Εθνικό Μετσόβιο Πολυτεχνειο

Σχολη Ηλεκτρολόγων Μηχανικών και Μηχανικών Υπολογιστών

Τομέας Ηλεκτρικής Ισχύος, Εργαστήριο Υψηλών Τάσεων

Technische Universität München

Fakultät für Elektrotechnik und Informationstechnik

Lehrstuhl für Hochspannungs- und Anlagentechnik

Συμβολή στη μελέτη της χωρικής αγωγιμότητας πολυμερών μονωτικών υλικών

Διπλωματική Εργασία

Μυρτώ Θωμά

Καθηγητές: Ιωάννης Αθ. Σταθόπουλος, ΕΜΠ

Josef Kindersberger, TUM

Επιβλέπων: Thomas Wendel

Αθήνα, Απρίλιος 2015

Εθνικό Μετσόβιο Πολυτεχνειο

Σχολη Ηλεκτρολόγων Μηχανικών και Μηχανικών Υπολογιστών

Τομέας Ηλεκτρικής Ισχύος, Εργαστήριο Υψηλών Τάσεων

Technische Universität München

Fakultät für Elektrotechnik und Informationstechnik

Lehrstuhl für Hochspannungs- und Anlagentechnik

Συμβολή στη μελέτη της χωρικής αγωγιμότητας πολυμερών μονωτικών υλικών

Διπλωματική Εργασία

Μυρτώ Θωμά

Καθηγητές: Ιωαννης Αθ. Σταθόπουλος, ΕΜΠ

Josef Kindersberger, TUM

Επιβλέπων: Thomas Wendel

Εγκρίθηκε τη 2α Απριλίου 2015 απο την τριμελή εξεταστική επιτροπή:

.....	.....	.....
Ι. Α. Σταθόπουλος	Φ. Β. Τοπαλής	Ι. Φ. Γκόνος
Καθηγητής ΕΜΠ	Καθηγητής ΕΜΠ	Επ. Καθηγητής ΕΜΠ

Αθήνα, Απρίλιος 2015

.....

Μυρτώ Θωμά
Διπλωματούχος Ηλεκτρολόγος Μηχανικός και Μηχανικός Υπολογιστών Ε.Μ.Π.

Στους γονείς μου

«Κι αν είσαι στο σκαλί το πρώτο, πρέπει
νάσαι υπερήφανος κ' ευτυχισμένος.
Εδώ που έφθασες, λίγο δεν είναι·
τόσο που έκαμες, μεγάλη δόξα.
Κι αυτό ακόμη το σκαλί το πρώτο
πολύ από τον κοινό τον κόσμο απέχει.
Εις το σκαλί για να πατήσεις τούτο
πρέπει με το δικαίωμά σου νάσαι
πολίτης εις των ιδεών την πόλι.
Και δύσκολο στην πόλι εκείνην είναι
και σπάνιο να σε πολιτογραφήσουν.
Στην αγορά της βρίσκεις Νομοθέτας
που δεν γελά κανένας τυχοδιώκτης.
Εδώ που έφθασες, λίγο δεν είναι·
τόσο που έκαμες, μεγάλη δόξα.»

Κ. Π. Καβάφης

Ευχαριστίες

Η παρούσα διπλωματική εργασία πραγματοποιήθηκε στον τομέα Υψηλών Τάσεων του Πολυτεχνείου του Μονάχου, στα πλαίσια του προγράμματος ανταλλαγής φοιτητών Εράσμους. Θα ήθελα να ευχαριστήσω θερμά τον Καθηγητή μου κύριο Ιωάννη Σταθόπουλο για την ευκαιρία που μου έδωσε να συμμετάσχω στη ερευνητική ομάδα του συγκεκριμένου τομέα, όπως επίσης και τον Καθηγητή Josef Kindersberger για την καθοδήγηση που μου παρείχε, καθώς και για την ευγένεια με την οποία αντιμετώπισε οποιαδήποτε απορία και δυσκολία μου. Επιπλέον, θα ήθελα να ευχαριστήσω τον επιβλέποντα μου Thomas Wendel για την πολύ καλή και εποικοδομητική μας συνεργασία, η οποία μετά από πολύ κόπο, πολλά τεχνικά προβλήματα και πολλή δουλειά, έφερε τα επιθυμητά αποτελέσματα, τα οποία θα μπορέσουν να χρησιμοποιηθούν και για περαιτέρω έρευνα.

Θα ήθελα επίσης να πω ένα τεράστιο ευχαριστώ στους γονείς μου και τον Φαέθωνα, που όλα αυτά τα χρόνια πιστεύουν σε μένα και με στηρίζουν σε ό,τι και αν επιλέξω. Ο καθένας με τον δικό του μοναδικό και ιδιαίτερο τρόπο.

Περίληψη

Η χρήση του συνεχούς ρεύματος (DC) αντί του εναλασσόμενου (AC) για τη μεταφορά της ηλεκτρικής ενέργειας, επεκτείνεται σταθερά. Οι αιτίες της επιλογής του Συνεχούς Ρεύματος Υψηλής Τάσης (HVDC) αντί του Εναλασσόμενου Ρεύματος, για μια συγκεκριμένη περίπτωση ειναι πολλές και σύνθετες. Μερικά απο τα πλεονεκτήματα της μεταφοράς ενέργειας μέσω HVDC ειναι τα παρακάτω:

- Οικονομικώτερη και πιο ικανοποιητική μεταφορά ηλεκτρικής ενέργειας σε μεγάλες αποστάσεις.
- Σύνδεση ασύγχρονων δικτύων ή δικτύων με διαφορετικές συχνότητες.
- Δυνατότητα ελεγχόμενης παροχής ρεύματος και προς τις δύο κατευθύνσεις.
- Επισκεψιμότητα δικτύου για κοντινή ή μακρυνή παραγωγή ρεύματος απο ανανεώσιμες πηγές ενέργειας.
- Έλεγχος αέργου ισχύος και καλύτερη ποιότητα ηλεκτρικής ενέργειας.

Αυτό που επέτρεψε την ευρεία χρήση HVDC είναι η μεγάλη τεχνολογική πρόοδος στον τομέα των ηλεκτρονικών ισχύος (κυρίως στους μετατροπείς), καθώς και η εξέλιξη των μονωτικών υλικών ώστε να αντέχουν αρκετά υψηλά επίπεδα τάσης.

Οι στερεοί ηλεκτρικοί μονωτές εχουν ευρεία χρήση στην ηλεκτρική και ηλεκτρονική βιομηχανία. Ιδιαίτερα η χρήση των πολυμερών μονωτών ειναι σταθερά αυξανόμενη. Τις τελευταίες δεκαετίες έχουν χρησιμοποιηθεί ευρέως λόγω των άριστων ηλεκτρικών και μηχανικών ιδιοτήτων τους. Εχουν ευρεία εφαρμογή, κυμαινόμενη απο καλώδια και ηλεκτρικές συσκευές, μέχρι τη μικροηλεκτρονική [IED-84]. Σε αμφότερες τη μεταφορά και τη διανομή ηλεκτρικής ενέργειας, τα πλεονεκτήματα των πολυμερών έναντι των απο προσελάνη ή γυάλινων μονωτών, έχουν οδηγήσει στην προοδευτική αποδοχή των πρώτων. Μερικά απο αυτά τα πλεονεκτήματα ειναι οι καλές υδροφοβικές ιδιότητες της επιφάνειάς τους, το μικρό βάρος, η μεγάλη μηχανική αντοχή τους κλπ [MAC-97]. Επιπρόσθετα, οι πολυμερείς μονωτές θεωρείται οτι εχουν μεγαλύτερη αντίσταση τάσης κάτω απο συνθήκες μόλυνσης έναντι των απο πορσελάνη ή γυάλινων μονωτών [MAE-98].
Η χρήση των πολυμερών μονωτών για εσωτερικές και εξωτερικές μονώσεις στη τεχνολογία της ηλεκτρικής ενέργειας εχει εφαρμογή σε καλώδια, ζυγούς συστημάτων ηλεκτρικής ενέργειας (bushings), μετασχηματιστές, αεριομονωμένους διακόπτες (gas-insulated switchgears) κ.α. [BAER-10].

Λόγω της αυξανόμενης ζήτησης για HVDC συστήματα παγκοσμίως, οι εποξεικές ρητίνες χρησιμοποιούνται όλο και συχνότερα ως στερεά μονωτικά σε εξοπλισμούς HVDC. Η διαστασιολόγηση των HVDC συσκευών απαιτεί τη γνώση των κατανομών του ηλεκτρικού πεδίου, που εξαρτώνται απο την αγωγιμότητα των μονωτικών που χρησιμοποιούνται σ' αυτα τα συστήματα. Δεδομένου ότι η χωρική κατανομή του συνεχούς ρεύματος, στα HVDC συστήματα, είναι ενα πεδίο αγωγιμότητας, προσδιοριζόμενο και απο την αγωγιμότητα των εμπεριεχομένων μονωτών, η συμπεριφορά τους πρέπει να διερευνηθεί κάτω απο μεταβαλλόμενες συνθήκες.

Η DC αγωγιμότητα ειναι ευαίσθητη σε πολλές παραμέτρους οπως η θερμοκρασία, το πεδίο, η υγρασία, οι συνθήκες περιβαλλοντικής ρύπανσης κλπ. Επιπλέον, η ανάπτυξη νέων πολυμερών υλικών με βελτιωμένη απόδοση κάτω απο ηλεκτρική τάση συνεχούς ρεύματος

και ταυτόχρονη θερμική διέγερση, απαιτεί ενδολεχή έρευνα των ιδιοτήτων που καθορίζουν την έγχυση φορέων από αγωγούς, τη μεταφορά των φορέων από το κύριο σώμα του μονωτικού υλικού, και την παγίδευση των φορέων στον όγκο του μονωτικού υλικού. Όμως, λόγω της πολύπλοκης φύσης των πολυμερών μονωτικών υλικών, μια λεπτομερής κατανόηση των θεμελιωδών ηλεκτρικών ιδιοτήτων τους και του τρόπου που οι φορείς δημιουργούνται και μεταφέρονται μέσα στα υλικά αυτά, ειναι απόλυτα απαραίτητη για την μελλοντική πρόοδο σε πρακτικές εφαρμογές.

Αντικείμενο της παρούσας μελέτης, ειναι η έρευνα της χωρική αγωγιμότητα δειγμάτων εποξεικής ρητίνης, εμποτισμένων με Al_2O_3 (fillers). Η χωρική αγωγιμότητα εξετάζεται ως συνάρτηση της θερμοκρασίας και του ηλεκτρικού πεδίου. Επιπροσθέτως θα προσπαθήσουμε να προσδιορίσουμε τους μηχανισμούς αγωγιμότητας που κυριαρχούν στην ηλεκτρική συμπεριφορά και τον τρόπο που οι φορείς δημιουργούνται και μεταφέρονται μέσα στο εξεταζόμενο υλικό.

Για τη διερεύνηση της χωρικής αγωγιμότητας του υλικού, πραγματοποιήθηκαν μετρήσεις του ρεύματος αγωγιμότητας σύμφωνα με τον κανονισμό VDE 0303-30, με εύρος ηλεκτρικού πεδίου 1 εως 12 KV/mm και θερμοκρασίες 40 και 80 °C.

Λεξεις κλειδια: Συνεχές ρελυμα υψηλής τάσης, πολυμερή μονωτικά υλικά, εποξεικές ρητίνες, μετρήσεις ρεύματος αγωγιμότητας, χωρική αγωγιμότητα, θερμοκρασία, ηλεκτρικό πεδίο.

Summary

The use of DC over AC voltage for the transmission of power is increasing steadily. The reasons for choosing High Voltage Direct Current (HVDC) instead of AC to transmit power in certain transmission applications are often numerous and complex. Some of the advantages of HVDC transmission are listed below:

- Economical and most efficient transmission of electrical power over long distances, using fewer lines
- Connecting asynchronous grids or grids with different frequencies
- Control of the reactive power, which supports the network stability and power quality
- Offering grid access for onshore and offshore power generation from renewable energy sources.

At the same time, the use of polymeric insulating materials for HVDC purposes is also steadily growing. Their advantages, compared to porcelain and glass insulators have led to the increased acceptance of the first ones. Some of these advantages are: good hydrophobic surface properties, low weight, high mechanical strength, higher withstand voltage under contaminated conditions etc. [MAC-97], [MAE-98]. The application of polymeric insulating materials in internal and external insulations of power engineering is considered for cables, bushings, transformers, gas-insulated systems and insulators [BAER-10]. In addition, the increasing demand on solid insulation for HVDC applications, has led to the introduction of composite insulating materials, where the use of functional fillers improve their electrical and other properties.

Research is focusing on the development of new polymeric insulating materials with improved performance under DC electrical stress and thermal excitation. And since the DC field distribution in HVDC insulation is a resistive field, the electrical conductivity, and in particular the volume conductivity of the insulators included has to be investigated in detail. However, an exact theoretical understanding of DC conduction in solid polymer insulation materials is currently impossible due to the underlying physical complexity of these materials [KAO-04], [TEY-05], as their structure consists of highly disordered, entangled, polymer chains [PHI-78]. Hence, the investigation of the volume conductivity requires a thorough investigation of the properties governing the charge injection, transport and trapping in these materials.

In the framework of this thesis, the volume conductivity of Al_2O_3 – filled epoxy resin is investigated as a function of temperature and electric field. For the study of the volume conductivity a conduction current measurement setup is used, and conduction current measurements are performed according to VDE 0303-30 (international norm: IEC 93) on plaque specimens of the material. The investigated fields are 1 to 12 kV/mm, and the investigated temperatures are 40 and 80 °C. The results are used in order to find the charge generation and transport mechanisms in the material, in the investigated field and temperature range.

In Chapter 2, a basic theoretical backgroung is given, containing information on the structure and applications of epoxy resins, the dielectric and electric response of insulating materials, the factors influencing DC conductivity (emphasizing on the temperature dependence), and the method of conduction current measurements on insulating materials.

In Chapter 3, the way carriers are generated, injected, and transported through polymeric insulating materials is discussed. In addition, the significant influence of the space charge accumulation on the investigation of volume conductivity is explained and conduction theories developed through the years are indicated.

In Chapter 4, experimental results from previous investigations concerning conduction current measurements on polymeric insulating materials, filled and unfilled, are presented, and the nature of the current density – electric field characteristic is analyzed.

In Chapter 5, the results from the conduction current measurements on the Al_2O_3 – filled epoxy resin specimens are shown. Good information and conclusions are drawn from the measurements.

In Chapter 5, the Thermally Stimulated Currents theory is presented as well as results from measurements on the investigated material.

Key words: High Voltage Direct Voltage (HVDC), polymeric insulating materials, epoxy resins, conduction current measurements, volume conductivity, temperature, electric filled.

Εισαγωγή:

Εποξεικές ρητίνες και εφαρμογές

Καθώς το εξεταζόμενο υλικό είναι εποξεική ρητίνη, εμπλουτισμένη με Al_2O_3 , ειναι απαραίτητο να γνωρίζουμε τη χημική σύνθεση των εποξεικών ρητινών καθώς και τις βασικές τους εφαρμογές στον τομέα των υψηλών τάσεων και μεταφοράς ηλεκτρικής ισχύος.

Χημική σύνθεση

Σε αντίθεση με πολλές άλλες κατηγορίες πολυμερών, οπως το πολυαιθυλαίνιο, το πολυπροπυλαίνιο, κλπ, οι εποξεικές ρητίνες αποτελούν μια περισότερο αντιθετική κατηγορία ρητινών τόσο στις χημικές, όσο και στις φυσικές ιδιότητες τους. Οι εποξεικές ρητίνες αποτελούν μια οικογένεια θερμοπλαστικών πολυμερών, στην οποία δυο στοιχεία αναμειγνύονται, με πιθανή δημιουργία ενος υαλώδους προιόντος σε θερμοκρασία δωματίου, το οποίο εχει καλες ηλεκτρομονωτικές ιδιότητες με υψηλή αδιαπερατότητα στο νερό [DIS92].

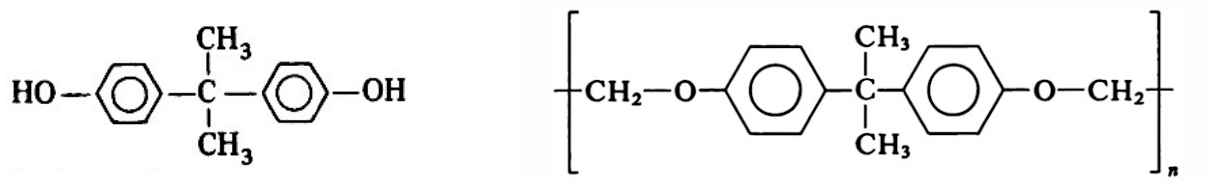

(a) (b)

Σχήμα 1 | (a) Bisphenol A, from [DOM-12]
(b) Diepoxide structure with Bisphenol A, from [DIS-92]

Οι εποξεικές ρητίνες ειναι χημικές συνθέσεις αποτελούμενες απο τουλάχιστον ενα στοιχείο της ομάδας των εποξεικων (επόξυ-ομάδα) και απο ενα στοιχείο της ομάδας των υδροξυλίων. Η επόξυ-ομάδα ειναι μια γέφυρα αποτελούμενη απο ενα άτομο οξυγόνου ενωμένο με με δυο αλλα άτομα ηδη συνδεδεμένα μεταξύ τους κατά καποιο τρόπο. Οταν τα δυο παραπάνω άτομα ειναι άτομα άνθρακα, τοτε έχουμε να κάνουμε με τις τριμερείς αλυσίδες α ή 1,2 επόξυ-ομάδες. Η τριμερής αλυσίδα ειναι ασταθής και συνακόλουθα ετοιμη να αντιδράσει με την υδροξυλική ομάδα. Μια κοινή μορφή ειναι αυτη της διεποξειδικής σύνθεσης (Σχήμα 1). Η σκλήρυνση ειναι επίσης ενας σημαντικός παράγοντας στην περίπτωση των εποξειδικών ρητινών. Οι εποξεικές ρητίνες πριν τη διαδικασία της σκλήρυνσης ειναι σε ρευστή μορφή και δεν εχουν καμμιά πρακτική ηλεκτρική ιδιότητα. Η διαδικασία της σκλήρυνσης ειναι η αντίδραση μεταξυ της εποξεικής ομάδας και ενος χημικού παράγοντα (καλουμένου επισης και σκληρυντικό). Σαν σκληρυντικά χρησιμοποιούνται οξέα ή αλκαλικά σκληρυντικά που σχηματίζουν συνθέσεις τριδιάστατων δικτύων, με αποτέλεσμα την μετατροπή των ρευστών ρητινών σε στερεά υλικά [LAU-05].

Εφαρμογές των εποξεικών ρητινών

Οι εποξεικές ρητίνες χρησιμοποιούνται σε πολλούς και διάφορους κλάδους όπως η αεροναυπηγική, η ιατρική, η ηλεκτρολογία, η κατασκευαστική δραστηριότητα, η βιομηχανία των αθλητικών ειδών κλπ [DOM-12]. Στη βιομηχανία της ηλεκτρικής ενέργειας, συγκεκριμμένα, οι εποξεικές ρητίνες, χρησιμοποιούνται ευρέως σαν μονωτικό υλικό, λόγω των εξαιρετικών διηλεκτρικών ιδιοτήτων τους, την υψηλή μηχανική αντοχή και την καλη αντίσταση στη διάβρωση [DAK-74]. Χρησιμοποιούνται σαν περιβλήματα σε αγωγούς καθώς και στις εφαρμογές ζυγών (bushings), ακροδεκτων, μετασχηματιστών, και ως μονωτικά συστημάτων τοποθέτησης, υποστήριξης και διακοπτών δικτυων [DAK-74], [DAK-72].

Άλλη μία σημαντική εφαρμογή των εποξεικών ρητινών στη μεταφορά HDVC, ειναι στα αεριομονωμένα συστήματα και συγκεκριμμένα στις αεριομονωμένες γραμμές μεταφοράς, Gas Insulated Lines (GILs). Μια πραγματική GIL παρουσιάζεται στο Σχήμα 2:

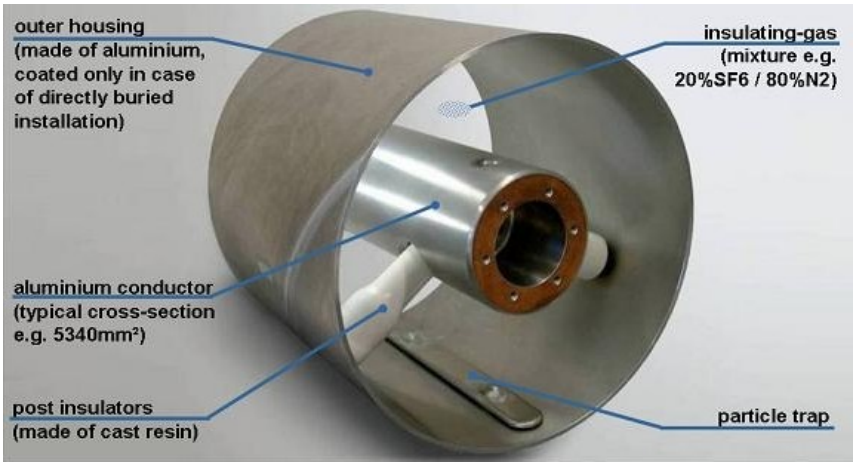

Σχήμα 2: Gas Insulated Line (GIL) of Siemens with all parts indicated

Οι GILs ειναι μια καλή εναλλακτική για μεταφορά υψηλής τάσης, οταν περιβαλλοντολογικοί ή κατασκευαστικοί περιορισμοί απαγορεύουν τη χρήση εναέριων γραμμών μεταφοράς. Η GIL αποτελείται απο δυο ομόκεντρους συνδεδεμένους σωληνωτούς αγωγούς. Ο εσωτερικός αγωγός στηρίζεται σε μονωτές ρητίνης που τον συγκρατούν στο κέντρο του εξωτερικού αγωγού. Για να εξασφαλίσει την αντιμετώπιση περιβαλλοντολογικών και τεχνικών περιορισμών, οι γραμμές GIL γεμίζονται με ένα μονωτικό μείγμα αερίων, κυρίως αζώτου και ενός μικρού ποσοστού εξαφθοριούχου θείου (SF6) [SIE-12]. Οι GILs μπορούν να τοποθετηθούν πάνω στο έδαφος, μέσα σε τούνελ ή και να είναι θαμμένες απ' ευθείας κάτω από τη γη, ανάλογα με τις εκάστοτε απαιτήσεις.

Οι χρησιμοποιούμενες σαν στερεά μονωτικά εποξεικές ρητίνες σε αυτές τις εφαρμογές θα πρέπει να ειναι ανθεκτικές στο ισχυρό ηλεκτρικό πεδίο, καθώς και τις εκάστοτε θερμοκρασιακές μεταβολές. Συνεπώς ειναι σημαντικό να μπορούμε να προβλέψουμε την κατανομή του ηλεκτρικού πεδίου και τη χωρικη αγωγιμότητα του υλικού κάτω απο συγκεκριμμένες συνθήκες πεδίου και θερμοκρασίας.

Διηλεκτρική απόκριση μονωτικού υλικού σε συνεχή τάση

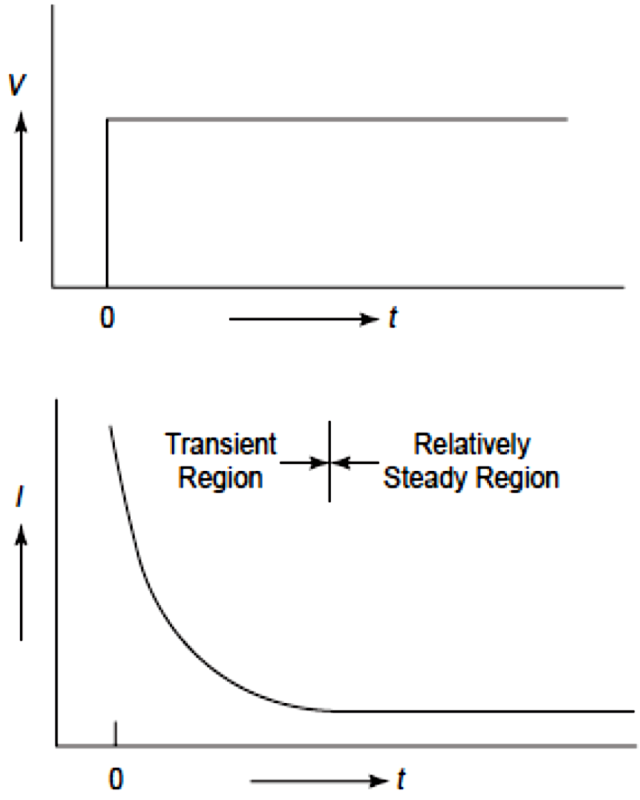

Σχήμα 3: Typical DC current response of insulation to a step voltage application, from [DAK-06]

Αμέσως μετά την εφαρμογή συνεχούς τάσης σε ένα μονωτικό υλικό, ένα πεδίο μετατόπισης επικρατεί, καθοριζόμενο από τη σχετική επιτρεπτότητα ε_r του υλικού. Το ρεύμα που μετράται οφείλεται κυρίως στις διαδικασίες πόλωσης που λαμβάνουν χώρα. Στη συνέχεια, το ρεύμα αυτό φθίνει ώσπου να φτάσει μια σταθερή τιμή, η οποία καθορίζεται από τη χωρική αγωγιμότητα του υλικού. Η τυπική απόκριση του μονωτικού φαίνεται στο σχήμα 3.

Ο συνολικός χρόνος που απαιτείται ωστε το ρεύμα να φθάσει σε μια κατάσταση σταθερής έντασης εξαρτάται από τη θερμοκρασία, καθώς οι μηχανισμοί πόλωσης εξαρτώνται από τη θερμοκρασία. Πειραματικά αποτελέσματα έχουν δείξει οτι, π.χ. για τα κοινά πολυμερη οου χρησιμοποιούνται σαν ηλεκτρικοί μονωτές (οπως πολυαιθυλαίνιο, πολυπροπυλαίνιο, εποξειδικές ρητίνες), η αποκατάσταση συνθηκών σταθερού καθεστώτος, μπορεί να απαιτήσει την παρέλευση ωρών [MON-11].

DC Αγωγιμότητα

Η ηλεκτρική αγωγιμότητα μπορεί να προκληθεί μέσω της κίνησης ηλεκτρονίων, οπών η ιόντων. Σε κάθε περίπτωση, ενα πρέπον σημείο εκκίνησης για συζήτηση της διαδικασίας της αγωγιμότητας, καθορίζεται απο την εξίσωση:

$$\kappa = \sum_{\mathrm{i}} q_{\mathrm{i}}\mu_{\mathrm{i}}e = n_{\mathrm{e}}\mu_e e + n_{\mathrm{h}}\mu_{\mathrm{h}}e + n_{\mathrm{I}}\mu_{\mathrm{I}}\,(Z_{\mathrm{w}}e) \qquad \text{Εξ.1}$$

όπου η αγωγιμότητα κ αποτελείται απο την αγωγιμότητα των ηλεκτρονίων, των οπών και των ιόντων και αναλύεται σε τρείς παράγοντες: το φορτίο του ηλεκτρονίου e, τη συγκέντρωση n και την κινητικότητα των φορέων μ. Το σθένος των ιόντων ειναι Zw. Η κινητικότητα (μ) χαρακτηρίζει την ευκολία με την οποία οι φορείς θα κινηθούν κατω απο την επίδραση του εφαρμοσμένου ηλεκτρικού πεδίου Ε και εκφράζεται συνήθως ως η ταχύτητα ανα μονάδα πεδίου ($m^2V^{-1}s^{-1}$).

Σε περίπτωση απουσίας ηλεκτρικού πεδίου, οι φορείς φαίνονται σαν να κινούνται ακανόνιστα σε ολες τις κατευθύνσεις, με μέση μηδενική ταχύτητα (v). Η παρουσία ενος

πεδίου θα οδηγήση σε κίνηση των φορέων με σημαντική ταχύτητα, κατα τη διεύθυνση του πεδίου ή αντίθετα απο αυτό, κάτι το οποίο εξαρτάται από το πρόσημο των φορέων [BLY-05]. Η κινητικότητα, όπως και η συγκέντρωση των φορέων, είναι συναρτήσεις του πεδίου, της θερμοκρασίας, και των περιβαλλοντικών συνθηκών. Συνεπώς , οι θεωρίες αγωγιμότητας τείνουν να εξηγήσουν πως οι μεταβλητές n και μ προσδιορίζονται απο τη μοριακή δομή και πως εξαρτώνται απο παράγοντες οπως είναι η θερμοκρασία και το ηλεκτρικό πεδίο [BLY-05].

Η DC αγωγιμότητα διαιρείται σε δυο κατηγορίες: τη χωρική και την επιφανειακή. Η χωρική αγωγιμότητα ορίζεται ως η αγωγιμότητα διαμέσου ενος κύβου του μονωτικού υλικου ενω η επιφανειακή αγωγιμότητα ορίζεται ως η ηλεκτρική αντίσταση μέσω της επιφάνειας του υλικού [Keithley-01]. Στην παρουσα εργασία θα ασχοληθούμε μονο με την πρώτη απο αυτές.

Η χωρική αγωγιμότητα των υλικών ειναι μια ιδιότητα που εκτείνεται σε ενα μεγάλο εύρος, οπως φαίνεται στο Σχήμα 4, και εξαρτάται απο τους παρακάτω παράγοντες [LUT-11]:

- το ηλεκτρικό πεδίο
- τη θερμοκρασία
- το χρόνο εξηλεκτρισμου (πόλωσης)
- τη σχετική υγρασία του υλικού
- τη σχετική υγρασία του περιβάλλοντος
- το υλικό του ηλεκτροδίου
- το πάχος του υλικού
- τη χημική και μορφολογική δομή (π.χ. για το υλικό πλήρωσης, η φύση το μεγεθος και η μορφή του)
- τους περιβαλλοντολογικούς παράγοντες οπως την ατμοσφαιρική ρύπανση, το θαλασσινό νερό κλπ.

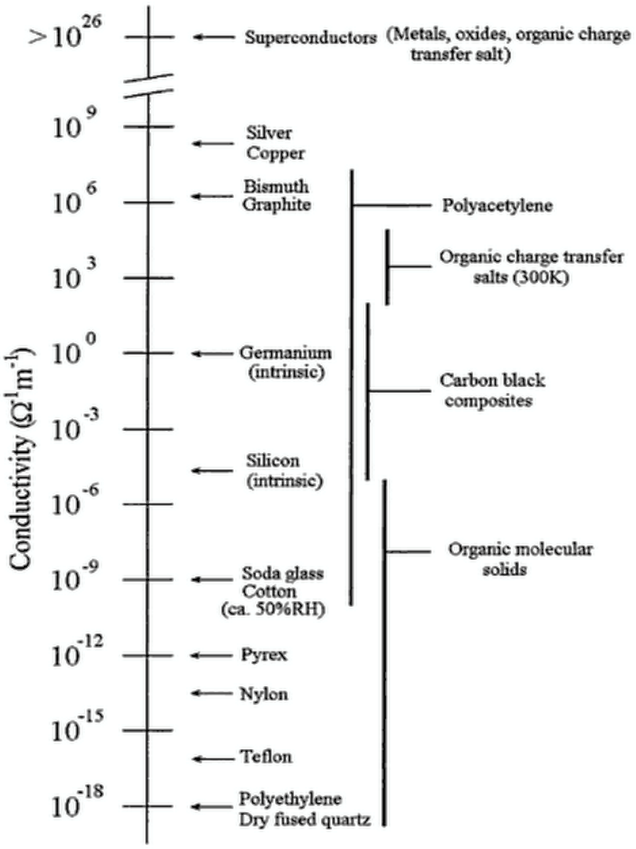

Fig. 2.9: Chart of typical volume conductivities, showing the wide range depending on the material, from [BLY-05]

Για να μετρήσουμε τη χωρική αγωγιμότητα ενος υλικού, εκτελούμε μετρήσεις του ρεύματος αγωγιμότητας.

Μετρήσεις ρεύματος αγωγημότητας (VDE 0303-30)

Για τον προσδιορισμό της χωρικής αγωγιμότητας, του υπο έρευνα υλικού, κατασκευάστηκε μια διάταξη μέτρησης χωρικής αγωγιμότητας. Οι μετρήσεις έγιναν σύμφωνα με τον κανονισμό VDE 0303-03. Η παρούσα εργασία εστιάζεται κυρίως στην επίδραση της θερμοκρασίας και του ηλεκτρικού πεδίου στη χωρική αγωγιμότητα του υλικού, συνεπώς οι μετρήσεις του ρεύματος αγωγιμότητας, έγιναν ως συνάρτηση αυτών των δύο παραμέτρων.

Το εξεταζόμενο υλικό ειναι εποξειδική ρητίνη εμπλουτισμένη με Al_2O_3. Το ποσοστό πλήρωσης δεν είναι γνωστό. Συνολικά χρησιμοποιήθηκαν πεντε κυκλικά πλακίδια, με παχος 1mm και διαμετρο 8 cm. Ολα τα δείγματα είχαν τοποθετηθεί στους 100 °C για τουλάχιστον 1 ημέρα πριν χρησιμοποιηθούν και είχαν καθαριστεί με ισοπροπανόλη. Επιπλέον, πριν από την εφαρμογή της τάσης, τα πλακίδια είχαν βραχυκυκλωθεί, ώστε εναπομείναντα ρεύματα να μην επηρεάσουν τη μέτρηση.

Η διαμόρφωση του εργαστηρίου (οπως φαινεται στο Σχήμα 5) βρίσκεται στο Εργαστήριο Υψηλών Τάσεων του Πολυτεχνείου του Μονάχου και αποτελείται απο τα εξης τμήματα:

Σχήμα 5: Test arrangement for Conduction Current Measurements on Al_2O_3-filled epoxy plaque specimen, in the laboratory of High Voltage Engineering and Switchgear Technology of TUM, showing: (1)The climate chamber, (2) The grounded cage, (3)The computer

Οι διαστάσεις των ηλεκτροδίων και τα όργανα μέτρησης, παρουσιάζονται αναλυτικά στο Appendix A. Τα αποτελέσματα των μετρήσεων παρουσιάζονται στο Appendix B. Μια πρώτη εικόνα των αποτελεσμάτων φαίνεται στο Σχήμα 6. Για πεδίο 1 kV/mm, χρησιμοποιήθηκαν τα αποτελέσματα από προηγούμενη διπλωματική εργασία [REM-12], η οποία αφορά το ίδιο υλικό. Στο Σχήμα 6, βλέπουμε καταρχάς τη διαφορά που υπάρχει στην τιμή της αγωγιμότητας στους 40 και στους 80 °C. Συγκεκριμένα, η αγωγιμότητα του υλικού στους 80 °C είναι 26 εώς 48 φορές υψηλότερη. Γι'αυτό κιόλας έχει χρησιμοποιηθεί λογαριθμικός άξονας για την απεικόνιση της αγωγιμότητας. Όσον αφορά την εξάρτηση της αγωγιμότητας από το ηλεκτρικό πεδίο, θα μπορούσαμε να πούμε ό,τι για πεδία απο 1 εώς 6 kV/mm η αγωγιμότητα παραμένει σχεδόν σταθερη και για τις δύο θερμοκρασίες, ιδιαίτερα λαμβάνοντας υπόψην και το τυχαίο σφάλμα των μετρήσεων. Στα 12 kV/mm αντιθέτως, η αγωγιμότητα είναι υψηλότερη και για τις δύο εξεταζόμενες θερμοκρασίες, δηλώνοντας πως έχει επηρεαστεί από την αύξηση του ηλεκτρικού πεδίου. Θα μπορούσαμε να πούμε ό,τι η χωρική αγωγιμότητα του υλικού, σαν συνάρτηση του ηλεκτρικού πεδίου, χωρίζεται σε δύο περιοχές: την περιοχή χαμηλού ηλεκτρικού πεδίου και την περιοχή υψηλού ηλεκτρικού πεδίου. Σύμφωνα με προηγούμενες μελέτες, οι δύο αυτές περιοχές χωρίζονται από ένα ηλεκτρικό πεδίο ονομαζόμενο και ως "κατώφλι" ($E_{threshold}$). Η τιμή του

πεδίου αυτού, σηματοδοτεί την έναυση μιας περιοχής αγωγιμότητας υψηλού πεδίου, η οποία οφείλεται σε διάφορους μηχανισμούς αγωγιμότητας.
Προηγούμενες μελέτες εστιάζουν κυρίως στην συγκέντρωση χωρικού φορτίου στον όγκο του μονωτικού, απο το πεδίο "κατώφλι" και μετά, η οποία επηρεάζει τη σχέση ρεύματος – ηλεκτρικού πεδίου, και συνεπώς και της αγωγιμότητας. Οι θεωρίες αγωγιμότητας που έχουν αναπτυχθεί ως τώρα παρουσιάζονται αναλυτικά στο κεφάλαιο 3.

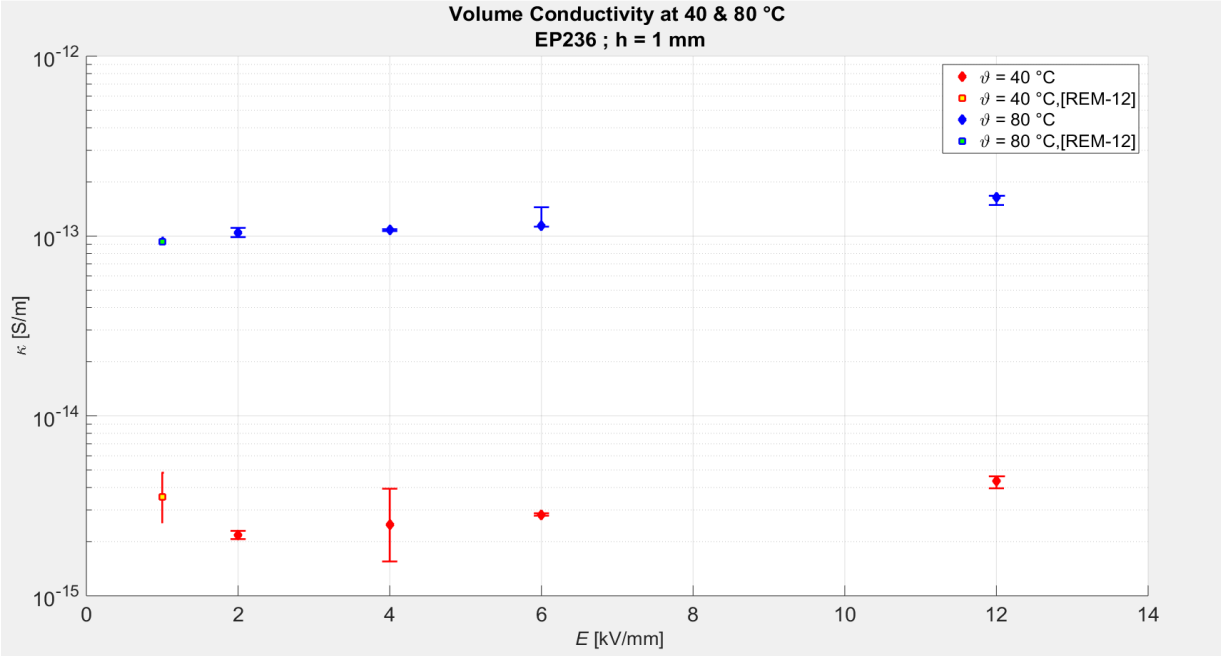

Fig. 5.4: Volume conductivity with respect to applied electric field, at 40 and 80 °C

Μέσω της μέτρησης της χωρικής αγωγιμότητας, συμπεράσματα μπορούν να εξαχθούν για τους μηχανισμούς αγωγιμότητας που διέπουν το υλικό, καθώς και για τη φύση των φορέων. Τα αναλυτικά αποτελέσματα των μετρήσεων, καθώς και τα συμπεράσματα για τους μηχανισμούς αγωγιμότητας στο εξεταζόμενο υλικό παρουσιάζονται στο κεφάλαιο 5.

Table of figures

Chapter 2

Fig. 2.1: Epoxy group, from [DOM-12]

Fig. 2.2: Diepoxide structure as a common configuration, from [DIS-92]

Fig. 2.3 (a) Bisphenol A, from [DOM-12]
(b) Diepoxide structure with Bisphenol A, from [DIS-92]

Fig. 2.4: Reaction of an epoxy resin with diamine compound as hardener, from [DIS-92]

Fig. 2.5: Gas Insulated Line (GIL) of Siemens with all parts indicated, from Siemens

Fig. 2.6: Typical DC current response of insulation to a step voltage application, from [DAK-06]

Fig. 2.7: Different types of dielectric response functions $f(t)$ in time domain, from [FAR-03]

Fig. 2.8: Principle types of Polarization, from [DAK-06]

Fig. 2.9: Chart of typical volume conductivities, showing the wide range depending on the material, from [BLY-05]

Fig. 2.10 (a) Test arrangement for the measurement of volume conductivity, from [VDE-93]
(b) Electrode arrangement for the measurement of volume conductivity, from [VDE-93]

Chapter 3

Fig. 3.1: Space charge accumulation at the metal-insulator interface, when the injected and transmitted currents differ.

Fig. 3.2: Field distribution in an insulator containing space charge regions extending From the electrodes at x = 0 and x = D.
(a) In the homocharge region the field is reduced and the injection is supressed
(b) in a heterocharge region the electrode field increases, from [DIS-92]

Fig. 3.3: Maxwell capacitor to describe the phenomena at the interface between dielectrics, from [KRE-95]

Fig. 3.4: Conduction and valence bands for insulators, semiconductors and conductors. Note the energy gaps in insulators and semiconductors, and how in a conductor there is no gap, while the conduction and valence bands are overlapped, from [KAS-01]

Fig. 3.5: Distribution of orbital levels going from methane to polyethylene. CB and VB stand for conduction and valence bands respectively, from [HOF-91]

Fig. 3.6: Representation of accessible localized states, i.e. traps, within the forbidden gap of a disordered dielectric material, from [KAH-89]

Fig. 3.7: Representation of shallow and deep traps for electrons and holes in a disordered dielectric material (Polyethylene), from [TEY-05]
Fig. 3.8: Insulator in contact with a metal:
(a) In the absence of a field
(b) With applied field, from [MOT-40]
Fig. 3.9: Bulk phenomena categorized into low and high field conduction mechanisms
Fig. 3.10: Diagram electron-transfer mechanisms between adjacent Sites separated by a potential-energy barrier, from [BLY-05]
Fig. 3.11: Poole-Frenkel mechanism: The potential $\Delta\Phi$ of the site is assumed to be of Coulombic form. Under high electric field, the energy of the site is modified, lowering of the barrier in the drift direction, from [TEY-05]
Fig. 3.12: Example of Laplacian (without accounting for space charge) and Poissonian (with space charge) electric field vs distance from a defect tip, from [ZHE-05]

Chapter 4

Fig. 4.1 (a) *J-E* characteristic for XLPE and EPR plaques, at 20 °C, from [BOD-04]
(b) *J-E* characteristic for XLPE mini-cables, at 20 °C, from [BOD-04]
Fig. 4.2 (a): *J-E* characteristic for commercial epoxy resin, unfilled and with Al_2O_3 filler, at 34 °C, from [MAC-00]
(b): *J-E* characteristic for commercial epoxy resin, unfilled and with ZnO filler, at 33 °C, from [MAC-00]
(c): *J-E* characteristic for a commercial epoxy resin, unfilled and with aluminum oxide or zinc oxide filler, at 33-34 °C, from [MAC-01]
Fig. 4.3: J-E characteristic for Epoxy and Polyethylene, at 25 °C, from [DAS-12].
Fig. 4.4: *J-E* characteristics for micro- and nanofilled epoxy resin specimens, from [CAS-11]
Fig. 4.5. Threshold field indication for PE and Epoxy, from conduction current and space charge measurements:
(a) Variation of charge density with respect to applied field, from [DAS-12]
(b) Variation of current density with respect to applied field, from [DAS-12]
Fig. 4.6: Mobility vs. electric field for micro- and nanofilled epoxy resin specimens, from [CAS-11]
Fig. 4.7: Plots of ln (J) vs. $E^{1/2}$ for the investigation of Schottky injection, for micro- and nanofilled epoxy resin specimens, at 25 °C, from [KRI-12]

Chapter 5

Fig. 5.1: Al_2O_3-filled epoxy plaque specimen, 1mm thickness
Fig. 5.2: Test arrangement for Conduction Current Measurements on Al_2O_3-filled epoxy plaque specimen, in the laboratory of High Voltage Engineering and Switchgear Technology of TUM, showing:
(1)The climate chamber, (2) The grounded cage, (3)The computer

Fig. 5.3: Conduction current measurements at 4 kV/mm and 40 °C
(a) Before the application of the silver lacquer
(b) After the application of the silver lacquer
Fig. 5.4: Volume conductivity with respect to applied electric field, at 40 and 80 °C
Fig. 5.5: Bar chart showing the difference in magnitude of the volume conductivity between 40 and 80 °C
Fig. 5.6: (a) Volume conductivity with respect to temperature, at 1 kV/mm,
(b) from [REM-12]
(c) Arrhenius equation fitting at 1 kV/mm, using the results of [REM-12]
Fig. 5.7: Conduction current measurement result at 2 kV/mm and 80 °C
Fig. 5.8: *I-t* characteristics for the first 1000 minutes of polarization, in log-log scale:
(a) At 40 °C
(b) At 80 °C
Fig. 5.9 Current density with respect to electric field
(a) At 40 °C
(b) At 80°C
Fig. 5.10: For the investigation of the Poole-Frenkel mechanism, the ln(J/E) versus $E^{1/2}$ characteristic is plotted:
(a) At 40 °C
(b) At 80 °C
Fig. 5.11: For the investigation of the Schottky mechanism, the ln(J) versus $E^{1/2}$ characteristic is plotted:
(a) At 40 °C
(b) At 80 °C
Fig. 5.12 For the investigation of the Fowler-Nordheim mechanism, the ln(J/E^2) versus E^{-1} characteristic is plotted:
(a) At 40 °C
(b) At 80 °C

Chapter 6

Fig. 6.1 Test arrangement for the performance of Thermally Stimulated Depolarization Currents (TSDC), from [KAO-05]
Fig. 6.2 Thermally Stimulated Depolarization Current measurement (TSDC) on EP236:
(a) Heating rate, from 80 to 150 °C
(b)Three subsequent depolarization current measurements with temperature elevated from 80 to 150 °C

Appendix A

Fig. A1: Keithley 6517B Electrometer
Fig. A2: FUG HCL 350-12500 DC High Voltage Power Supply
Fig. A3: Electrode arrangement for plaque specimens
Fig. A4: WEISS WT3 Climate chamber
Fig. A5: LabVIEW file for the data acquisition and recording
Fig. A6: Keithley 6517B Diode protection circuit
Fig. A7: Silica gel bags for the control of humidity

Table of contents

1. Introduction ... 3
2. Theoretical Background ... 5
2.1. Epoxy resins and applications ... 5
2.2. Dielectric and electrical response of insulating materials ... 8
2.2.1. Switching on a DC voltage U ... 8
2.2.2. Dielectric response function ... 9
2.3. Polarization mechanisms ... 9
2.4. DC Conductivity ... 11
2.5. Conduction current measurements according to VDE 0303-30 ... 12
2.6. Temperature dependence of the conductivity ... 14
3. Charge generation and transport in polymers ... 15
3.1. Space charge accumulation ... 15
3.1.1. Electrode-Insulation interface ... 15
3.1.2. Insulation-Insulation interface ... 17
3.1.3. Temperature gradient ... 19
3.1.4. Material inhomogeneity ... 19
3.2. Why is space charge related to the conductivity? ... 19
3.3. The Band Theory applied in polymers ... 20
3.4. Trapping in polymers ... 22
3.5. Charge generation and Injection at the electrodes ... 24
3.5.1. Schottky model approach: contact emission phenomenon ... 25
3.5.2. Fowler-Nordheim injection ... 26
3.6. Charge transport ... 27
3.6.1. Low-field conduction bulk phenomena ... 28
3.6.2. High-field conduction bulk phenomena ... 29
4. Conduction current measurements - Previous investigations ... 38
4.1. The threshold field and its dependence ... 38
4.1.1. Conduction current measurements on XLPE and EPR insulation, from [BOD-04] 38
4.1.2. Conduction current measurements on filled and unfilled epoxy, from [MAC-00], [MAC-01] ... 40
4.1.3. Conduction current measurements in Epoxy and Polyethylene, from [DAS-12] 42
4.1.4. Conduction current measurements on composite epoxy resin materials, from [CAS-11] ... 43
4.2. Possible origins of the non-linear *J-E* behavior ... 44
4.3. Detection of the conduction mechanisms from the J-E characteristics ... 46
5. Conduction current measurements on EP236 ... 51
5.1. Conduction current measurements procedure ... 51

5.1.1. Samples....51
5.1.2. Instrumentation....52
5.1.3. Experimental procedure....53
5.2. Noise reduction....53
5.3. Experimental results....57
5.3.1. Temperature dependence....58
5.3.2. Transient currents and dielectric response....60
5.3.3. Steady-state currents analysis....63
6. Thermally Stimulated Currents (TSC)....72
6.1. Theory of TSC spectroscopy....72
6.2. Experimental procedure....73
6.3. Conclusions....74
7. Appendix A....75
8. Appendix B....78
9. Bibliography....80

1. Introduction

The use of DC over AC voltage for the transmission of power is increasing steadily. The reasons for choosing High Voltage Direct Current (HVDC) instead of AC to transmit power in certain transmission applications are often numerous and complex. Some of the advantages of HVDC transmission are listed below:

- Economical and most efficient transmission of electrical power over long distances, using fewer lines
- Connecting asynchronous grids or grids with different frequencies
- Control of the reactive power, which supports the network stability and power quality
- Offering grid access for onshore and offshore power generation from renewable energy sources.

At the same time, the use of polymeric insulating materials for HVDC purposes is also steadily growing. Their advantages, compared to porcelain and glass insulators have led to the increased acceptance of the first ones. Some of these advantages are: good hydrophobic surface properties, low weight, high mechanical strength, higher withstand voltage under contaminated conditions etc. [MAC-97], [MAE-98]. The application of polymeric insulating materials in internal and external insulations of power engineering is considered for cables, bushings, transformers, gas-insulated systems and insulators [BAER-10]. In addition, the increasing demand on solid insulation for HVDC applications, has led to the introduction of composite insulating materials, where the use of functional fillers improve their electrical and other properties.

Research is focusing on the development of new polymeric insulating materials with improved performance under DC electrical stress and thermal excitation. And since the DC field distribution in HVDC insulation is a resistive field, the electrical conductivity, and in particular the volume conductivity of the insulators included has to be investigated in detail. However, an exact theoretical understanding of DC conduction in solid polymer insulation materials is currently impossible due to the underlying physical complexity of these materials [KAO-04], [TEY-05], as their structure consists of highly disordered, entangled, polymer chains [PHI-78]. Hence, the investigation of the volume conductivity requires a thorough investigation of the properties governing the charge injection, transport and trapping in these materials.

In the framework of this thesis, the volume conductivity of Al_2O_3 – filled epoxy resin is investigated as a function of temperature and electric field. For the study of the volume conductivity a conduction current measurement setup is used, and conduction current measurements are performed according to VDE 0303-30 (international norm: IEC 93) on plaque specimens of the material. The investigated fields are 1 to 12 kV/mm, and the investigated temperatures are 40 and 80 °C. The results are used in order to find the charge generation and transport mechanisms in the material, in the investigated field and temperature range.

Thesis outline

In Chapter 2, a basic theoretical backgroung is given, containing information on the structure and applications of epoxy resins, the dielectric and electric response of insulating materials, the factors influencing DC conductivity (emphasizing on the temperature dependence), and the method of conduction current measurements on insulating materials.

In Chapter 3, the way carriers are generated, injected, and transported through polymeric insulating materials is discussed. In addition, the significant influence of the space charge accumulation on the investigation of volume conductivity is explained and conduction theories developed through the years are indicated.

In Chapter 4, experimental results from previous investigations concerning conduction current measurements on polymeric insulating materials, filled and unfilled, are presented, and the nature of the current density – electric field characteristic is analyzed.

In Chapter 5, the results from the conduction current measurements on the Al_2O_3 – filled epoxy resin specimens are shown. Good information and conclusions are drawn from the measurements.

In Chapter 5, the Thermally Stimulated Currents theory is presented as well as results from measurements on the investigated material.

2. Theoretical Background

2.1. Epoxy resins and applications

In this thesis, the material under investigation is Al_2O_3 - filled epoxy resin. Thus, it is important to be aware of the chemical structure of epoxy resins and their basic applications in power engineering.

Chemical structure

Contrary to many other classes of polymers, such as polyethylene, polypropylene, etc., epoxy resins are a much more diverse class of resins, chemically and in their physical properties. Epoxy resins are a family of thermoset polymers in which two components are mixed to eventually form a glassy product at room temperature, which has good electrical insulating properties and is highly impermeable to water [DIS-92]. Epoxy resins are chemical compounds that consist of at least one epoxy and one hydroxyl group. The epoxy group is a bridge consisting of an oxygen atom bonded to two other atoms already united in some way. When the other two atoms are carbon, we deal with the three membered ring a- or 1,2-epoxides.

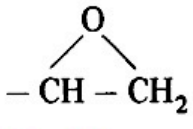

Fig. 2.1: Epoxy group, from [DOM-12]

The three membered ring is instable, and thus ready to react with the hydroxyl group. A common configuration is that of the diepoxide structure shown in Fig. 2.2:

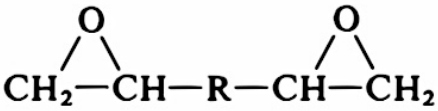

Fig. 2.2: Diepoxide structure as a common configuration,
from [DIS-92]

In Fig. 2.2, R is the hydroxyl group, which is a phenol. In commercial epoxy resins, used in high voltage insulation applications, R is almost exclusively bisphenol-A, as shown in Fig. 2.3 [DOM-12].

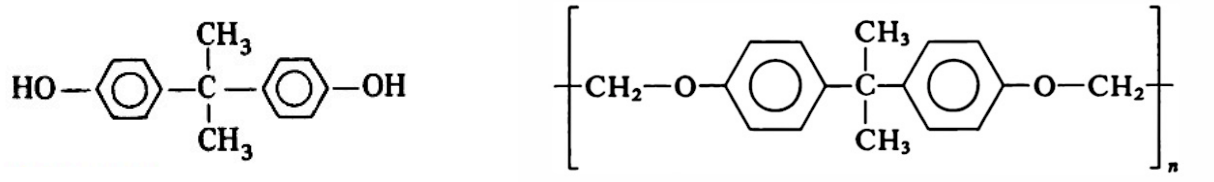

(a) (b)

Fig. 2.3 | (a) Bisphenol A, from [DOM-12]
(b) Diepoxide structure with Bisphenol A, from [DIS-92]

The index n in Fig. 2.3(b) varies from 0 to 10, which is quite low for a polymeric chain. Curing is necessary in case of epoxy resins. The epoxy resins before curing are liquid and do not have any practical electrical properties. The curing process is the reaction between the epoxy group and a curing agent (also called hardener). As hardeners, acids or alkaline hardeners are used that form a three- dimensional network structure, and so the epoxy resins are cured into solid materials [LAU-05]. An example of curing, using diamine compounds is shown in Fig. 2.4:

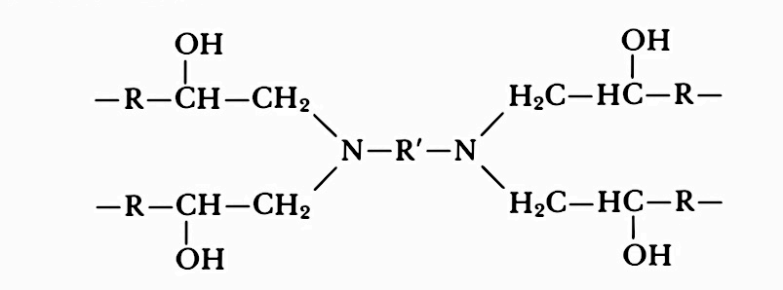

Fig. 2.4: Reaction of an epoxy resin with diamine compound as hardener, from [DIS-92]

Applications of Epoxy resins

Epoxy resins are used in many different branches such as aerospace, medicine, electrical and civil engineering, sports equipment, adhesives, etc. [DOM-12]. In the electric power industry, in particular, epoxy resin has been widely used as an insulation material owing to its excellent dielectric properties, high mechanical strength, and good erosion resistance [DAK-74]. They are used as coatings for conductors as well as in applications of bushings, cable terminations, instrument transformers, various post and support insulators, and parts for circuit breakers [DAK-72], [DAK-74].

Another important application of epoxy resins in HVDC transmission is in Gas Insulated Systems and in particular in Gas Insulated Lines (GILs), as solid insulation. A real GIL of Siemens is shown in Fig. 2.5.

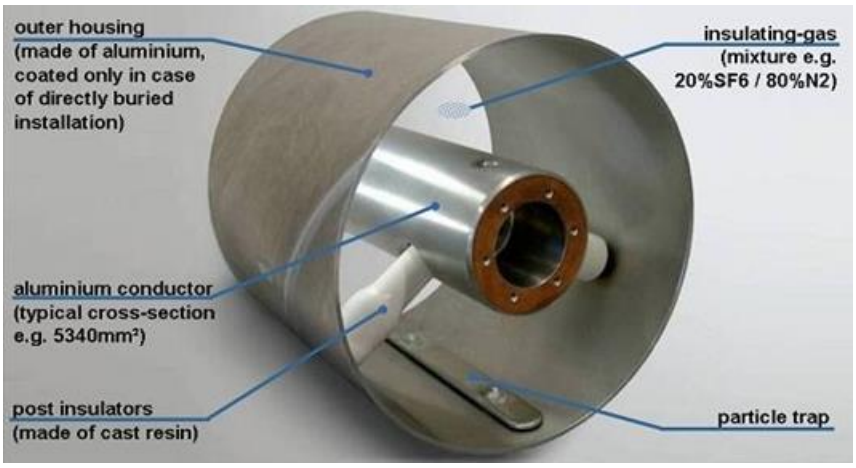

Fig. 2.5: Gas Insulated Line (GIL) of Siemens with all parts indicated, from Siemens

GILs are a good alternative for high power transmission, when the environmental or structural considerations rule out the use of overhead transmission lines. GILs consist of two concentric conductive tubes; the inner conductor is resting on cast resin insulators, which center it within the outer enclosure. To meet the environmental and technical aspects, GILs are filled with an insulating gas mixture of mainly nitrogen and a smaller percentage of SF_6 (sulphur hexafluoride) [SIE-12]. GILs can be laid aboveground, installed in tunnels or buried directly in the soil, depending on the individual requirements. The epoxy resin used as solid insulation in these applications has to withstand the electric field applied. Thus, it is important to be able to foresee the electric field distribution and volume conductivity of the material under specific field and temperature conditions.

Epoxy-based composites and applications

The use of either nano- or microfillers leads to the creation of nano- and microcomposite insulating materials respectively. Nano and micro fillers are used in polymeric dielectric materials for improving electrical and other properties, and their use in power engineering is steadily increasing. In addition, the use of inorganic fillers reduces the cost of components [DIS-92]. The most commonly used fillers are: silica oxide (SiO_2), alumina oxide (Al_2O_3), zinc oxide (ZnO), magnesium oxide (MgO), aluminum nitride (AlN), etc. The effect of fillers on the volume conductivity of epoxy resin specimens is investigated in many studies, like [AND-10], [MAC-01], etc. Some of these studies are presented analytically in chapter 4. The effect of the fillers depends strongly on their nature, concentration in the host material, shape, etc. In addition, the effect of pre-processing of the fillers is also investigated in studies like [MAI-08], [PAT-08]. In general, fillers tend to either increase or decrease the volume conductivity, depending on the above mentioned parameters and mostly the applied electric field.

One example of epoxy-based composites is the dry-type bushing, which is used in converter transformers of ultra HVDC transmission systems [NIN-13]. Another application of epoxy composites is in field grading. Field grading, or stress control, refers to the technique of reducing local enhancements of the electric field in various devices [KRE-95], [QI-04]. Resistive field grading in particular, is based on the use of materials with appropriate current-voltage characteristics. That means current-voltage characteristics that reveal a non-linear relation above a certain value of the electric field [CHR-10]. The fillers impart a strongly field dependent and non-linear conductivity to the host materials and could thus be used as the means for the creation of resistive field grading materials. Such materials can be used for the "absorption" of field enhancements during test conditions, overvoltages, etc.

The use of functional fillers is also promising for the development of GILs. An advantage of their use is indicated in [WIN-14]; according to this study, the aspired goals for the composite insulators are improved electric field distribution, reduction of maximum electric field stress (field grading), minimization of electric field inversion effects under the impact of non-uniform temperature distribution and fast decay of charges from the insulator surfaces.

2.2. Dielectric and electrical response of insulating materials

The response of an insulating material when exposed to a DC voltage is different of that to an AC voltage. The field distribution at AC is determined by the relative permittivity, or dielectric constant, ε_r of the material, which is not affected by temperature, or by field strength. At DC, a dielectric displacement field is developed because of the permittivity, which subsequently approaches a steady-state condition, determined by the conductivity κ of the material, which contrariwise depends strongly on temperature and electric field [KRE-95].

2.2.1. Switching on a DC voltage U

When switching on a DC voltage U, the dielectric is stressed as if it were an AC voltage. A capacitive current I_c flows through the dielectric and the field is a displacement field determined by the permittivity ε_r [KRE-95]. After hours, the current falls back to a small steady-state leakage current. The electric field is a steady-state conduction field, which is determined by the DC conductivity. The typical DC current response of insulation to a step voltage application is shown in the Fig. 2.6.

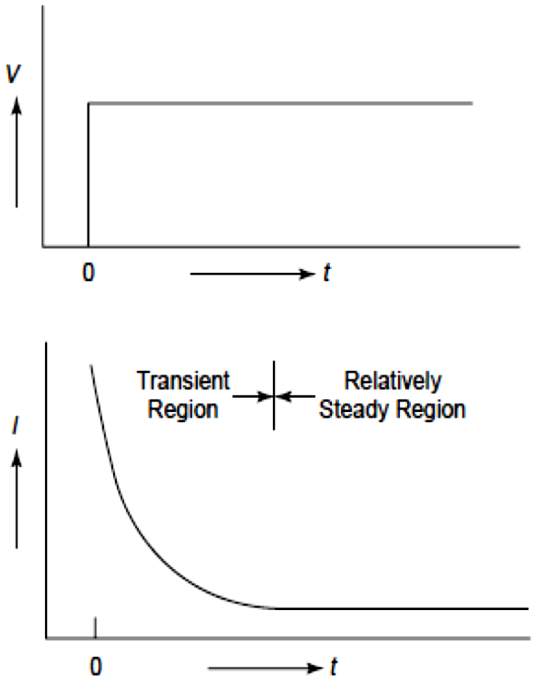

Fig. 2.6: Typical DC current response of insulation to a step voltage application, from [DAK-06]

The total time that the current needs to reach a steady-state (constant) value is called electrification time [PAT-08]. Experimental results have shown that, e.g. for the most common polymers used as electrical insulation (such as polyethylene, polypropylene, epoxy resin), the onset of steady state regime conditions may require hours [MON-11], or in extreme cases even weeks [KRE-95].

The total current after the application of the electric field can be given as follows [LUT-11]:

$$i(t) = K \cdot f(t) + I_{ss} \qquad \text{Eq. 2.1}$$

where K is a constant dependent on the electric field and temperature, $f(t)$ the dielectric response function of the material, and I_{ss} the current at the steady-state. When the applied voltage is removed, the discharge current is usually a mirror image of the charging one, but without the steady-state current [DAS-97]. Thus, the total discharge current is given by:

$$i(t) = K \cdot f(t) \qquad \text{Eq. 2.2}$$

2.2.2. Dielectric response function

Typical response functions are shown in Fig. 2.7:

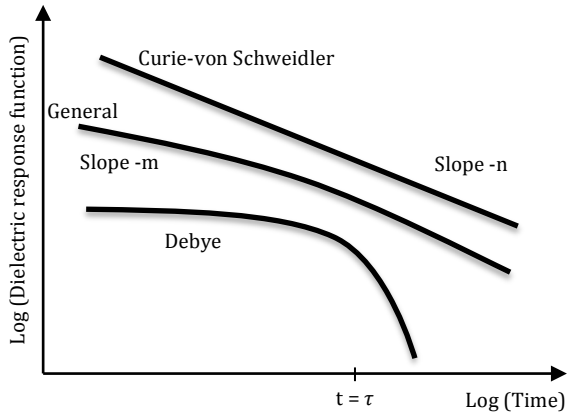

Fig. 2.7: Different types of dielectric response functions $f(t)$ in time domain, from [FAR-03]

Each material has its own and unique dielectric response function [JON-83]. The most common are the following:

- Debye function: $f(t) = \frac{\Delta\varepsilon}{\tau_D} e^{-t/\tau_D}$
- Curie-von Schweidler: $f(t) = A \cdot t^{-n}$
- General response function: $f(t) = \frac{A}{\left(\frac{t}{\tau}\right)^m + \left(\frac{t}{\tau}\right)^n}$

The Debye function is commonly found in polar liquids, while the Curie-von Schweidler has a universal character [JON-83] and is found to follow the dielectric response of many solid materials [FAR-03]. An example of the suitability of the Curie-von Schweidler function on filled and unfilled epoxy resins is indicated in the studies of [LOV-74], [GUI-06]. The parameter n is between 0 and 1 for most dielectrics [GUO-83]. The General response function represents a transition at $t = \tau$ between different processes (Fig. 2.7) and is also often found in dielectrics, with parameter values: $m > 1 > n > 0$ [CIGRE-01]. For $m = n$, the General response function gives the Curie-von Schweidler law.

2.3. Polarization mechanisms

The transient phenomenon taking place before the current stabilizes at its steady state value is called polarization current [KUE-10] or absorption current [KRE-95]. Every kind of dielectric consists, at an atomic level, of negative and positive charges balancing each other on the microscopic and macroscopic scale. As soon as a dielectric is exposed to an electric field, the positive and negative charges become oriented and form different kind of dipoles. This phenomenon, referred in the bibliography as the electric polarization, can be thought of as charge redistribution in a material caused by an external electric field [KAO-04].

During polarization, the relative displacement of the negative and positive charges of atoms and molecules, the orientation of existing dipoles toward the direction of the field, or the separation of mobile charge carriers at the interfaces of impurities or other defect boundaries take place [KAO-04]. Due to chemical interactions between dissimilar atoms forming molecules, permanent dipoles will be formed, which are usually randomly oriented and distributed within the material, as long as no external field is applied [ZAE-03].

A dielectric material is made up of atoms or molecules that possess one or more of five major types of electric polarization, also shown in Fig. 2.8, from [KAO-04], [DAK-06]:

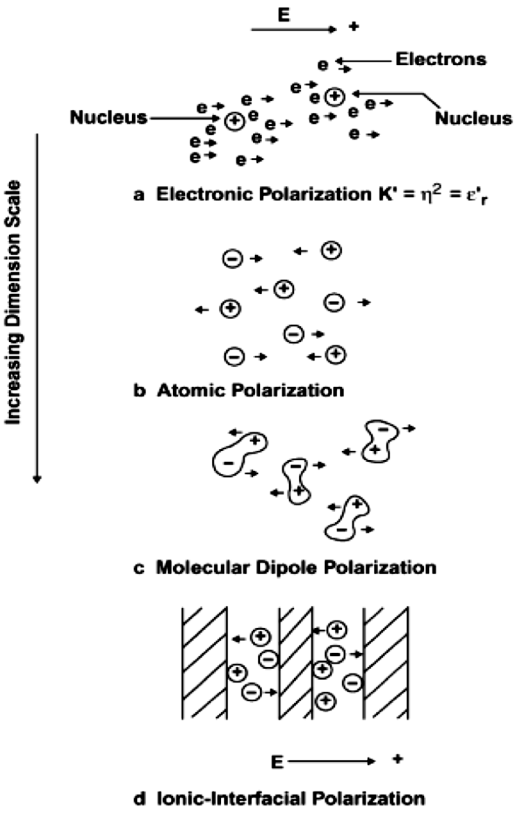

Fig. 2.8: Principle types of Polarization, from [DAK-06]

- Electronic or optical (a_e): the electric field causes deformation or translation of the originally symmetrical distribution of the electron clouds of atoms or molecules.
- Atomic or ionic (a_i): the electric field causes the atoms or ions of a polymeric molecule to be displaced relative to each other.
- Orientational or molecular dipole (a_0): occurs only in materials consisting of molecules or particles with a permanent dipole moment. The electric field causes the reorientation of the dipoles toward the direction of the field.
- Interfacial or space charge (a_d): occurs when carrier injection is important. For materials consisting of a high field concentration of charge carriers polarization due to the migration of charge carriers to form space charges at interfaces or grain boundaries becomes important.

The total polarizability of a material a comprises four components:

$$a = a_\mathrm{e} + a_\mathrm{i} + a_0 + a_\mathrm{d} \qquad \text{Eq.2. 3}$$

Each type of polarization requires time to perform. In addition, some polarization mechanisms are slow and some are fast. This is why the degree of the overall polarization depends on the time variation of the electric field. After the polarization processes are finished, a steady-state current called conduction current passes through the material. It is important to note that the time needed for the current to reach the steady-state value (i.e. the electrification time) varies with temperature, as polarization is a temperature

dependent phenomenon. Lower temperatures require higher electrification times [PAT-08].

2.4. DC Conductivity

Electrical conduction may occur through the movement of electrons, holes, or ions. In each case, a suitable starting point for discussion of the conduction processes is the basic equation [LUT-11]:

$$\kappa = \sum_{\mathrm{i}} q_{\mathrm{i}}\mu_{\mathrm{i}}e \; = \; n_{\mathrm{e}}\mu_e e + \; n_{\mathrm{h}}\mu_{\mathrm{h}}e + n_{\mathrm{I}}\mu_{\mathrm{I}}\,(Z_{\mathrm{w}}e) \qquad \text{Eq. 2.4}$$

where the conductivity κ consists of the conductivity of electrons (e), holes (h) and ions (I), and is resolved into three factors: the charge e, concentration n_i and mobility μ_{i} of the carriers. The valence of the ions is Z_{w}. The mobility (μ) characterizes the ease with which the charged species will move under the influence of the applied electric field E and is usually expressed as a velocity per unit field ($m^2V^{-1}s^{-1}$). The mobility is the drift velocity of the carriers, $\langle v \rangle$ per unit field, where $\langle v \rangle$ is defined as the average carrier velocity. In the absence of an electric field, carriers are as likely to be travelling in any one direction as any other and v averages to zero. In the presence of a field there will be a mean carrier velocity, either in the direction of the field or in the opposite direction, depending on whether the carrier has positive or negative charge on it, respectively [BLY-05]. Mobility is given as a function of:

$$\mu = \mu(\mathrm{V}, \mathrm{T}, \mathrm{A}, \mathrm{X}) \qquad \text{Eq.2.5}$$

Where V is the voltage, T is temperature, A is the ambient condition, and X indicates direction. The concentration of the carriers is thereafter dependent on the voltage, the temperature and the ambient condition [DAS-97]. Thus, theories of conduction aim to explain how n and μ are determined by molecular structure and how they depend on such factors as temperature and electric field [BLY-05].

The conductivity is divided into two categories: the volume conductivity and the surface conductivity. The volume conductivity is defined as the electrical conductivity through a cube of insulating material, while the surface conductivity is defined as the electrical resistance of the surface of an insulating material [Keithley-01]. In this thesis only the first one will be dealt with.

Volume conductivity of materials is measured in Siemens per meter (S/m) and is a property which spans in a very wide range, as may be judged from Fig. 2.9. Volume conductivity is dependent on the following factors [LUT-11]:

- Electric Field
- Temperature
- Electrification time
- Relative Humidity of the material
- Relative Humidity of the environment
- Electrode material
- Material thickness

- Chemical and morphological structure (e.g. fillers: nature, size and shape)
- Environmental factors such as pollution, sea salt etc.

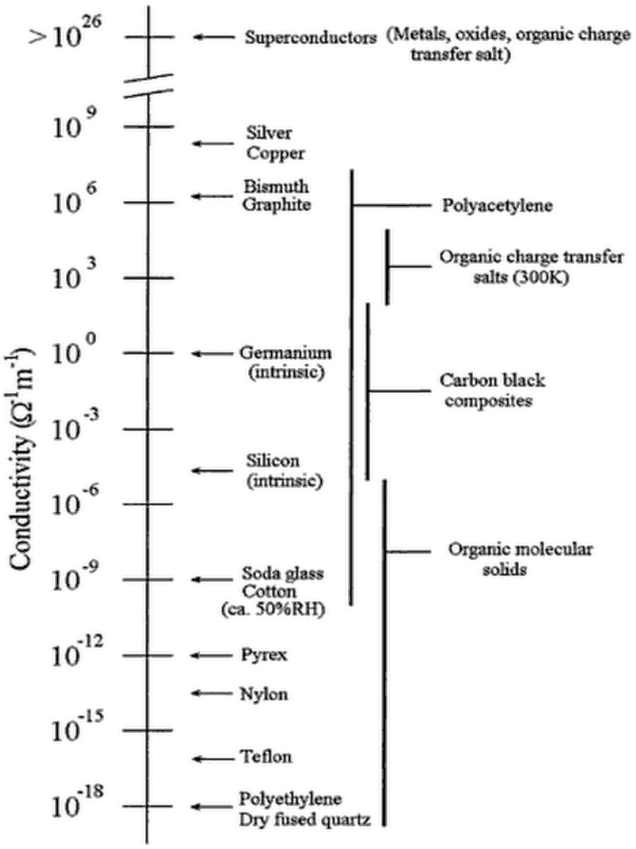

Fig. 2.9: Chart of typical volume conductivities, showing the wide range depending on the material, from [BLY-05]

In order to measure the volume conductivity of a material, conduction current measurements are performed.

2.5. Conduction current measurements according to VDE 0303-30

The conduction current measurements are performed according to the method of test for insulating materials for technical purposes VDE 0303-30 (international norm: IEC 93). The specimens used in this thesis are flat plaques, and so the respective electrode setup will be presented here. The volume conductivity is measured by applying a voltage potential (5) across opposite sides of the insulator sample and measuring the resultant current through the sample. The measurement technique is shown in Fig. 2.10 (a) and the geometry of the electrodes in Fig. 2.10 (b). The sample is placed between two main electrodes: the top electrode (1) and center electrode (2). The center electrode is connected in series with an electrometer (4) that measures the value of the current flowing through the bulk of the material. For the measurement of the volume conductivity, it is necessary to avoid the currents flowing from one electrode to the other via surface path. This is accomplished by means of the ring electrode (3), which is so placed with reference to the center electrode in a distance g, that any surface leakage current is collected and led to the ground and not the measuring instrument.

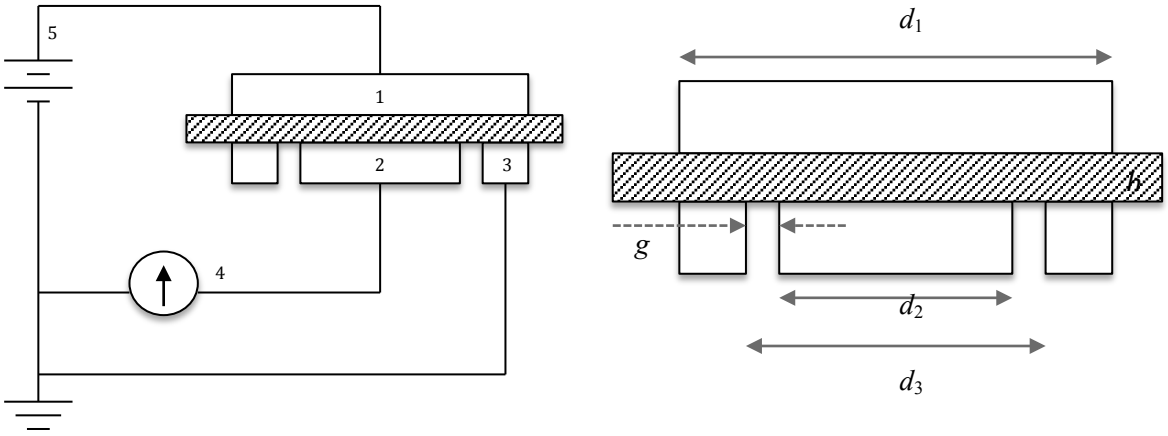

(a) (b)

Fig. 2.10 (a) Test arrangement for the measurement of volume conductivity, showing the top electrode (1), the center electrode (2), and the ring electrode (3), from [VDE-93]
(b) Electrode arrangement for the measurement of volume conductivity, from [VDE-93]

The typical response of the insulating material was shown analytically in paragraph 2.2. Let $i(t)$ be the detected current, V_{applied} the applied voltage and I_{ss} the final conduction current. According to the norm VDE 0303-30, the volume conductivity κ is calculated as follows:

$$\kappa = \frac{J}{E} = \frac{I/A}{V/h} = \frac{h}{R_{\text{x}} \cdot A} \qquad \text{Eq. 2.6}$$

where κ is the volume conductivity in S/m, h is the thickness of the specimen in m, $R_{\text{x}} = V_{\text{applied}} / I_{\text{ss}}$ is the resistivity in Ω and A is the effective area of the measuring electrode in m² given by:

$$A = \frac{\pi (d_1+g)^2}{4} \qquad \text{Eq. 2.7}$$

where d_1, g are in m. The value of the calculated conductivity is accurate by $\pm$ 10% for resistivities lower than 10^{10} Ω and $\pm$ 20% for higher resistivities. However, the accuracy also depends strongly on the measuring instrument.

Before the application of voltage, the specimen is short-circuited until the value of the current is very low. If the short-circuit current I_0 before the application of the voltage is not negligible compared to the steady-state current after the polarization, then it has to be taken into account in the calculation of the resistance:

$$R_{\text{x}} = V_{\text{applied}} / (I_{\text{ss}} \pm I_0) \qquad \text{Eq. 2.8}$$

The minus-sign is used when the sign of the short-circuit current has the same direction with the conduction current. Otherwise, the plus-sign is used.

2.6. Temperature dependence of the conductivity

In the framework of this Thesis, only the dependence of the conductivity on Electric field and temperature is investigated. Through the years, many studies have investigated DC volume conductivity and its dependence on electric field and temperature. The most often used materials in these studies were polyethylene type (XLPE, LDPE or HDPE) and epoxy-resin. Studies have also been made, in order to find empirical formulas for the DC conductivity as a function of electrical field and temperature. Here we will focus on the dependence of the ionic conductivity on temperature and the models that have been built to describe it.

The presence of ions in insulating polymers is inevitable, and in addition, the mobility of ions increases with the increase of temperature [SEA-82]. This leads to an increased ionic conductivity that often exhibits an exponential dependence on the temperature. There are two empirical equations developed in order to describe this relation; the Arrhenius and the Vogel-Tammann-Fulcher Equation:

i. Arrhenius Equation:

$$\kappa = \kappa_0 \, exp\{-\frac{E_a}{k_B T}\} \qquad \text{Eq. 2.9}$$

where κ_0 is a pre-exponential factor proportional to the number of charge carriers, k_B is the Boltzmann constant in eV K^{-1}, T is the absolute temperature in K, and E_a is the activation energy. The activation energy is a measure of the dependence of the volume conductivity on the temperature variation. The higher the activation energy, the bigger the variation of the volume conductivity with temperature [FAS-05], [LUT-11]. At temperatures below the glass transition temperature T_g, the conductivity obeys generally an Arrhenius-type law.

ii. Vogel-Tammann-Fulcher (VTF) Equation:

$$\kappa = A \, exp\{-\frac{B}{k_B(T-T_0)}\} \qquad \text{Eq. 2.10}$$

where A is a pre-exponential factor, B a pseudo-activation energy related to the segmental motions of the polymer, and T_0 is called equilibrium glass transition temperature and is usually 30-50 degrees below the glass transition temperature T_g [KNA-08]. Above T_g the conductivity usually follows the VTF equation. The VTH equation is not so common as the Arrhenius, but it is however sometimes more suitable (e.g. in the study of [NIN-13] on pure epoxy resin).

3. Charge generation and transport in polymers

Due to the underlying physical complexity of polymeric insulating materials, the charge generation and transportation processes in these materials are still not fully understood [KAO-04], [TEY-05]. The conduction currents in insulating polymers under DC fields may be electronic or ionic or both and it may be difficult to determine their origins unambiguously [DAS-97]. Furthermore, factors like temperature, electric field, thickness, electrode material, fillers etc. are determinant for the conduction processes taking place every time, while the generation of space charge makes it even more complex to determine its conductivity. In this chapter, the significant influence of the space charge accumulation is explained and conduction theories developed through the years are indicated.

3.1. Space charge accumulation

Another difference between AC and DC voltage, which is also a reason for the degradation of polymer insulation under high DC stresses [CHO-08], is that at DC the space charge plays an important role, as it has time to be formed. Consequently, the space charge distorts the electric field distribution and makes the determination of the DC conductivity much more complex [BAER-10].

Space charge is a surplus of electric charges distributed over a region of space rather than a distinct point. Space charges are present when the rate of charge accumulation differs from the rate of extraction. Charges may be attributed to electrons, holes, or ions depending on the mechanism of charge transfer. Space charge accumulation occurs only when the total current density J through a region of space is divergent. A divergence in the total current density means that the flow of charged particles into a region of space is not equal to the flow of charged particles coming out of that region. This difference between incoming and outgoing charge leads to the space charge buildup inside that region [DIS-92].

A divergence in the current density J can be found in the following locations and conditions [KRE-95]:

- Electrode-Insulation interface
- Insulation-Insulation interface
- Case of temperature gradient
- Case of material inhomogeneity

3.1.1. Electrode-Insulation interface

The buildup of space charge at an electrode-insulation interface is defined by the difference of the current density ΔJ_{inj} between two charge flows: the flow $J_{\text{inj}}(E,T)$, which is defined by the charge injection and extraction process and the flow $J_{\text{trans}}(E,T)$ through the dielectric, which is defined by the conduction or transport process in the bulk material (Fig. 3.1).

This current density difference at the electrode-insulation material is represented by the equation:

$$J_{\text{inj}}(E,T) - J_{\text{trans}}(E,T) = \Delta J_{\text{inj}}(E,T) \qquad \text{Eq. 3.1}$$

The relation between injected and transmitted current determines the space charge that will accumulate in the insulation, as well as its polarity compared to the adjacent electrode.

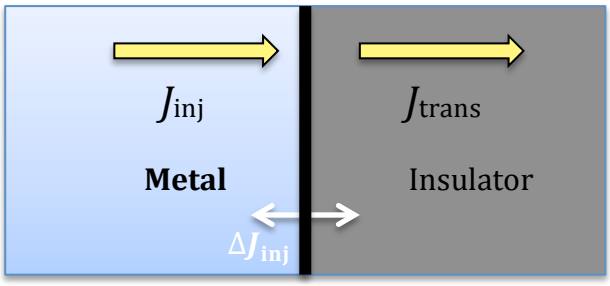

Fig. 3.1: Space charge accumulation at the metal-insulator interface, when the injected and transmitted currents differ.

The terms homo-charge and hetero-charge refer to the polarity of space charge compared to the polarity of the adjacent electrode (Fig. 3.2). When the polarity of the space charge is the same with the polarity of the adjacent electrode, we have the so called homo-charge. On the other hand, when the polarity of the space charge is opposite to the polarity of the adjacent electrode, we have the so called hetero-charge. Homo-charge results in an enhanced electrical field in the material bulk, while the field at the interface between the material and the electrode drops. In contrast to this, hetero-charge enhances the electrical field at the electrode-insulation interface, while the field in the material bulk drops [DIS-92].

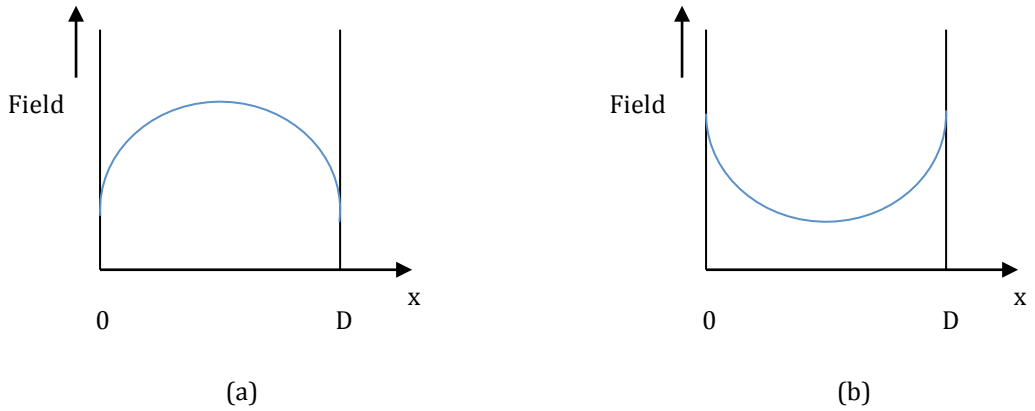

Fig. 3.2: Field distribution in an insulator containing space charge regions extending from the electrodes at x = 0 and x = D.
(a) In the homocharge region the field is reduced and the injection is supressed
(b) in a heterocharge region the electrode field increases, from [DIS-92]

Now, going back to Eq. 3.1, three different situations can occur at the interface:

- $J_{\text{inj}}(E,T) = J_{\text{trans}}(E,T)$: In this case we have an Ohmic interface and there is no space charge accumulation. In other words, the amount of charges injected/extracted from the electrodes is just enough to replace the charges that are removed from/towards the interface by transport.

- $J_{\text{inj}}(E,T) < J_{\text{trans}}(E,T)$: In this case the electrode interface cannot convey the charges as fast as the dielectric can conduct them. Thus, positive hetero-charge will build up in front of the cathode and negative hetero-charge in front of the anode. The hetero-charge increases the electric field in front of the electrode and hence the injection current, while reducing the bulk field and the transport current. Eventually a steady state situation is achieved when the two currents coincide.

- $J_{\text{inj}}(E,T) > J_{\text{trans}}(E,T)$: In this case the electrodes yield more charges than the dielectric can dissipate. Therefore, negative homo-charge builds up in front of the cathode and positive homo-charge in front of the anode. The homo-charge decreases the electric field in front of the electrode and hence the injection current, while increasing the bulk field and the transport current. Eventually a steady-state situation is achieved when the two currents coincide.

3.1.2. Insulation-Insulation interface

Maxwell-Wagner Effect or Maxwell-Wagner Capacitor

The Maxwell-Wagner effect is referring to the charge buildup occurring in dielectrics that are layered or inhomogeneous. In the following figure (Fig. 3.3) we can see two dielectrics with permittivity ε_1 and ε_2, and conductivity κ_1 and κ_2 respectively. The two dielectrics have thicknesses d_1 and d_2, and at t=0 a voltage U is applied [KRE-95].

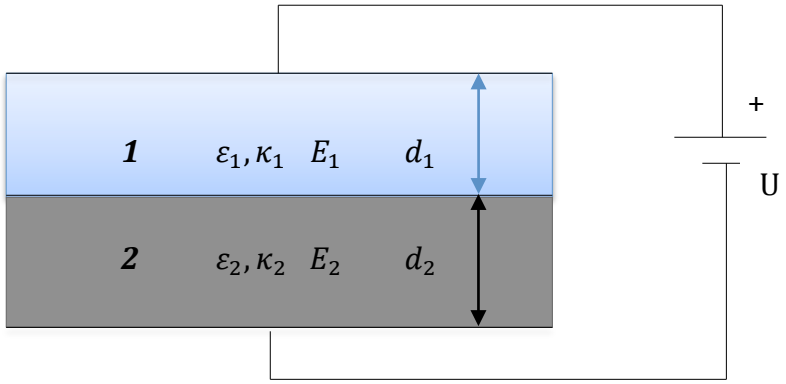

Fig. 3.3: Maxwell capacitor to describe the phenomena at the interface between dielectrics, from [KRE-95]

This two-layer capacitor (Fig. 3.3) is also referred in the bibliography as the Maxwell-Wagner capacitor [WAG-24].

From the continuity equation at the surface between them we have [KRE-95], [LUT-11]:

$$\kappa_1 E_1(t) + \frac{\partial \varepsilon_0 E_1(t)}{\partial t} + \frac{\partial P_1(t)}{\partial t} = \kappa_2 E_2(t) + \frac{\partial \varepsilon_0 E_2(t)}{\partial t} + \frac{\partial P_2(t)}{\partial t} \quad \text{Eq. 3.2}$$

By neglecting the slow polarization mechanisms:

$$\kappa_1 E_1(t) + \frac{\partial \varepsilon_0 E_1(t)}{\partial t} = \kappa_2 E_2(t) + \frac{\partial \varepsilon_0 E_2(t)}{\partial t} \quad \text{Eq. 3.3}$$

Further, for the applied voltage:

$$U = \int_0^{d_1+d_2} E(t)\, dy = \int_0^{d_1} E_1(t)\, dy + \int_{d_1}^{d_1+d_2} E_2(t)\, dy = E_1(t) \cdot d_1 + E_2(t) \cdot d_2 \quad \text{Eq.3.4}$$

By using the Eq. 3.3 and eliminating the term $E_2(t)$, the solution of the differential Eq. 3.3 is given by Eq. 3.5:

$$E_1 = \frac{\kappa_2 U}{d_2\kappa_1 + \kappa_1\sigma_2}\left(1 - exp\left(\frac{-t}{\tau}\right)\right) + \frac{\varepsilon_2 U}{d_2\varepsilon_1 + d_1\varepsilon_2} exp\left(\frac{-t}{\tau}\right) \quad \text{Eq. 3.5}$$

where τ is the time constant and it is calculated according to the equation Eq. 3.6:

$$\tau = \frac{d_2\varepsilon_1 + d_1\varepsilon_2}{d_2\sigma_1 + d_1\sigma_2} \quad \text{Eq. 3.6}$$

The growth of the surface charge σ is finally calculated with the use of the Eq. 3.7:

$$\sigma = \frac{d_2\varepsilon_1 - d_1\varepsilon_2}{d_2\sigma_1 + d_1\sigma_2} U\left((1 - exp\left(\frac{-t}{\tau}\right)\right) \quad \text{Eq. 3.7}$$

As seen from the Eq. 3.7, the difference in permittivities and conductivities between the two materials leads to a discontinuity in the electric field at the interface. As a result, a difference in conduction current density occurs, which results in the formation of space charge at the interface.

3.1.3. Temperature gradient

As discussed in chapter 2, the electrical conductivity depends strongly on temperature, and thus, any temperature gradient in the material will cause a conductivity gradient. As a result, the permittivity to conductivity ratio $\frac{\varepsilon}{\kappa}$ varies as well, and space charge ρ is generated according to the equation [KRE-95]:

$$\rho = J \cdot \nabla(\frac{\varepsilon}{\kappa}) \qquad \text{Eq. 3.8}$$

3.1.4. Material inhomogeneity

The introduction of material inhomogeneity in polymers is inevitable. Inhomogeneity can occur either in the bulk of the insulator or at the insulator/electrode interface [DIS-92]. Typical inhomogeneities include [DIS-92]:

- Electrode aberrations penetrating the insulation or surface scratches, asperities and depressions;
- Regions of free volume in the polymer due to morphological irregularities with sizes typically less than $\sim 10\ nm$, small voids due to movement of additives etc., and larger voids generally due to imperfections in the manufacturing technique;
- Impurities in the insulation, including impurity particles, moisture and sites of imperfect mixing and coagulation of fillers.

The inhomogeneity of materials is a factor that becomes more intensive regarding new materials, where chemical or physical doping (by micro- and nano-fillers, like in the case epoxy resins, as explained in chapter 2) are present, and can introduce great inhomogeneity into the material. Fillers, for example, which have a different conductivity and permittivity than the host material result in a large amount of boundaries in the material. Space charge will accumulate at those boundaries [TEY-05].

3.2. Why is space charge related to the conductivity?

One would wonder why the study of DC conductivity is connected with the space charge accumulation. At low electric fields the voltage-current relation tends to follow Ohm's law [DIS-92]. The steady-state current-field characteristic is linear expressed in mathematics with the relation:

$$\vec{J} = \kappa \vec{E} \qquad \text{Eq. 3.9}$$

where $\vec{J}$ and $\vec{E}$ are the current density and electric field in the insulation respectively and κ is the electrical conductivity at the steady-state region and is constant.

However, at high fields, a space charge formation is indicated, which distorts the field distribution and the conductivity of the material. This space charge builds a Poisson electric field and the voltage-current relation is not Ohmic anymore, but it obeys a power law [CHR-10].

The Poisson field can be expressed as:

$$\nabla \cdot \vec{D} = \rho \qquad \text{Eq. 3.10}$$

where ρ is the distribution of space charge.

The addition of expressions Eq. 3.9 and Eq. 3.10 reflects the characteristics of the DC insulation material, so that it is necessary to consider Ohmic conductivity and space charge in the calculation of the electric field [BOG-01]. As mentioned in chapter 2, the conductivity is strongly dependent on the electric field. Thus, a non-Omhic behavior is also influencing the DC conductivity.

In total, the formation of space charge influences the way carriers are transported through the material and so it is taken into consideration when studying the transport mechanisms in polymers and, consequently, the DC conductivity

3.3. The Band Theory applied in polymers

Electronic conduction in polymers differs in several important ways from the more familiar kind in metals and semiconductors. That is not to say that they are separate subjects and, indeed, the well-known band theory of atomic lattices has provided the essential basis of concepts and language for the discussion of conduction in polymers [BLY-05]. In order to understand trapping and microscopic space charge physics in polymer insulating materials one should be aware of the band theory. Although the idealized band theory is not applicable to an insulating polymer, it can be useful in giving a background for describing and understanding the insulating properties of polymers.

The "idealized" Band Theory

All solids can be classified into three categories: conductors, semiconductors and insulators, according to the availability of conduction electrons in their structures. The band theory gives an explanation for the differences in electrical properties of these materials and accounts for the availability, or not, of those conduction electrons.

Although individual atoms have certain permitted energy levels for their electrons, as defined by quantum theory, when large groups of atoms are incorporated into a solid mass these energy levels become reorganized in such a way to form bands of possible energy levels. As the number of electrons in a solid mass increases, the discrete energy levels become essentially continuous and form permitted energy level bands (see example with polyethylene in Fig. 3.5). The two uppermost bands are considered and are known as valence band and conduction band. Electrons fill the valence band from the lowest to the highest energy level. The top of the valence band for a material is the highest level, which would theoretically be filled by all the available electrons within an atom at T = 0 K [KAS-01]. Whether a material is a metal, a semiconductor or an insulator will depend on the band structure and the filling of the energy states within the bands. In insulators and semiconductors the valence band is completely filled with electrons, and the conduction band is empty. Concerning the conduction band, in insulators the electrons in the valence band are separated by a large gap band (forbidden gap) from the conduction band, in conductors like metals the valence band overlaps the conduction band, and in

semiconductors there is a small enough gap between the valence and the conduction band that thermal or other excitations can bridge (Fig. 3.4).

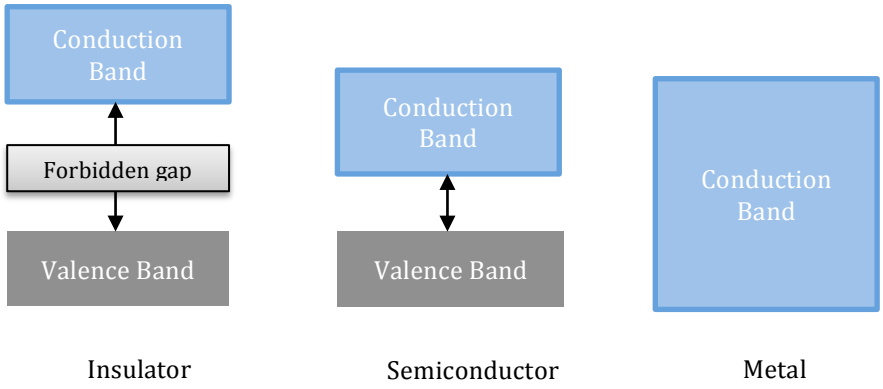

Fig. 3.4: Conduction and valence bands for insulators, semiconductors and conductors. Note the energy gaps in insulators and semiconductors, and how in a conductor there is no gap, while the conduction and valence bands are overlapped, from [KAS-01]

The building of the band structure of polyethylene was analyzed by [TEY-05] and is shown in Fig. 3.5. Going from methane to polyethylene leads to a correspondingly separation between the orbital electrons and finally to the formation of discrete energy bands. From this diagram, it can be seen that polyethylene is a large band gap material, which means that there are no accessible energy levels for the charges between the top of the valence band and the bottom of the conduction band [TEY-05]. The value of the forbidden band as derived from calculation or an experimental measurement is of the order of 8.8 eV [LES-73] meaning that we have a perfect insulator which would have an intrinsic conductivity of $10^{-45}\,\frac{\mathrm{S}}{\mathrm{m}}$ [COE-93].

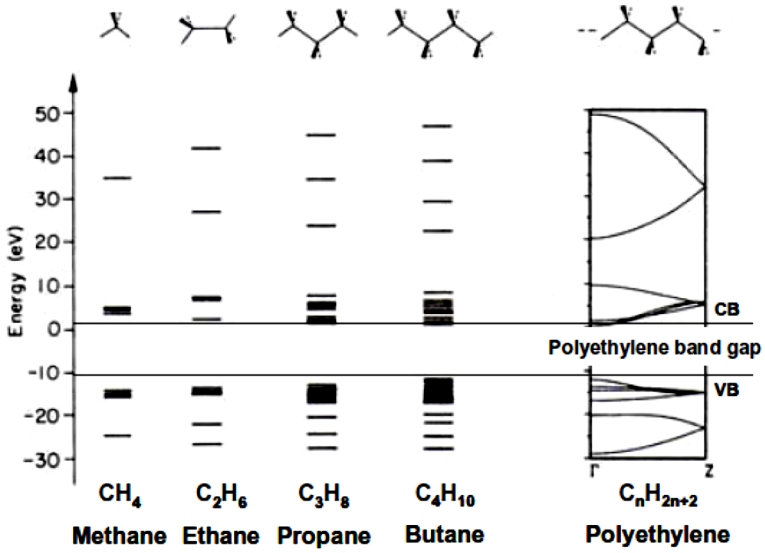

Fig. 3.5: Distribution of orbital levels going from methane to polyethylene. CB and VB stand for conduction and valence bands respectively, from [HOF-91]

However, such a conductivity value has never been measured, as the reality is much more complex. Although the "idealized" band theory is a good starting point for the investigation of the conduction processes, the microscopic structure of polymers is much more different. The main statement, which explains the true value of the conductivity in polyethylene and polymers, is the existence of trapping sites in these materials, which will be analyzed in the next paragraph.

3.4. Trapping in polymers

Trapping is the fastening of charges at a fixed location in the material and is closely related to the existence of either chemical or physical defects [TEY-05]. As mentioned in paragraph 3.1, polymers have complex structure, which contains defects. These structural defects are responsible for the existence of intrinsic charge sources and hence, the measured conductivity of those materials is much higher than the one derived from the "idealized" band theory (Fig. 3.6).

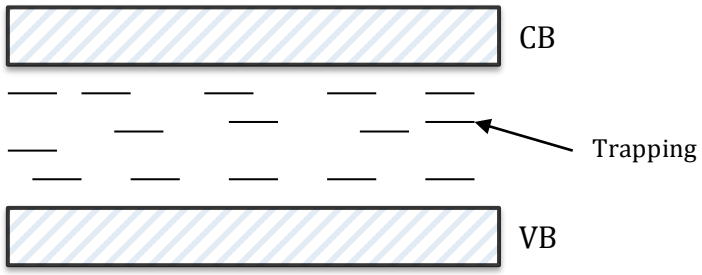

Fig. 3.6: Representation of accessible localized states, i.e. traps, within the forbidden gap of a disordered dielectric material, from [KAH-89]

A charge carrier that is trapped in a potential well can leave the trap when a sufficient amount of thermal energy is acquired. The amount of energy needed to escape from a certain trap is called the trap depth. The amount of time a charge carrier resides in a charge trap is determined by the trap depth: the deeper the trap, the longer the time a carrier will spend inside the trap (the chance of acquiring enough thermal energy is smaller for deeper traps) [DIS-92].

The difference between physical and chemical defects is explained here [TEY-05]:

- Physical defects are referring to the different conformations of the molecules, like amorphous and crystalline regions, and chain conformation. This has consequences to the energy band diagram, introducing accessible, localized states for carriers in the forbidden gap. These states are usually shallow traps (Fig.3.7) and assist charge transport. Two reasons can be given for this. Either the localized states are in thermal equilibrium with extended states of conduction and/or valence band: transport can occur by thermal activation of carriers to a band, leading to the concept of conduction through multiple trapping/detrapping steps. The term "shallow trap" comes from this point of view, because charges move from trap to trap, experiencing each time a transition to the extended states of the band. The second situation makes reference to a large density of localized states in interaction

(meaning that the wave functions of the traps overlap). In this situation, carriers can tunnel from one level to another one without undergoing a transition to the extended state. This is referred to as the phonon-assisted tunneling (also quoted as the "hopping" mechanism and will be dealt with analytically later).

- Chemical defects are referring to the presence of one or several atoms that are not part of the repeated unit that constitutes the backbone of the molecular chain like branching, in-chain defects, residues, additives, by-products etc. Chemical disorder introduces also physical disorder in its surroundings due to the difference in size and position of the foreign atoms as regards the atoms constituting the polymer itself. Because the electronic properties of the foreign atom can be different, it can introduce additional energy levels in the forbidden gap, generally at a deeper level. The chemical disorder is thought to control the space charge and these energy levels are often named "deep traps" or "real traps" (Fig. 3.7).

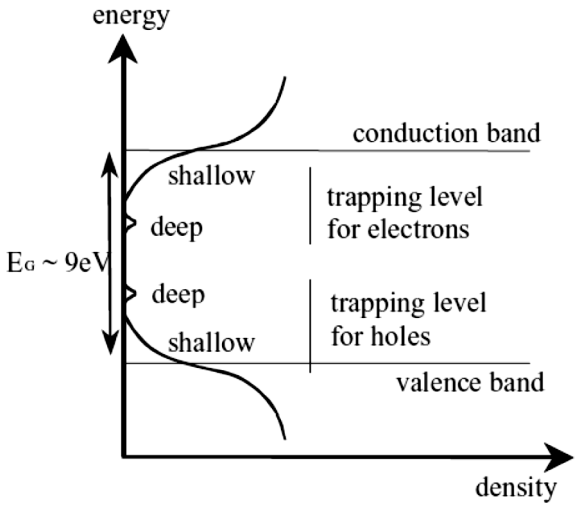

Fig. 3.7: Representation of shallow and deep traps for electrons and holes in a disordered dielectric material (Polyethylene), from [TEY-05]

The density of deep traps is much lower than the density of shallow traps. Furthermore, the contribution of the deep traps to the conduction process is low, as opposed to shallow traps that assist the conduction [MAZ-13], [BLY-05].

Another distinction of traps is associated with the type of carriers they accept. Traps for electrons are called acceptors and traps for holes are called donors. Electrons or holes travelling from the valence band to the conduction band may get trapped in such an energy state [TEY-05].

Another type of trap called self-trap is also present in polymers. The electric field of an electron can locally change the structure of the polymer molecular chain creating a local drop in the potential (potential well). The electron thus traps itself. Self-traps are usually deep. Hence, charge remains in such traps for many hours or even days [KRE-95].

3.5. Charge generation and Injection at the electrodes

A release of carriers in the material is possible from two different sources [CHR-98]:

- Carriers can be generated intrinsically via a bulk instability
- Carriers can enter due to injection at the electrodes

So, neglecting charge generation due to discharges in the environment of the insulation, as well as any other irradiation source (photo-generation, X-rays, electron irradiation, etc.) [TEY-05], we consider here the charge injection and in the next paragraph the transport mechanisms that have been developed until now.

As discussed in paragraph 3.1, the nature of the electrode-insulation interface is complex. That is because of the presence of physical, chemical and electrical defects such as: surface roughness, imperfect contact, chemical impurities, donor-acceptor states, trap states etc. [DIS-92]. The two electron-injection mechanisms described here are the Schottky effect and the Fowler-Nordheim injection. Both are based on the very simple electron energy diagram of the metal-insulator contact shown in Fig. 3.8.

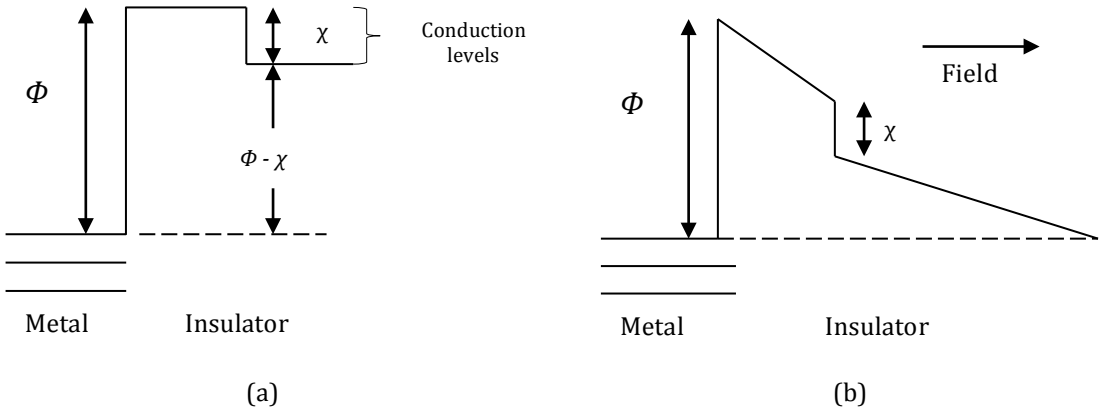

Fig. 3.8: Insulator in contact with a metal:
(a) In the absence of a field
(b) With applied field, from [MOT-40]

In Fig. 3.8, Φ stands for the work function of the metal and is defined as the minimum energy that has to be expended to remove an electron from the metal to the vacuum. So, in Fig. 3.8, electrons must overcome a potential barrier to leave the metal and enter the insulation. The height of the barrier depends on the interface. The theories were initially developed for electron injection from a metal into a vacuum in which case the barrier height was equal to the work function of the metal, Φ. In the case of metal-polymer interface however, this barrier height and shape is modified by the local conditions obtaining. In an ideal case the electrons would have to be excited into a conduction band in the polymer, in which case the barrier height would be decreased by the electron affinity of the polymer [DIS-92]. The electron affinity χ is the energy required to bring an electron from the vacuum to the conduction band [TEY-05].

3.5.1. Schottky model approach: contact emission phenomenon

The Schottky effect (or field assisted thermionic injection) occurs when the presence of an electric field modifies the emission current by lowering the potential barrier for thermionic emission [RAJ-03]. In this case, the electrons are injected from an electrode into the conduction band of the insulation material [DIS-92], [CAS-11].

The current density emitted due to the Schottky effect is expressed by [LEN-66]:

$$J_s = AT^2\, exp\left[-\frac{\Phi_0 - \beta_s E_c^{\frac{1}{2}}}{kT}\right] \qquad \text{Eq.3.10}$$

where:

- A is the Richardson-Dushman (in $\frac{\mathrm{A}}{\mathrm{m^2 K}}$) constant for thermionic emission given by:

$$A = \frac{4\pi e m k^2}{h^3} \qquad \text{Eq. 3.11}$$

  where m and e are the mass (in kg) and charge (in C) of an electron respectively, k is the Boltzmann constant (in J/K), and h is Planck's constant (in J · s)).

- β_s is the Schottky constant (in C · m) and is given by:

$$\beta_s = \left[\frac{q^3}{4\pi\varepsilon_0\varepsilon_\infty}\right]^{\frac{1}{2}} \qquad \text{Eq. 3.12}$$

  where:

  - ε_0: the permittivity of free space ($\varepsilon_0 \cong 8.854$ F/m)
  - ε_∞: the relative permittivity at high frequencies
  - q: the electronic charge (in C)

- Φ_0 is the height of the potential barrier at the metal-dielectric interface without any applied field, or, more precisely, the difference in energy between the Fermi energy in the cathode metal and the potential energy of a conduction electron in the polymer.

- E_c corresponds to the electrical state at the contact

For a plane-parallel electrode system, an ideal insulator would lead to a homogeneous field distribution of the magnitude V/d where V is the applied voltage and d is the thickness of the specimen. However, the accumulation of space charge leads to a different field value near the electrodes and this effect has to be taken into account by a multiplying factor [LEN-66].

For this reason, a dimensionless constant γ is used as follows:

$$E_c = \gamma \frac{V}{d} \qquad \text{Eq. 3.14}$$

In most experiments γ turns out to be greater than 1, showing a concentration of the field at the injecting electrode [LEN-66]. In the study of [CAS-11] it is indicated that $\gamma < 1$ stands for a contact with dominant homo-charge and $\gamma > 1$ for a contact with dominant hetero-charge. The Schottky equation (Eq. 3.10) after the field distortion correction becomes:

$$J_s = AT^2 \, exp\left[-\frac{\varphi - \beta_s\left(\gamma\frac{V}{d}\right)^{\frac{1}{2}}}{kT}\right] \qquad \text{Eq. 3.15}$$

According to equation Eq. 3.15, a plot of ln (J) versus $E_c^{1/2}$ gives a straight line, although at low fields space charges and surface inhomogeneities tend to cause deviations [DIS-92]. The intercept is the pre-exponential and the slope is the term in brackets [RAJ-03]. The value of the γ parameter near the injection-electrode can be calculated from the slope of this curve [CAS-11], [KRI-12] and is given using the equation:

$$\gamma = \frac{(slope \times kT)^2 4\pi\varepsilon_0\varepsilon_r}{q^3} \qquad \text{Eq. 3.16}$$

Although the Schottky emission theory is considered an important mechanism in describing conduction in insulators, the range of it is estimated to lie between 1 and 100 kV/mm [MOR-60]. For field strengths above that value field emission based on the Fowler-Nordheim effect is more appropriate.

3.5.2. Fowler-Nordheim injection

Field emission (or the quantum-mechanical tunneling) of electrons from a metal surface into a vacuum under the influence of a strong electric field, was first explained by Fowler and Nordheim (1928). The Fowler–Nordheim injection is valid for "high" fields, above ~100kV/mm. In this case the barrier becomes very thin, less than 1nm at 1000kV/mm [DIS-92]. In classical mechanics a particle cannot enter a region in which its total energy is less than the potential required. However, particles that exhibit particle-wave duality such as electrons and photons have a finite probability of existing in such regions. It is found that electrons may pass through thin potential barriers despite having insufficient energy to surmount them; this is also known as tunneling. When this occurs at the contact barrier it is known as Fowler-Nordheim injection and the emission current is given by [DIS-92]:

$$J_{FN} = \frac{q^3E^2}{8\pi h\varphi} \, exp\left\{-\frac{4}{3}\left(\frac{2m^*}{\hbar^2}\right)^{\frac{1}{2}}\frac{\varphi^{3/2}}{qE}\right\} \qquad \text{Eq. 3.17}$$

where h is the Planck's constant ($4.1357 \cdot 10^{-15}$ eV· s), $\hbar = h/2\pi$, m* is the effective mass of the carriers (in Kg), and all the other parameters have the same meaning as previously.

The injection current density, according to equation Eq. 3.17, depends strongly on electric field E and there is no or small temperature T dependence. The Fowler-Nordheim equation relates the current density to the work function and electric field and the plot of ln (J/E^2) versus $1/E$ must give a straight line.

Depending on their nature, carriers can be extracted or not at the opposite electrodes. In case of ions, it is difficult to envisage mass transport through the electrodes. However, they can interact with carriers of opposite polarity being injected at the electrode, providing electrical neutralization. In case of electronic carriers, extraction can occur with or without barrier height [TEY-05].

3.6. Charge transport

A coherent categorization of the bulk conducting phenomena taking place in polymers is shown in Fig. 3.9 below.

.

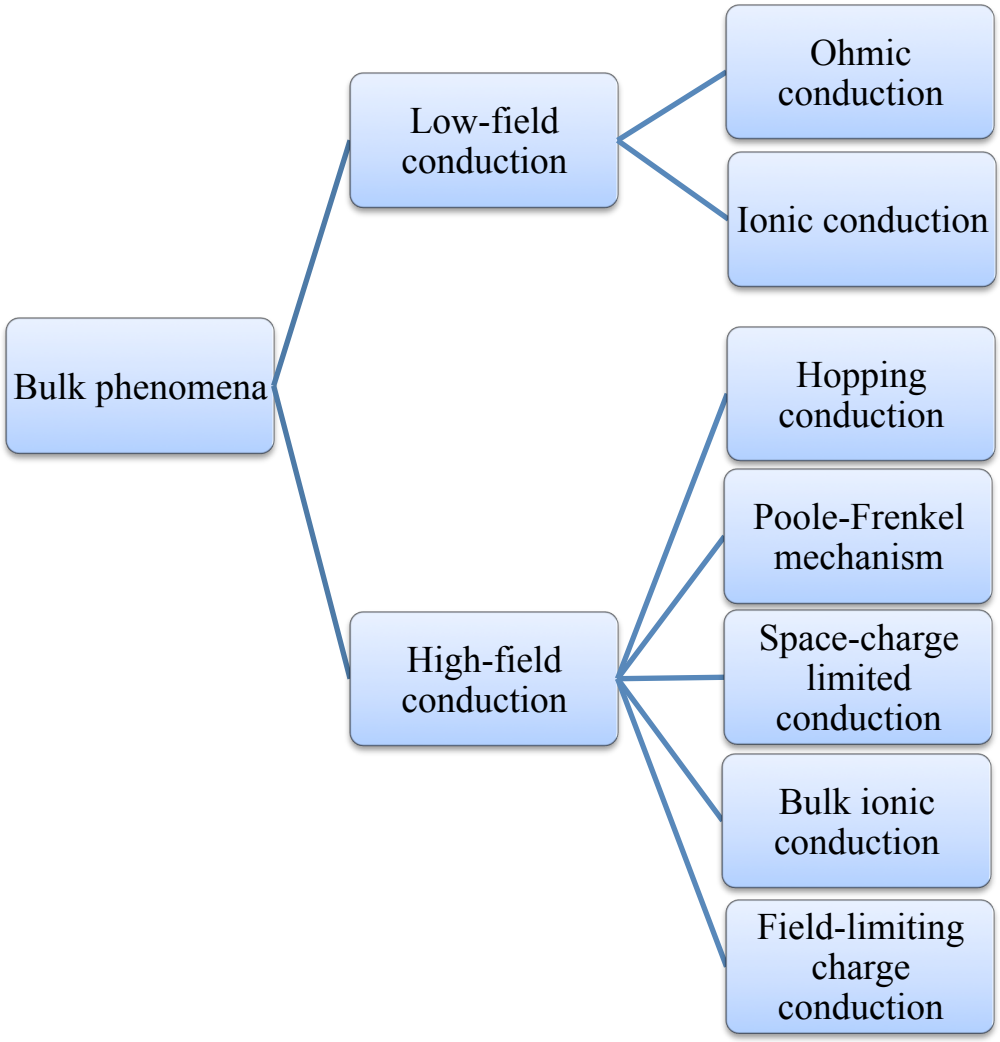

Fig. 3.9: Bulk phenomena categorized into low and high field conduction mechanisms

Charge transport processes depend primarily on the nature of carriers. The first classification is a distinction between low-field and high-field conduction mechanisms, both involving ionic and electronic processes. Within processes at higher fields, a second classification can be made referring to processes involving band transport (Poole-Frenkel mechanism) and those that do not (Hopping and Bulk ionic conduction). Diffusion is somewhat apart as it involves mass transport. Furthermore, the Space Charge Limited Current (SCLC) model combines Ohmic conduction, involving band mobility or trap-limited mobility, and local field distortion due to space charge accumulation. Additionally there is the field-limiting space charge (FLSC) model, which is in some ways analogous to the SCLC model at the trap-filled limit and takes into account the increase of the mobility with the electric field.

3.6.1. Low-field conduction bulk phenomena

(A) Ohmic conduction

At low electric fields the voltage-current characteristic tends to obey Ohm's Law. This is usually explained in terms of Ohmic conduction, in which the carriers, usually electrons or holes, acquire an average velocity proportional to the field. In this situation, as explained in chapter 2, the equation dominating the steady-state current density-electric field behavior is:

$$\vec{J} = \kappa \vec{E} \qquad \text{Eq. 3.18}$$

where the conductivity κ is independent of the applied field.

In Ohmic conduction, the representation of the steady-state current density with respect to applied electric field in log-log coordinates yields a slope of 1. Charge hopping motions between localized states can also lead to Ohmic conduction [DAS-97].

(B) *Ionic conduction*

Ionic conduction in a dielectric is the process in which electric current is carried by the motion of ions [DIS-92]. This could arise in two different manners:

- In an ionic crystal physical imperfections alone can be responsible for mechanisms of current flow;
- In a non-ionic substance chemical imperfection is required to supply the mobile species

In addition, a low concentration of ions may be present in a polymeric material, as a result of chemical reactions involving sulfur in antioxidants, or organic ions resulting from oxidation of the material [GIL-92]. An alternative for the generation of ions is dissociation of impurities or absorbed water under the effect of the field [PAI-75]. Finally, ionic species can be generated at the metallic electrodes and from there can be injected to the bulk material [TAK-99], [HO-01].

Ionic conduction at low fields can also lead to an Ohmic relation between the current density and the field. For high fields, the bulk ionic conduction is discussed in the next

paragraph. Finally, ionic conduction is strongly dependent on the temperature, as discussed in Chapter 2, obeying either the Arrhenius or VTF equation.

3.6.2. High-field conduction bulk phenomena

(A) Hopping conduction

Hopping conduction makes charge transport possible in situations where band conduction no longer occurs. Hopping can simply occur from one trapping site to the other [RAJ-03]; just as carriers can be generated thermally by excitation of electrons across the band gap, from the valence band to acceptor states or from donors to the conduction band- so it is also possible to move charge between localizes states by thermal excitation. Such conduction requires the electrons to execute discrete jumps across an energy barrier and through space from one site to the next (see Fig. 3.10 below).

The concept of hopping transport has been familiar for a long time in connection with ionic conduction (i.e. bulk ionic conduction), since ions move essentially by hopping, whether through interstices or vacancies. This concept has been extended to electrons, particularly for electronic conduction in amorphous and disordered nonmetallic solids [KAO-04].

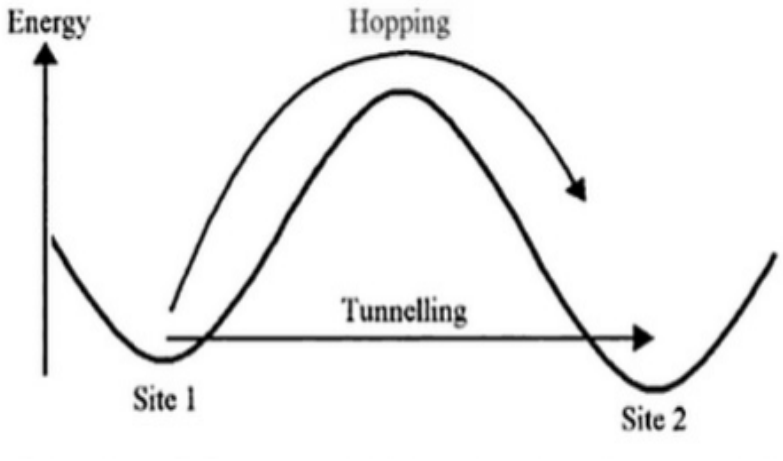

Fig. 3.10: Diagram electron-transfer mechanisms between adjacent
Sites separated by a potential-energy barrier, from [BLY-05]

An electron may either hop over or tunnel through the barrier, going from one site to the other, depending on the shape of the barrier, the separation of the sites and the availability of thermal energy. To hop between sites the electron must acquire sufficient thermal energy to surmount the barrier, while for tunneling the site separation must be small enough for the tail of the electron wave-function to extend through the barrier. A concerted process, in which the electron is thermally excited sufficiently far up the barrier that tunneling can occur, is also possible. This process becomes important for sites beyond nearest neighbors, since the probability of long distance hopping will be influenced by the spatial extent of the tails of the wave-functions [BLY-05].

In high quality crystals the density of defects will be too small for hopping to occur between defect sites on account of their large physical separation. However, if the defect levels lie close in energy to either the valence band or the conduction band then transitions to and from the band states are possible [BLY-05].

The conductivity in the case of hopping between localized states is given by Mott's law:

$$\kappa_{HOP} = \kappa_0 \cdot exp\left(-\frac{T_0}{T^{-n}}\right) \qquad \text{Eq. 3.19}$$

where T_0 is constant at sufficiently low temperature, κ_0 is a pre-exponential factor, and n=1/4. However, in less simplifies analyses, n, which expresses the temperature dependence of the hopping conductivity, lies between one half and one quarter ($1/4 \leq n \leq 1/2$) [BLY-05]. These values have been verified for various amorphous materials [DIS-92].

(B) Poole-Frenkel Mechanism

The Poole-Frenkel mechanism is the bulk analogue of the Schottky effect [DIS-92]. Both the Poole-Frenkel mechanism and the Schottky effect exhibit a current flow, which increases exponentially with the square root of the applied voltage for high electric fields [MAS-71].

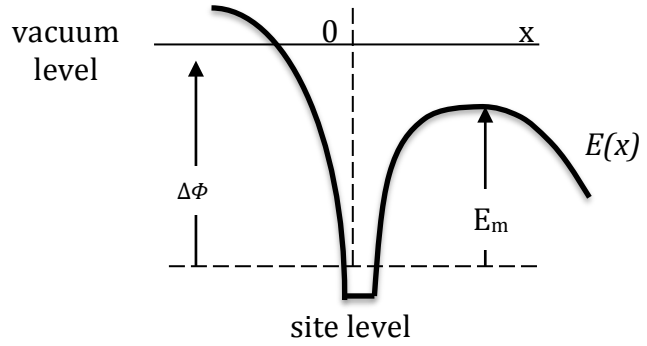

Fig. 3.11: Poole-Frenkel mechanism: The potential $\Delta\Phi$ of the site is assumed to be of Coulombic form. Under high electric field, the energy of the site is modified, lowering of the barrier in the drift direction, from [TEY-05]

The Poole-Frenkel mechanism occurs within the bulk of the dielectric where the Coulombic potential barrier can be lowered due to the influence of the high electric field (see Fig. 3.11 above). The potential $\Delta\Phi$ of the site is assumed to be of Coulombic form. In the presence of high electric field, the energy of the site is modified, lowering the barrier in the direction of the field.

For the mechanism to occur, the polymer must have a wide band gap and must have donors or acceptors. For the sake of simplicity we assume that the insulator has only donors, as the treatment is similar in both cases. Additionally, we further assume that there are no thermally generated carriers in the conduction band and the only carriers that are present are those that have moved from donor states due to high electric field [DIS-92], [RAJ-03].

Let:

- N_{D} = the number of donor atoms or molecules per m^3.
- N_o = the number of non-donating atoms or molecules per m^3.
- N_{c} = the number of electrons in the conduction band.

Then the relationship:

$$N_{\mathrm{c}} = N_{\mathrm{D}} - N_{\mathrm{o}} \qquad \text{Eq. 3.20}$$

holds assuming that each atom or molecule donates one electron for conduction. As an electron is ionized it moves away from the parent atom but a Coulomb force of attraction exists between the electron and the parent ion is given by:

$$F = \frac{-e^2}{4\pi\varepsilon_0\varepsilon_{\mathrm{r}}r^2} \qquad \text{Eq. 3.21}$$

where ε_r the dielectric constant of the material and r the distance between charge centers.

With potential energy reference for $r \to \infty$, the potential energy associated with this force is:

$$V(r) = \frac{-e^2}{4\pi\varepsilon_0\varepsilon_{\mathrm{r}}r} \qquad \text{Eq. 3.22}$$

And the electric field changes the potential energy to:

$$V(r) = \frac{-e^2}{4\pi\varepsilon_0\varepsilon_{\mathrm{r}}r} - eEr \qquad \text{Eq. 3.23}$$

To find the condition for the potential energy to be maximum, we differentiate the equation and equate it to zero. Then, solving for r and noting the maximum by r_m, the change in the maximum height of the barrier is:

$$\Delta V_m = -2\left(\frac{e^3E}{4\pi\varepsilon_0\varepsilon_{\mathrm{r}}}\right)^{\frac{1}{2}} = -\beta_{\mathrm{P}}E^{1/2} \qquad \text{Eq. 3.24}$$

Where $\beta_{\mathrm{P}} = 2\left(\frac{e^3}{4\pi\varepsilon_0\varepsilon_{\mathrm{r}}}\right)^{\frac{1}{2}}$ is the Poole-Frenkel coefficient that depends only on the charge of the carrier and the dielectric constant of the material, assuming a Coulombic potential well [BÖT-85], [BRU-06].

The Poole-Frenkel conductivity is given on the form:

$$\kappa_{PF} = \kappa_0 exp\,(\beta_{\mathrm{P}}E^{\frac{1}{2}}/2kT) \qquad \text{Eq. 3.24}$$

where κ_0 is the low field conductivity.

On the Poole-Frenkel effect, several investigators have pointed out that the slope of ln(J/E) versus $E^{1/2}$ gives a value between β_P/kT and β_P/2kT, which means between β_s and $2\beta_s$, where β_s is the Schottky constantm[MAR-67].

(C) Space charge limited Currents (SCLC)

The Space Charge Limited Current (SCLC) current model is found generally in thin insulating films and is highly dependent upon thickness. The prime objective of SCLC models was to calculate the steady state current produced when the carrier concentration is high enough to bring significant spatial variation of the field. In a thin film which is insulating but has good contacts, although there may only be a very small amount of free charge in the material at first, more free charge may be injected. If the dielectric constant of the material is high this may lead to a high space charge accumulation within the material.

Charge injected from the electrode moves through the bulk and eventually reaches the opposite electrode. If the rate of injection is equal to the rate of motion charges do not accumulate in a region close to the interface and the electrodes are called Ohmic. Ohmic conductors are sources of unlimited number of charge carriers [KAO-04]. If the mobility is low, which is the normal situation with many polymers, then the charges are likely to accumulate in the bulk and the electric field due to the accumulated space charge influences the conduction current. A linear relationship between current and electrical field does not apply anymore except at very low fields. At higher fields the current increases much faster than linearly and it may increase as the square or cube of the electric field. This mechanism is usually referred to as Space Charge Limited Current (SCLC). The SCLC theory provides the external current for electronic carriers in either a trap-free medium, a single trapping level, or in situations of an exponential distribution of trap levels [ROS-55], [MAR-62].

Following, in developing a theory for SCLC, we assume that the charge is distributed within the polymer uniformly, there is only one type of charge carrier and the contacts are Ohmic. This model was formally developed to explain the nonlinear character of the steady-state current vs. field characteristic. In experiments it is possible to choose electrodes to inject a given type of charges and if both charges are injected from electrodes recombination should be taken into account. With increasing electric field the regions of space charge move towards each other within the bulk and coalesce. The number and type of charge carriers, and its mobility and thickness of space charge layer influence SCLC. Mott and Gurney first derived the current due to space charge limited current in crystals assuming that there were no traps. For a better understanding of the SCLC theory we will analyze first the case where the traps are absent and then we will include traps in the theory according to [DIS-92], [RAJ-03], [CAS-69], [TEY-05].

Trap free dielectric

Consider an ideal dielectric in which there are:

- No thermally generated carriers
- No traps
- Ohmic contacts implying good injection

- Only negatively-charged carriers (i.e. electrons)

The total current density in the dielectric is made up from the three components of drift, diffusion and displacement:

$$J = ne\mu E - eD_{\mathrm{n}}\frac{dn}{dx} + \varepsilon_0\varepsilon_{\mathrm{r}}\frac{dE}{dt} \quad \text{Eq. 3.24}$$

Where D_{n} is the Fick's diffusion coefficient for electrons and the other symbols have their usual notation. Assuming steady-state conditions ($dE/dt = 0$), as we are investigating the DC conductivity, the equation Eq. 3.24 becomes:

$$J = ne\mu E - eD_{\mathrm{n}}\frac{dn}{dx} \quad \text{Eq. 3.25}$$

From Poisson's equation:

$$\frac{dE}{dx} = \frac{ne}{\varepsilon_0\varepsilon_{\mathrm{r}}} \quad \text{Eq. 3.26}$$

So that the total current is:

$$J = \varepsilon_0\varepsilon_{\mathrm{r}}\mu\mathrm{E}\frac{\mathrm{dE}}{\mathrm{dx}} - \varepsilon_0\varepsilon_{\mathrm{r}}\mathrm{D_n}\frac{\mathrm{d^2E}}{\mathrm{dx^2}} \quad \text{Eq. 3.27}$$

If we neglect diffusion and assume a constant electric field across the bulk of the dielectric the current will be as follows:

$$J \cong \varepsilon_0\varepsilon_{\mathrm{r}}\mu\mathrm{E}\frac{\mathrm{dE}}{\mathrm{dx}} \quad \text{Eq. 3.28}$$

Rearranging this expression and integrating both sides gives:

$$E = \left(\frac{2\mathrm{J}}{\varepsilon_0\varepsilon_{\mathrm{r}}\mu}(\mathrm{x} + \mathrm{x}_0)\right)^{1/2} \quad \text{Eq. 3.29}$$

Where x_0 is a constant of integration. This may be estimated using the boundary condition that at $x = 0$, n is given by the concentration of electrons injected over the electrode-insulator barrier, $N_0 = n(x = 0)$ which at low fields (i.e. much less than those at which Schottky or Fowler-Nordheim processes would have a role) is approximately given by:

$$N_0 = 2\left(\frac{2\pi m^* k_{\mathrm{B}}T}{h^2}\right)^{1/2} exp\left\{\frac{x_{\mathrm{i}} - \varphi_{\mathrm{m}}}{k_{\mathrm{B}}T}\right\} \quad \text{Eq. 3.30}$$

where x_i is the electron affinity of the insulator and φ_m is the work function of the metal. Finally x_0 is given as:

$$x_0 = \frac{\varepsilon_0\varepsilon_{\mathrm{r}}J}{2N_0^2e^2\mu} \quad \text{Eq. 3.31}$$

The current density to voltage relationship is then:

$$V = \int_0^L Edx = \frac{2}{3}\left(\frac{2J}{\varepsilon_0\varepsilon_{\mathrm{r}}\mu}\right)^{\frac{1}{2}}\left((d + x_0)^{\frac{3}{2}} - x_0^{3/2}\right) \quad \text{Eq. 3.32}$$

where d is the thickness of the material.

It is usual to assume that $x_0 \ll L$ so that the current density is given by:

$$J = \frac{9\varepsilon_0\varepsilon_r\mu V^2}{8L^3} \quad \text{Eq. 3.33}$$

And the current is proportional to the square of the voltage. This is known as the Mott & Gurney square law (or sometimes Child's law for solids, whereas Child's law for a vacuum predicts $J \propto V^{3/2}$). The inequality constraint $x_0 \ll L$ is only true for electrodes with good injection properties.

The charge density in the dielectric is made up from two components, n_0 and n_1 where n_1 is an injection term. The current density can therefore be thought of as being made up of two parts:

$$J_{SCLC} = n_0 e\mu\frac{V}{L} + \frac{9\varepsilon_0\varepsilon_r n_1\mu V^2}{8L^3} \quad \text{Eq. 3.34}$$

$$(Ohmic) \qquad (Space\ charge\ limited)$$

And if $n_1 \gg n_0$ then space charge limited current dominates. A transition voltage V_{tr} may be defined such that above this voltage the space charge limited current dominates over the Ohmic component. This is easily found experimentally by plotting $\log(J)$ versus $\log(V)$ and observing the voltage at which the slope changes from unity to two.
Equating the Ohmic and space charge limited currents gives:

$$V = \frac{9en_0L^2}{9\varepsilon_0\varepsilon_r} \quad \text{Eq. 3.35}$$

From Eq. 3.35, the space charge in the material can be found.

Dielectric with traps

If traps are present (which is inevitable in the case of polymers) the space charge limited current will be reduced by several orders of magnitudes, since most of the injected carriers are removed by empty traps. It was proposed, by [ROS-55], that neither the space charge density nor the field distribution is altered by trapping, but the voltage-current relationship should be modified by a trapping parameter θ, which is given by

$$\theta = \frac{n_c}{n_t + n_c} \quad \text{Eq. 3.36}$$

Where n_c the number density of conduction band electrons and n_t the number density of occupied trap states.

The current density due to SCLC is then given by:

$$J_{SCLC} = \theta\,\frac{9\varepsilon_0\varepsilon_r\mu V^2}{8s^3} \quad \text{Eq. 3.37}$$

The trapping parameter θ expresses actually the proportion of electrons that are available for conduction. Its value is very small at low voltages, as all carriers injected from the electrodes are led into traps and do not contribute to the conduction current. At sufficiently

high fields, when all traps are filled (also referred in the bibliography as the trapped filled limit), the parameter θ returns to its previous unit value.
The numbers n_t and n_c are given by:

$$n_c = N_{\mathrm{v}} \exp\left(-\frac{E_{\mathrm{F}} - E_{\mathrm{v}}}{kT}\right) \quad \text{Eq. 3.38}$$

$$n_t = \frac{N_t}{1+\exp\left[(E_{\mathrm{F}} - E_{\mathrm{t}})/kT\right]} \quad \text{Eq. 3.39}$$

where N_v the density of states in the valence band and N_t is the density of traps.

(D) Field-Limiting Space Charge (FLSC) model

Several works on HVDC polymeric insulation showed that significant space charge buildup starts when the applied field is above a critical value, the so-called threshold for space charge accumulation [BOD-04]. A mechanism that could explain this observation is an abrupt increase of the mobility at a critical field value (mobility edge) that leads to homo-charge injection. Recently, this parameter has also been associated with the startup of electrical ageing. For these reasons, the threshold for space charge accumulation can be considered as a parameter of utmost interest not only for insulation design, but also for material characterization and comparison [BOD-04].

Space charge accumulation is known to play a very important role not only in the aging, but also in the breakdown of HVDC solid polymeric insulation, due to local electric field enhancement. If the applied field exceeds the threshold for space charge accumulation, charge injected from the electrodes can accumulate in traps located at the interface with electrodes and in the insulation bulk. Buildup of injected charge can be observed often close to the injecting electrode, forming a homo-charge distribution after relatively short times of voltage application, depending on electric field and temperature [FAB-09].

In electrical engineering applications charge injection occurs in most cases at very high voltages. Approaches involving directly the effect of space charge in terms of Poisson equation electric field modification and contribution to conduction current mechanism have been proposed, mainly to deal with high-field, thus short-term, breakdown. These approaches consider highly inhomogeneous conditions, from divergent electrical field to composite or filled dielectrics, which can be not uncommon in real insulation [MON-00].

Regarding high and divergent fields, the mechanisms proposed by Zeller and Boggs have the common background of the so-called Field Limited Space Charge Current (FLSC) theory. These two mechanisms are indicated here:

- [ZEL-84]: Modeling of the tip-plate geometry in the limit of an infinitely high mobility edge and by neglecting diffusion. In this model, a space charge forms near the tip when the mobility reaches the mobility edge. The mobility edge is described with a mobility $\mu(E)$ which vanishes for $E < E_c$, but is very large for $E > E_c$, where Ec is the critical value of the electric field. The space charge, in turn, screens the electric field enhancement at the tip, and pins it to the mobility edge.

- [BOG-93], [BOG-95]: Proof of usefulness of the screening by the injected space charge in ac driven field-grading materials. This model, however, is based on the concept of conductivity which cannot lead to a consistent physical description of charge injection. The theory assumes a conductivity which is only a function of the field and which does not distinguish between intrinsic and injected charge carriers.

According to the FLSC theory, there is a threshold field, Ec, below which injected space charge possess a low but finite mobility, so that over a long period of time the equilibrium situation predicted by the Space Charge Limited Current (SCLC) model will result. Above the strongly nonlinear dependence of the mobility on the electric field causes space charge clouds to penetrate rapidly into the insulation bulk from a conductive protrusion/particle tip, thereby reducing the electric field at the interface between dielectric and electrode/defect in a very short time. When the FLSC conductivity is reached, the resistive current density is equal to the capacitive current density and space charge is generated to limit the field to close to Ec. This has the practical effect of reducing the Laplacian field at the defect tip to a near constant Poissonian value of ~*E*c for a length inside the dielectric that is established by the extent of the difference between Laplacian and FSCL threshold field, as shown in the following figure:

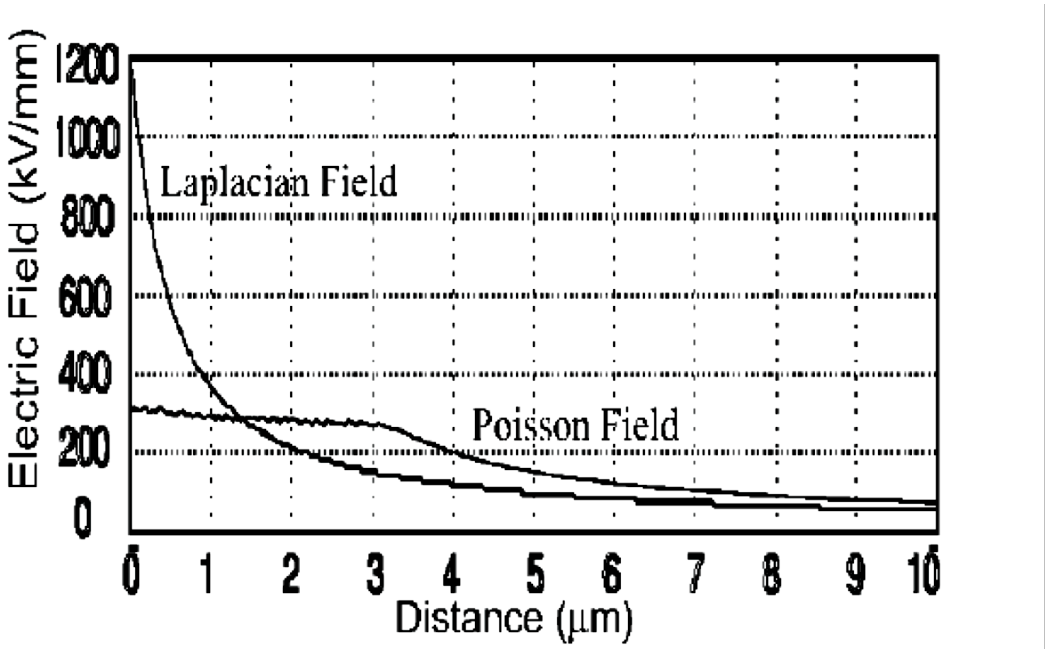

Fig. 3.12: Example of Laplacian (without accounting for space charge) and Poissonian (with space charge) electric field vs distance from a defect tip, from [ZHE-05]

In Fig. 3.12 we can see that: when the Laplacian field at the tip is appreciably above the threshold field, the FSCL mechanism is present. In this case, the space charge limited field region extends from the defect tip for approximately 3μm in the insulator [ZHE-05].

Damage can penetrate into the polymer from the defect tip through electron avalanches generated by very high local field, but as the electrons for such a process must be extracted from the defect/polymer interface and electromechanical fatigue at the defect/polymer

interface is not involved (injection and extraction), the degradation under constant voltage takes much longer times than those resulting from an AC supply [MON-11].

(E) Bulk Ionic conduction model

According to [MOT-40], the theoretical equation for ionic conduction, relating current density with electric field strength is:

$$J_{\mathrm{BIC}} = J_0 \sinh\left(\frac{\lambda q_{\mathrm{i}} E}{2kT}\right) \qquad \text{Eq. 3.40}$$

where λ is an ionic jump distance, used to express the movement of ions in the material and q_{i} is the ionic charge. The mean jump distance can derive from the current versus electric field strength characteristic. The bulk ionic conduction model is the analogous of the hopping conduction, but not for tunneling, as it refers to ionic carriers.

Conclusion:

Summarizing, the electrical conductivity can be classified into three categories [KAO-04]:

- Intrinsic conductivity: charge carriers are generated in the material based on its chemical structure only.
- Extrinsic conductivity: charge carriers are generated by impurities in the material, which may be introduced into it by fabrication processes or deliberately doped into it for a specific purpose.
- Injection-controlled conductivity: charge carriers are injected into the material mainly from metallic electrodes through a metal-material interface.

Through the years, studies have been developed in order to sufficiently describe the way carriers are generated and transported in polymeric insulating materials. However, each polymeric material has a different chemical and physical structure and is influenced differently from the various parameters, such as temperature and electric field. In addition, more than one conduction mechanism can be present in a material, and especially at steady-state, an injection mechanism must be combined with a charge transport mechanism to fully describe the conduction phenomena taking place. The suitability of these mechanisms will be dealt with in the next chapter, giving also examples from previous investigations.

4. Conduction current measurements - Previous investigations

Conduction current measurements are used as a way to determine the conduction mechanisms that are present in a material. Previous studies on polymeric insulating materials have shown that the current-voltage (*I*-*V*), or current density-electric field (*J*-*E*) characteristics exhibit a transition from Ohmic behavior to high-field behavior (chapter 3), above a critical electric field strength. This critical field strength is also known as threshold field.

Previous investigations have tried to determine the value of this threshold field, find its dependence on factors like temperature, fillers, material geometry etc. and specify its origins. Some of these investigations, the most relevant to this thesis, are indicated in the next paragraphs.

4.1. The threshold field and its dependence

4.1.1. Conduction current measurements on XLPE and EPR insulation, from [BOD-04]

The study of [BOD-04] is focusing on the conduction currents of two different insulating materials and their dependence on the applied electric field and the specimen geometry.

Samples and Experimental conditions

- Materials:
  - EPR
  - XLPE
- Electrode material: aluminum
- Specimen geometry:
  - Plaques
  - Cables
- Range of applied electric field:
  - 3.3 to 23.3 kV/mm for the cables
  - 3.3 to 20 kV/mm for the plaques
- Temperature: 20 °C

Result summary

Material	Geometry	ϑ (°C)	$E_{threshold}$
XLPE	Cable	20	8.5 kV/mm
	Plaque	20	13 kV/mm
EPR	Plaque	20	5.5 kV/mm

J–E characteristic

A logarithmic plot of the *J-E* characteristic, shown in Fig. 4.1, indicates the transition between low-field and high-field conduction, with:

- Slope ≈ 1 indicating Ohmic conduction
- Slope ≥ 2 indicating a high-field conduction region

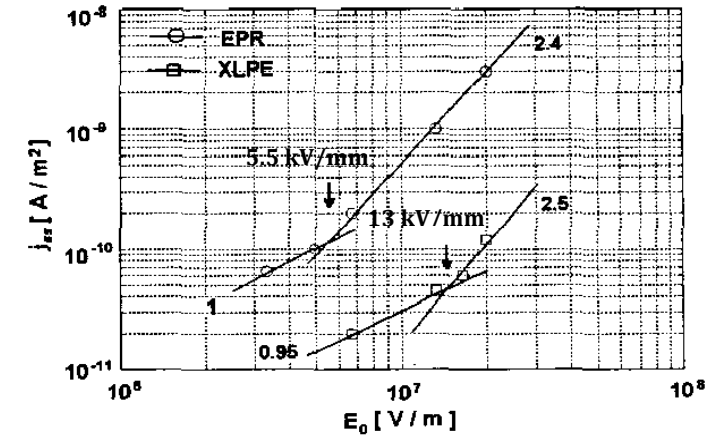

(a)

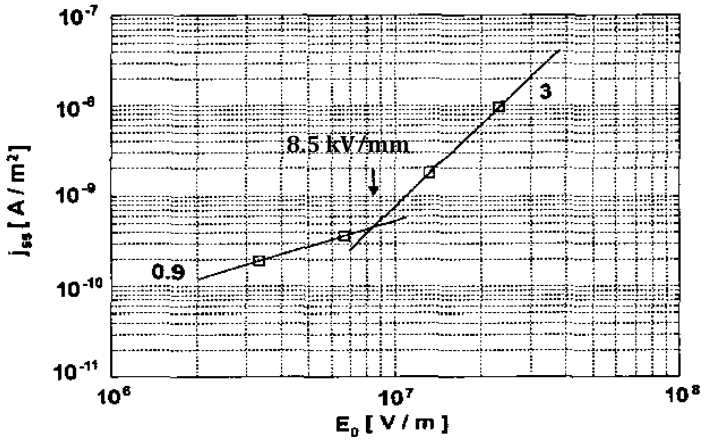

(b)

Fig. 4.1 | (c) *J-E* characteristic for XLPE and EPR plaques, at 20 °C, from [BOD-04]
(d) *J-E* characteristic for XLPE mini-cables, at 20 °C, from [BOD-04]

Conclusion

Both materials exhibit a transition from a low-field to a high-field conduction regime. The influence of the specimen geometry is remarkable, and indicates that the nonlinear behavior starts at lower fields for the cable specimens. No interpretation is given in [BOD-04] for this result.

4.1.2. Conduction current measurements on filled and unfilled epoxy, from [MAC-00], [MAC-01]

The study of [MAC-00] is focusing on the conduction currents of filled and unfilled epoxy resin specimens and their dependence on the applied electric field and the fillers (quantity and nature). In [MAC-01] the author is using the same results to accentuate the influence of the filler nature on the threshold field value.

Samples and Experimental conditions

- Materials:
  - Unfilled epoxy resin
  - Epoxy filled with either 10% or 15% aluminum oxide Al_2O_3
  - Epoxy filled with either 10% or 15% zinc oxide ZnO
- Electrode material: aluminum
- Specimen geometry: Square plaques
- Range of applied electric field: Up to 11 kV/mm
- Temperature: 33 or 34 $\pm$0.5 °C

Result summary

Material	ϑ (°C)	$E_{threshold}$
Epoxy, unfilled	34	Not found
Epoxy, 10% Al_2O_3	34	Not found
Epoxy, 15% Al_2O_3	34	6-7 kV/mm
Epoxy, unfilled	33	Not found
Epoxy, 10 % ZnO	33	Not found
Epoxy, 15% ZnO	33	4 kV/mm

J–E characteristic

The *J-E* characteristics are shown in Fig. 4.2 and do not reveal a transition from a low-field to a high-field conduction regime for all materials.

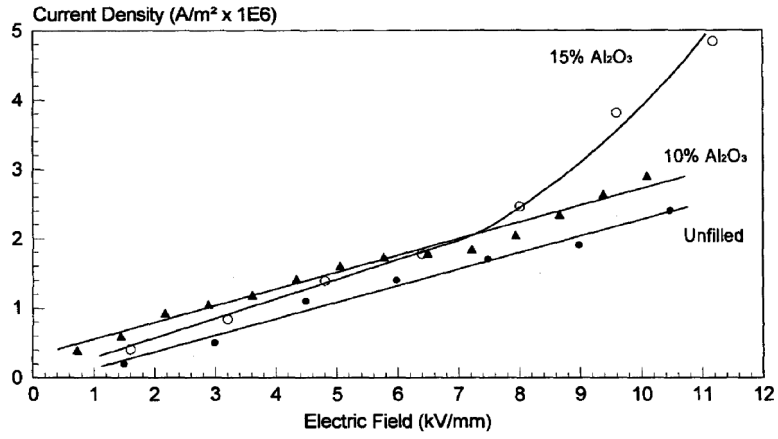

(a)

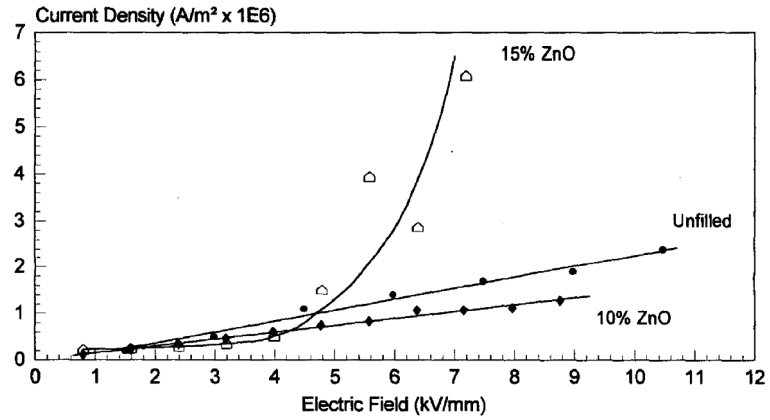

(b)

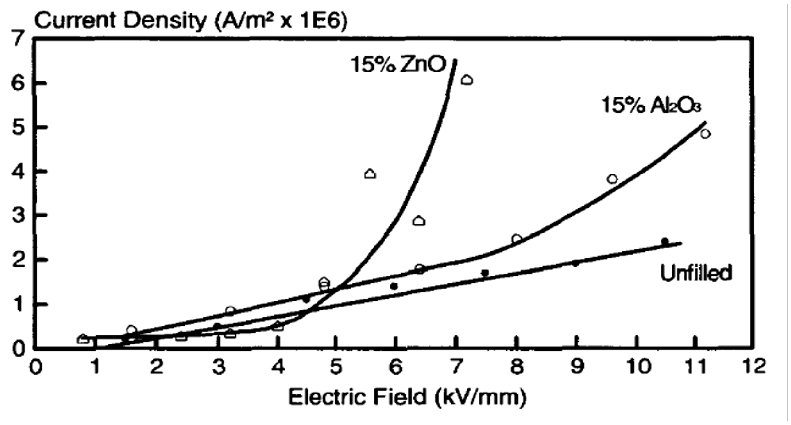

(c)

Fig. 4.2 (a): *J-E* characteristic for commercial epoxy resin, unfilled and with Al_2O_3 filler, at 34 °C, from [MAC-00]
(b): *J-E* characteristic for commercial epoxy resin, unfilled and with ZnO filler, at 33 °C, from [MAC-00]
(c): *J-E* characteristic for a commercial epoxy resin, unfilled and with aluminum oxide or zinc oxide filler, at 33-34 °C, from [MAC-01]

Conclusion

The influence of the concentration and the nature of the fillers on the conduction currents in epoxy square plaque measurements is clear. The addition of either aluminum oxide or zinc oxide in the epoxy specimens can produce a composite material, which exhibits a non-linear behavior above a threshold field. It is also remarkable from the *J-E* characteristics that the influence of the ZnO fillers is more intensive compared to the Al_2O_3. At the linear region, it is not clear whether the current of the filled or unfilled specimens is greater. Concerning the Al_2O_3 filled specimens the current is lower for unfilled specimens. For ZnO filled specimens the current is greater for the unfilled specimens, however, with a lower magnitude.

4.1.3. Conduction current measurements in Epoxy and Polyethylene, from [DAS-12]

The study of [DAS-12] is focusing on the conduction currents of two different insulating materials and their dependence on the applied electric field.

Samples and Experimental conditions

- Materials:
  - Epoxy
  - Polyethylene (PE)
- Electrode material: aluminum
- Specimen geometry: Plaques
- Temperature: 25 °C

Result summary

Material	ϑ (°C)	$E_{threshold}$
Epoxy	25	17 kV/mm
PE	25	13 kV/mm

J-E Characteristic

A logarithmic plot of the *J-E* characteristic can show the transition between low-field and high-conduction, with:

- Slope ≈ 1 indicating Ohmic conduction
- Slope ≥ 2 indicating a high-field conduction region

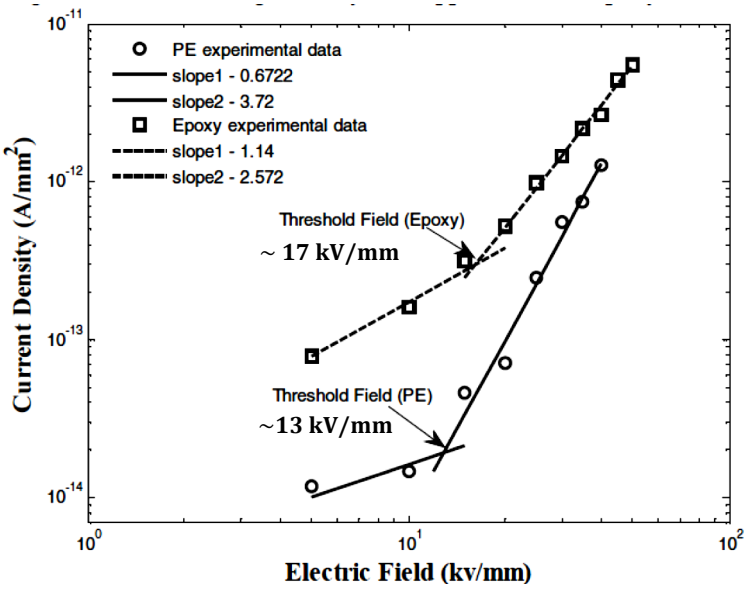

Fig. 4.3: J-E characteristic for Epoxy and Polyethylene, at 25 °C, from [DAS-12].

Conclusion

Both materials exhibit a transition from a low-field to a high-field conduction regime. The threshold field value for this transition is higher for the epoxy specimens. The authors refer to the structural properties of the materials for a possible explanation of the results. Epoxy is an amorphous material, while PE is a semi crystalline material. The crystalline-amorphous boundaries of PE, and thus the introduction of traps or localized states at these boundaries, could be one of the reasons behind its low threshold field value.

4.1.4. Conduction current measurements on composite epoxy resin materials, from [CAS-11]

The study of [CAS-11] deals with the conduction mechanisms that are present in micro and nano composite epoxy resin materials. For this reason, conduction current measurements are performed and the threshold field is detected.

Samples and Experimental conditions

- Materials:
  Six kinds of epoxy-based materials with different weight % contents of micro and nano SiO_2 filler, with amounts ranking up to 65%wt micro and 5%wt nano, as shown in the following table:

	Nano %wt	Micro %wt
M0N0	0	0
M60N5	60	5
M62.5N2.5	62.5	2.5
M65N0	65	0
M65N5	65	5

Table 4.2. Micro and nanofiller contents in % by weight, from [CAS-11]

- Specimen geometry: plaques, 1mm thick
- Range of applied electric field: 1 to 13 kV/mm
- Temperature: 25 °C

Result summary

All samples showed a non-linear behavior for fields greater than 2 kV/mm.

J-E characteristic

A logarithmic plot of the *J-E* characteristic can show the transition between low-field and high-conduction, with:

- Slope ≈ 1 indicating Ohmic conduction
- Slope ≥ 2 indicating a high-field conduction region

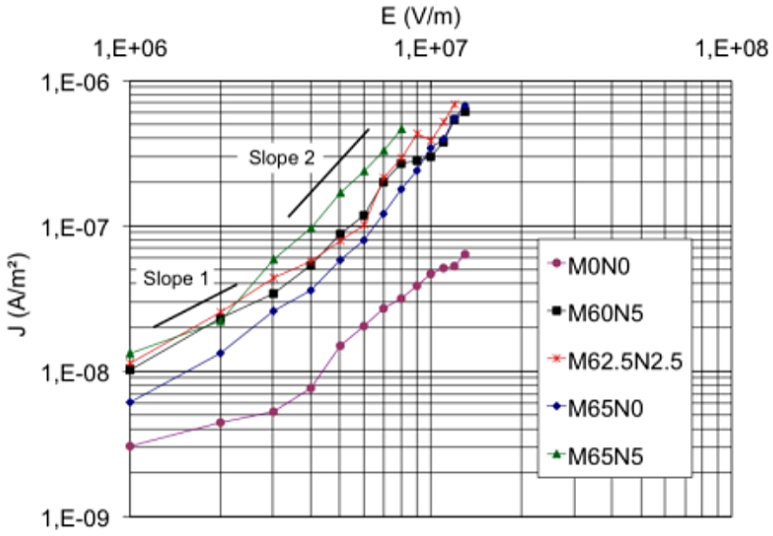

Fig. 4.4: *J-E* characteristics for micro- and nanofilled epoxy resin specimens, from [CAS-11]

4.2. Possible origins of the non-linear *J-E* behavior

Previous studies performing conduction current measurements on polymeric insulating materials tried to give an explanation for the non-linear behavior of the *J-E* characteristic above the threshold field. It has been proved in a number of cases (e.g. [DIS-05], [DAS-12]), that the point at which the slope of the *J-E* characteristic changes determines the electric field above which space charge starts accumulating. As discussed in chapter 3, space charge and Ohmic behavior cannot coexist. The presence of space distorts the distribution of the electric field in the material, and inevitably results to a non-linear *J-E* characteristic.

The space charge accumulation is taken into account in the Space Charge Limited Conduction (SCLC) theory, which was explained in the previous chapter. In the SCLC theory, the *J-E* characteristic reveals the transition from a low-field regime where Ohm's law prevails (represented with a straight line with a slope approximately equal to 1 in a log-log coordinate system) to a high-field behavior determined by the establishment of steady trapped space charges. In the latter case, the conduction model is described by a power law, providing a straight line in log-log coordinates with a slope equal or larger than two. According to the SCLC theory, this critical field corresponds to the onset of space charge accumulation within the material.

However, space charge is not the only origin for nonlinear currents. Generation and transport mechanisms such as the Schottky injection, Hopping conduction etc., may occur even when there is no space charge and might also create non-linearity in the *J-E* characteristic. The functions describing these mechanisms may fit the data almost as well as the expressions for SCLC [MON-00]. The crucial point is whether or not the I-V characteristic can be non-linear when there is no space charge accumulation

The question as to the existence of space charge at voltages for which the current is non-linear can easily be settled by complementary techniques such as space charge detection, or electroluminescence, or both. Modern equipment allows space charge (or electroluminescence) and conduction current measurements to be performed simultaneously, thereby giving the opportunity of clearing up the coincidence or not of the non-linear behavior with the existence of space charge [TEY-01] and comparing the sensitivity and efficiency of the methods [MON-00]. In the study of [DAS-12], which was indicated in the previous paragraph, both space charge and conduction current measurements were performed. The results are shown in Fig. 4.5 below:

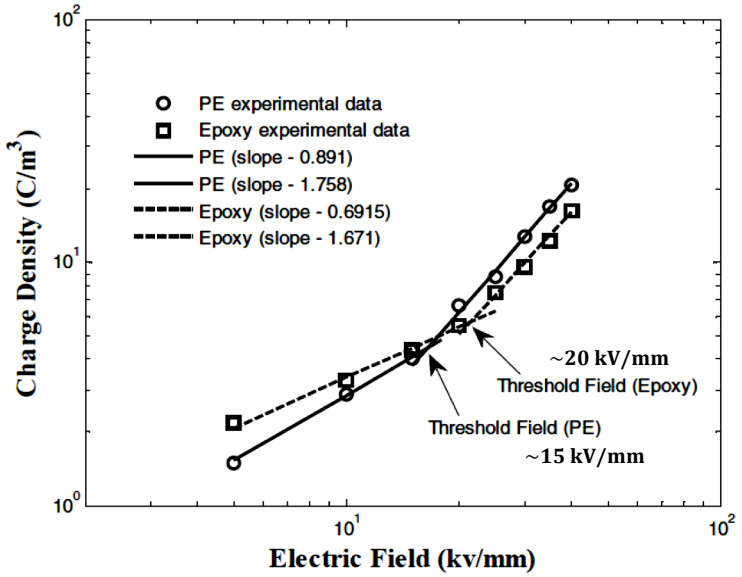

(a)

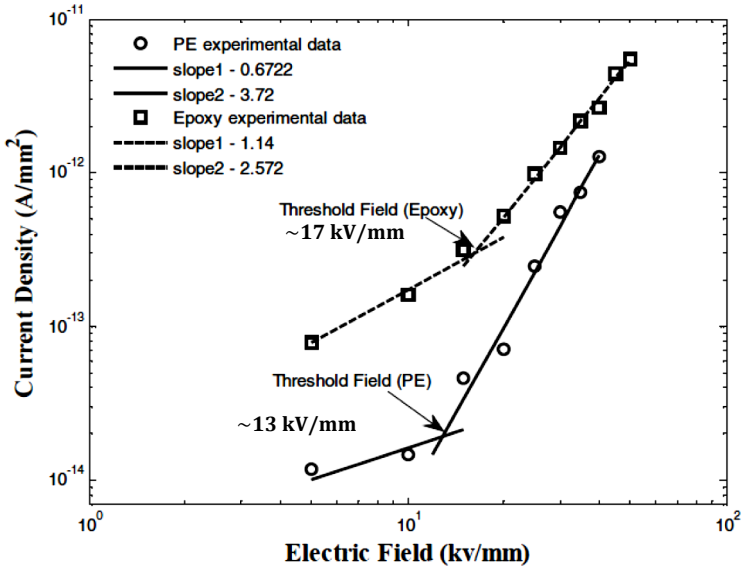

(b)

Fig. 4.5. Threshold field indication for PE and Epoxy, from conduction current and space charge measurements:
(a) Variation of charge density with respect to applied field, from [DAS-12]
(b) Variation of current density with respect to applied field, from [DAS-12]

The threshold field value deriving from the two techniques differs somewhat, either because of a mechanism different from SCLC, or because of the sensitivity of the test techniques and the physics behind the measurement [DIS-05].

When studying conduction phenomena in dielectrics we should expect more than one conduction mechanism to be present. In particular, as the current enters, travels through the bulk, and finally exits the material, we should expect the coexistence of injection and bulk mechanisms. Especially in the case of steady-state conditions, the current at the electrode-material interface and the current in the bulk are equal [CAS-11]. The injection and bulk conduction mechanisms analyzed in chapter 3 are summarized in the following table:

Conduction mechanism	Dependence of κ (and J) on temperature and field	Representation of results
Schottky	$\sim T^2 \exp\left(\frac{c\sqrt{E}}{kT}\right)$	$\ln\left(\frac{1}{T^2}\right)\ vs.\sqrt{E}$
Nordheim-Fowler	$\sim E^2 \exp\left(-\frac{c}{E}\right)$	$\ln\left(\frac{1}{E^2}\right) vs.\frac{1}{E}$
Poole-Frenkel	$\sim \exp\left(-\frac{\Delta\varphi}{2kT}+\frac{c\sqrt{E}}{kT}\right)$	$\ln(\kappa)\ vs.\sqrt{E}$
Hopping conduction	$\sim \exp\left(-\frac{\Delta W}{kT}\right)\cdot\sinh\left(\frac{cE^{\frac{1}{a}}}{kT}\right)$	$\ln(\kappa)\ vs.\frac{1}{T}$
Ionic conduction	$\sim \exp\left(-\frac{W_A}{kT}\right)\cdot\sinh\left(\frac{cE}{kT}\right)$	$\ln(\kappa)\ vs.\frac{1}{T}$ $J\ vs.\sinh\left(\frac{cE}{kT}\right)$
SCLC	$\sim E^2$	$\ln(J)\ vs.\ln(U)$

Table 4.1. Representation of the possible injection and bulk mechanisms in polymeric insulating materials, from [LUT-11], [LOV-74].

4.3. Detection of the conduction mechanisms from the J-E characteristics

From the curve fitting of the steady J-E characteristic, the conduction mechanisms that are present in a material are detected. For the curve fitting, the results must be represented in the way the third column of the table 4.1 dictates. If the representation of the results in such a way gives a straight line and sensible parameter values, then the respective conduction mechanism is present in the material. For the explanation of the latter the study of [KRI-12], [CAS-11] is indicated again here.

(A) J-E fitting, Bulk phenomena

1. Space charge limited conduction (SCLC)

The SCLC theory is the first conduction mechanism that comes to mind when the slope of the log-log J-E characteristic changes from about 1 to 2 or higher than 2. The SCLC, as explained in the previous paragraph, refers to the start of space charge accumulation above the threshold field. At the high-field conduction region *J* is given from Eq. 4.1:

$$J = \frac{9}{8}\varepsilon\varepsilon_0\mu\frac{V^2}{L^3} \qquad \text{Eq.4.1}$$

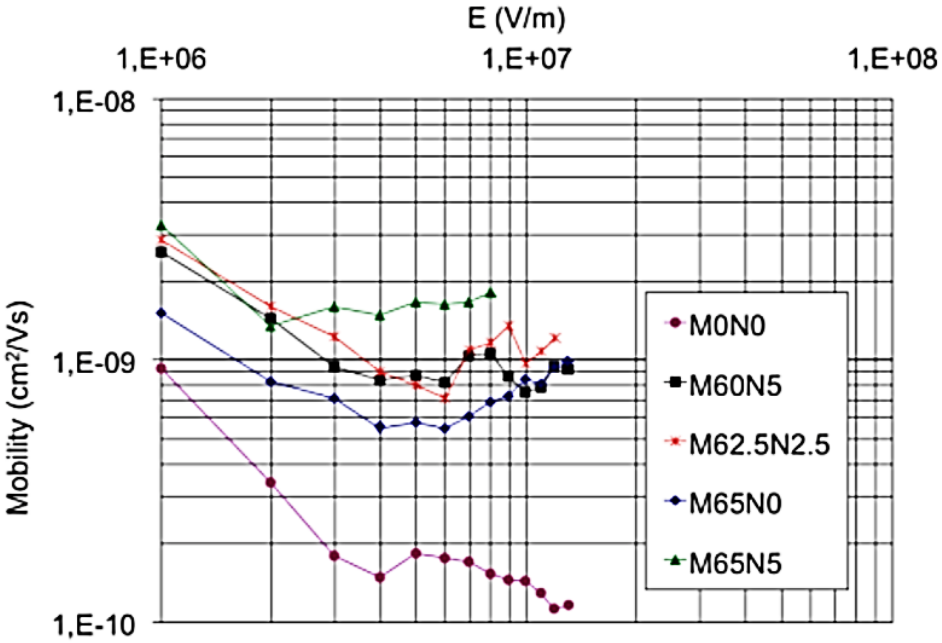

Fig. 4.6: Mobility vs. electric field for micro- and nanofilled epoxy resin specimens, from [CAS-11]

From the curve fitting of the results the mobility of the carriers with respect to applied field has been found and the values seem to agree with the respective in literature. That means that the SCLC is present in the material, but is not necessarily the only conduction mechanism. A validation for that can be given from the fact that the SCLC theory foresees only accumulation of homo-charge. The same study conducts also space charge measurements, finding out that under the same conditions, there is also hetero-charge accumulating in the material. That suggests that SCLC is present, but also other conduction mechanisms contribute to the conduction process. In order to determine if SCLC is dominant, one should change the thickness of the specimens and see if the change in the current is proportional.

2. Bulk ionic conduction

The ionic conduction model is expressed as:

$$J = J_0 \exp\left[(q_i \lambda E)/(2kT)\right] \qquad \text{Eq. 4.2}$$

The parameters J_0 and λ are calculated from Eq. 4.2, are in a reasonable range and are shown in the following table:

Material	$J_0 \times 10^{-8}$ $(\frac{\mathbf{A}}{\mathbf{m^2}})$	λ (nm)
M0N0	1.25	9.8
M60N5	4.47	13.8
M62.5N2.5	3.9	15.9
M65N0	2.11	17.1
M65N5	2.84	23.0

Table 4.3: Calculated parameters for the ionic conduction model for the epoxy composites, from [KRI-12]

So the bulk ionic conduction fits the results as well.

3. Poole-Frenkel mechanism

According to the Poole-Frenkel conduction mechanism, the conductivity is expressed as:

$$\sigma = \sigma_0 \exp\left(\beta_P E^{\frac{1}{2}}/2kT\right) \qquad \text{Eq. 4.3}$$

Where the Poole-Frenkel constant β_P must be between β_S and $2\beta_S$, where β_S is the Schottky constant and depends on the relative permittivity of the material under investigation. The slope of $\ln(J/E)$ versus $E^{1/2}$ yields values between 0.001 and 0.0008, which is outside the expected range of 0.0001 to 0.0008, suggesting that the Poole-Frenkel model is not suitable.

(B) J-E fitting, contact phenomena

1. Schottky injection

According to the Schottky injection model:

$$J_S = AT^2 \exp\left[-\frac{\varphi - \beta_S E_C^{\frac{1}{2}}}{kT}\right] \qquad \text{Eq. 4.4}$$

or with the field correction constant γ:

$$J_s = AT^2 \exp\left[-\frac{\varphi-\beta_s\left(\gamma\frac{V}{d}\right)^{\frac{1}{2}}}{kT}\right] \qquad \text{Eq. 4.5}$$

For the investigation of the Schottky model ln (J) versus $E^{1/2}$ is plotted:

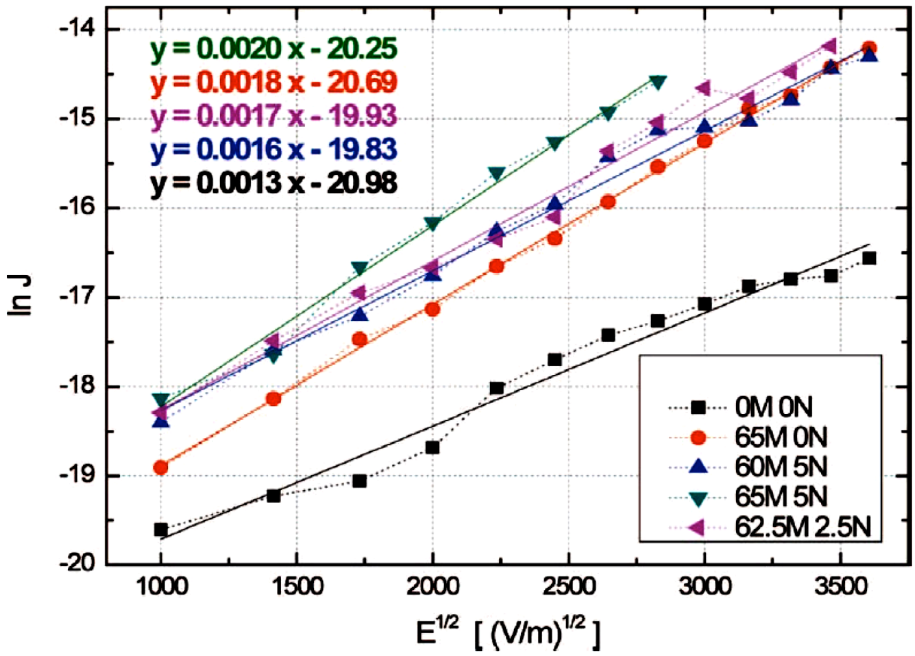

Fig. 4.7: Plots of ln (J) vs. $E^{1/2}$ for the investigation of Schottky injection, for micro- and nanofilled epoxy resin specimens, at 25 °C, from [KRI-12]

The data plotted in Fig. 4.7 show good correlation to the Schottky emission model, and the values of the calculated parameters showed in Table 4.4 are in a reasonable range.

Material	Slope	ε_r (at 1 MHz)	γ
M0N0	0.0013	3.29	2.5
M60N5	0.0016	3.95	4.6
M62.5N2.5	0.0017	3.95	5.2
M65N0	0.0018	4.05	6
M65N5	0.0020	4.05	7.4

Table 4.4: Slope and unknown parameter values derived from the Schottky emission fitting of the results, from [KRI-12]

From Table 4.4 it can be seen that the constant γ is increasing with the silica content.

2. Fowler-Nordheim injection

The Fowler-Nordheim conduction model is valid for fields above 100 kV/mm so it is expected that it would not fit the results. This can be proved with the representation of the results in a $\ln\left(\frac{J}{E^2}\right)$ versus $\frac{1}{E}$ graph. The plot does not yield a straight line and so the Fowler-Nordheim mechanism is not present in this case, as expected.

Conclusion

As seen from the studies of [KRI-12], [CAS-11], the J-E characteristic can be used to determine satisfactory the conduction mechanisms that are present in a material as well as the values of some important parameters. Except for the studies of [KRI-12], [CAS-11] there are also several other studies concerning the same field of interest, like the study of [IED-71], which focuses on the applicability of the Poole-Frenkel effect on polymeric insulators, the study of [LEN-66], which focuses on the Schottky Emission, the study of [KOS-71], which focuses on the Bulk Ionic Conduction as well as other studies like [LOV-74], [MON-00], [GUI-06] that examine the applicability of different conduction mechanisms on filled and unfilled epoxy resins and PE. This "fitting" method will be used also in this thesis for the results of the conduction current measurements on Al_2O_3, in chapter 5.

5. Conduction current measurements on EP236

5.1. Conduction current measurements procedure

For the determination of the volume conductivity of the material under investigation a conduction current measurement setup is used. The conduction current measurements are performed according to VDE 0303-30 (international norm: IEC 93), as explained in Chapter 2. This work is specifically focused on the influence of temperature and electric field on the volume conductivity of the material and thus, conduction current measurements varying these two parameters are performed.

5.1.1. Samples

The material under investigation is epoxy resin, filled with Al_2O_3 fillers. In total 5 plaque specimens (*spi*, *i*=1 to 5) with thickness h = 1 mm and diameter d = 80 mm were used (Fig. 5.1). All specimens were dried in the oven, at 100 °C, before they were used.

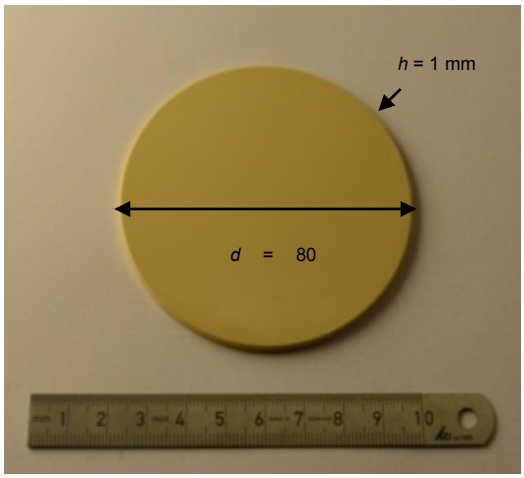

Fig. 5.1: Al_2O_3-filled epoxy plaque specimen, 1mm thickness

The material has been investigated before at the institute (TUM), from [REM-12], at 1 kV/mm and temperatures from 40 to 100 °C. The results of the volume conductivity are shown in Table 5.1 below:

ϑ (°C)	κ (S/m)
40	3,53E-15
50	6,76E-15
60	1,61E-14
70	3,89E-14
80	9,26E-14
90	1,78E-13
100	2,51E-13

Table 5.1

From the results of [REM-12], the significant influence of temperature on the volume conductivity is clear. Going from 40 to 100 °C, the conductivity is about 71 times higher. These results will also be used later and will be compared with the results of this research, in order to have a more complete profile of the influence of temperature and electric field on the material.

5.1.2. Instrumentation

The test arrangement (shown in Fig. 5.2) is in the laboratory of High Voltage Engineering and Switchgear Technology of the Technical University of Munich and consists of the following parts:

1. Climate chamber
    - Electrode setup
    - Silica gel bags for humidity control
2. Grounded cage:
    - High Resolution Electrometer
    - DC Voltage Power Supply
3. Computer for the data acquisition

The dimensions of the electrodes and the technical specifications of the instruments used in the test arrangement are analytically presented in Appendix A.

Fig. 5.2: Test arrangement for Conduction Current Measurements on Al_2O_3-filled epoxy plaque specimen, in the laboratory of High Voltage Engineering and Switchgear Technology of TUM, showing:
(1)The climate chamber, (2) The grounded cage, (3)The computer

5.1.3. Experimental procedure

The range of the examined poling fields was 2 to 12 kV/mm. At 1 kV/mm, the results were compared with the results of [REM-12]. The investigated temperatures were 40 and 80 °C. The relative humidity was always kept lower than 5 %. Three measurements were performed at each field and temperature combination. To measure stabilized DC conduction current and avoid the influence of polarization, a long measurement time was needed, especially because the samples were completely dry and their resistivity was very high. Each measurement was investigated separately and the voltage was switched off only when the current had reached steady-state. The specimens were cleaned with isopropanol before their use, to remove human fat or impurities. In order to obtain reliable and reproducible results, a depolarization procedure was applied to the sample prior to the field application, so that any residual charge could dissipate. Between consecutive measurements at different temperatures and fields, the sample was again depolarized until the depolarization current fell to negligible levels. After days of depolarization it was noticed that the minimum absolute current that was measured was about 0.6 pA. Thus, all specimens were depolarized until they reached a current of about 0.6 pA. Regarding the electrode material, the electrodes were normally made of aluminum, but a conductive silver layer was applied on both sides of the specimens.

5.2. Noise reduction

Low current measurements often encounter noise. Some possible causes of noise are the following:

- Electrostatic coupling: this occurs when an electrically charged object is brought near an uncharged object.
- Vibration can cause noise currents to flow due to the triboelectric effect.
- Offset currents usually because of temperature changes in the device and the electrometer.
- Poor contacting between the specimen and the electrodes

The elimination of noise is of great importance for the correct interpretation of the results. Thus, in order to tackle the above mentioned problems the following solutions were applied:

- The electrode set up was in the climate chamber and the inner metallic surface of the climate chamber was grounded.
- Low noise cables that cut down the friction between insulators in the cable were used for the reduction of the vibrations.
- Before every measurement the temperature was stabilized at its value.
- The electrode setup stands on special silicon pads that reduce the vibration.
- To improve the contacting between the specimens and the electrodes, conductive silver lacquer was applied on the specimens, according to the norm VDE 0303-30.

For the application of the silver, stencil patterns were used and the following procedure was performed:

Step 1: Design of stencil patterns according to the guard-ring electrode arrangement, for both sides of the specimen and printing of the stencil patterns on one sided adhesive sticker paper

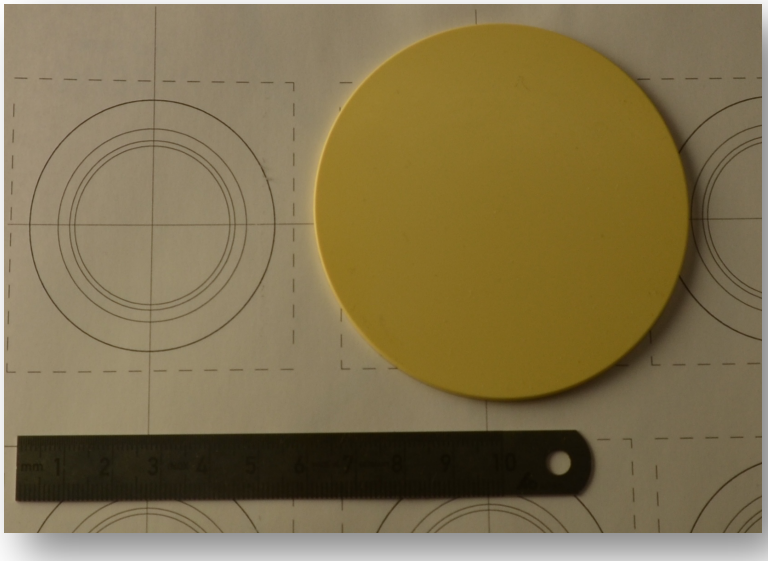

Step 1

Step 2: Cut the stencil patterns using a cutting compass

Step 2

Step 3: Placement of stencil patterns on both sides of the specimen

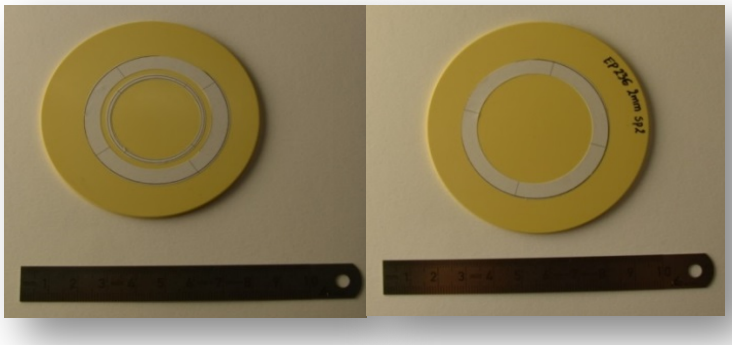

Step 3

Step 4: Color with conductive silver lacquer

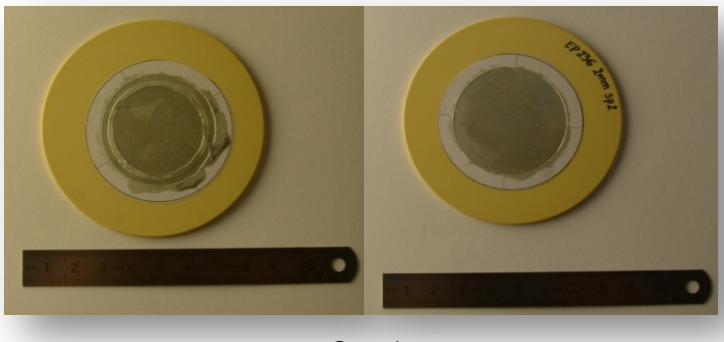

Step 4

Step 5: Put the specimen in the climate chamber for conditioning, until the silver has dried (~ 30 min)

Step 6: Take off stencil patterns and the specimen is ready for a new measurement!

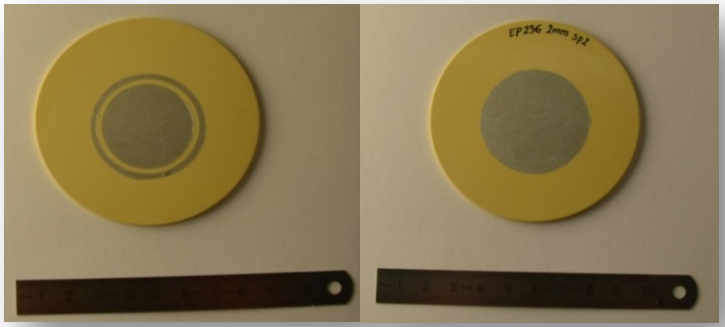

Step 6

The application of the conductive silver lacquer improved the contact between the electrode and the specimen and reduced the noise significantly. This can be seen in Fig. 5.3 below, in a measurement performed at 40 °C and 4 kV/mm.

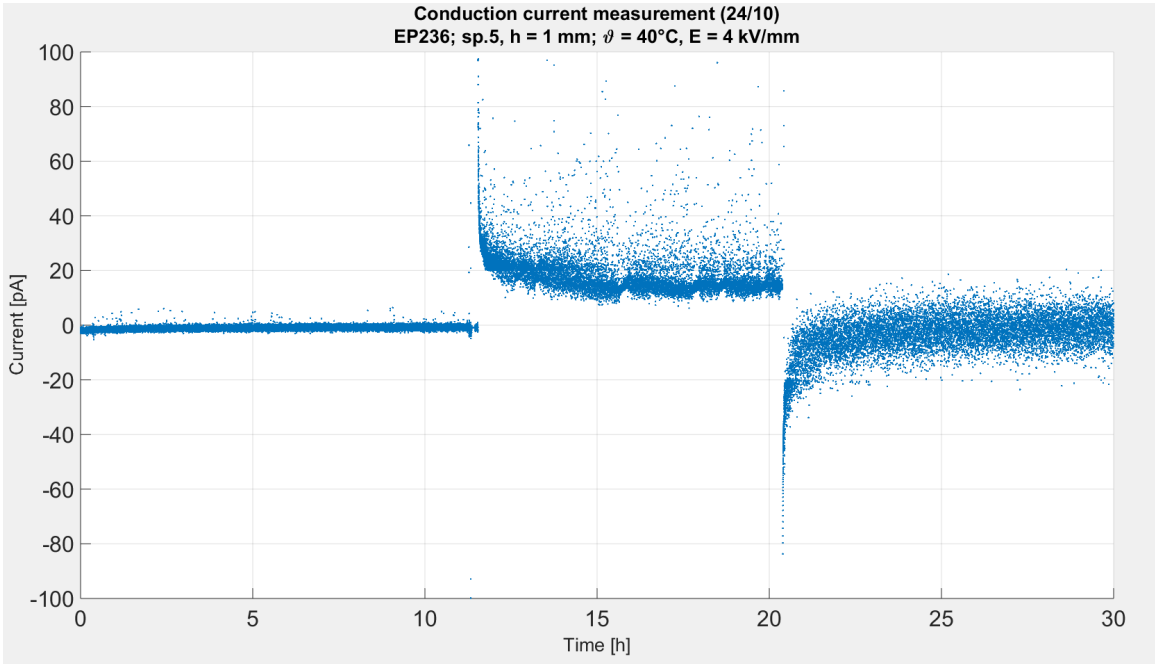

(a)

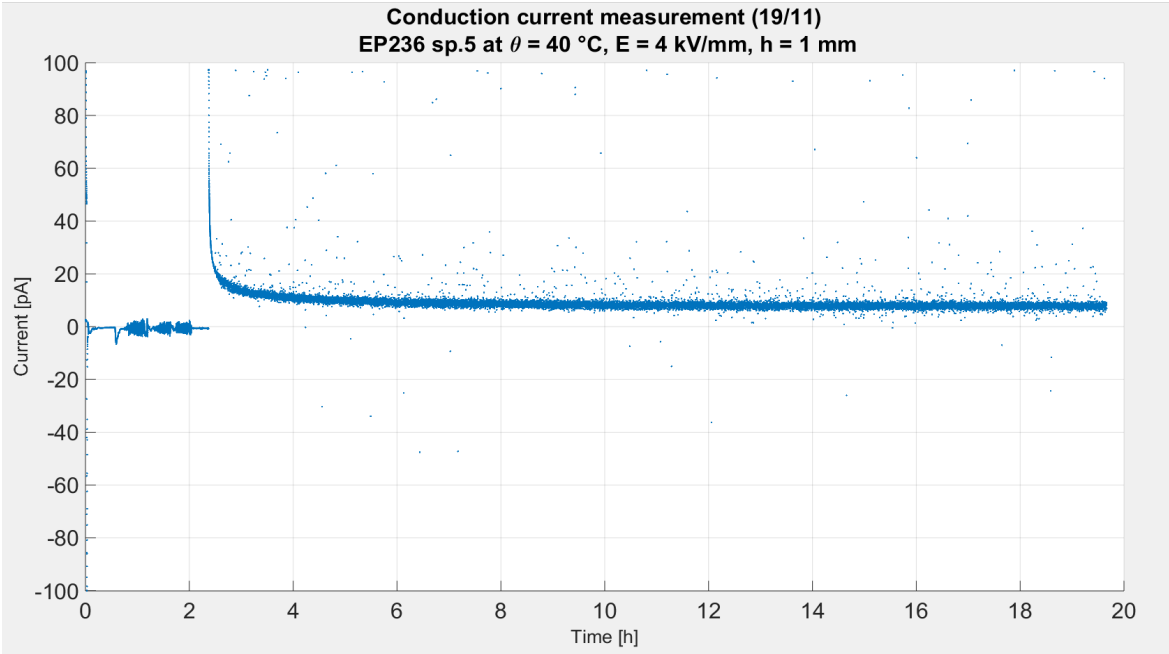

(b)

Fig. 5.3: Conduction current measurements at 4 kV/mm and 40 °C
(c) Before the application of the silver lacquer
(d) After the application of the silver lacquer

5.3. Experimental results

Using the recorded current values, the volume conductivity was calculated according to the norm, as shown in chapter 2. The table with all the results is shown in Appendix B. For the representation of the results the median and not the mean value of conductivity is used. The median value is the middle value of a list of numbers, while the mean value is the average value of a list of numbers. The median value is considered better in case of skewed distributions like this one, because of the small number of measurements at each filed and temperature combination and the random error influencing the measurements.

The effect of the applied field and temperature on the volume conductivity of the material investigation is shown in Fig. 5.4, where the median, max and min values are represented using error bars, at each field and temperature combination. Because of the big difference in the volume conductivity at 40 and 80 °C, the conductivity axis is represented in log coordinates.

As seen from the graph, the value of the volume conductivity is almost constant for fields between 1 and 6 kV/mm, at both temperatures. At 12 kV/mm the conductivity is slightly higher, but in the same magnitude. Regarding the temperature dependence, the graph clearly shows the strong temperature dependence of the volume conductivity of the studied samples. The temperature dependence will be investigated furtherly in the next paragraph.

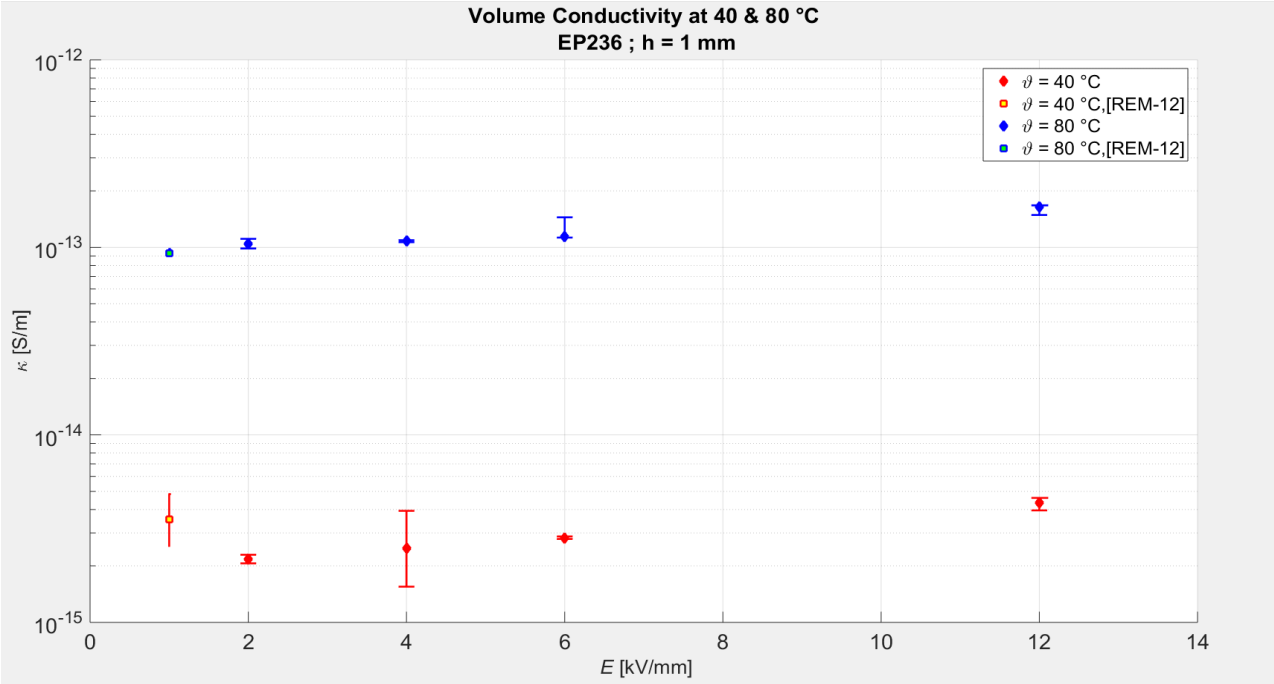

Fig. 5.4: Volume conductivity with respect to applied electric field, at 40 and 80 °C

5.3.1. Temperature dependence

Going from 40 to 80 °C, the magnitude of the conductivity is 26 to 48 times higher, which is better seen in Fig. 5.5 below.

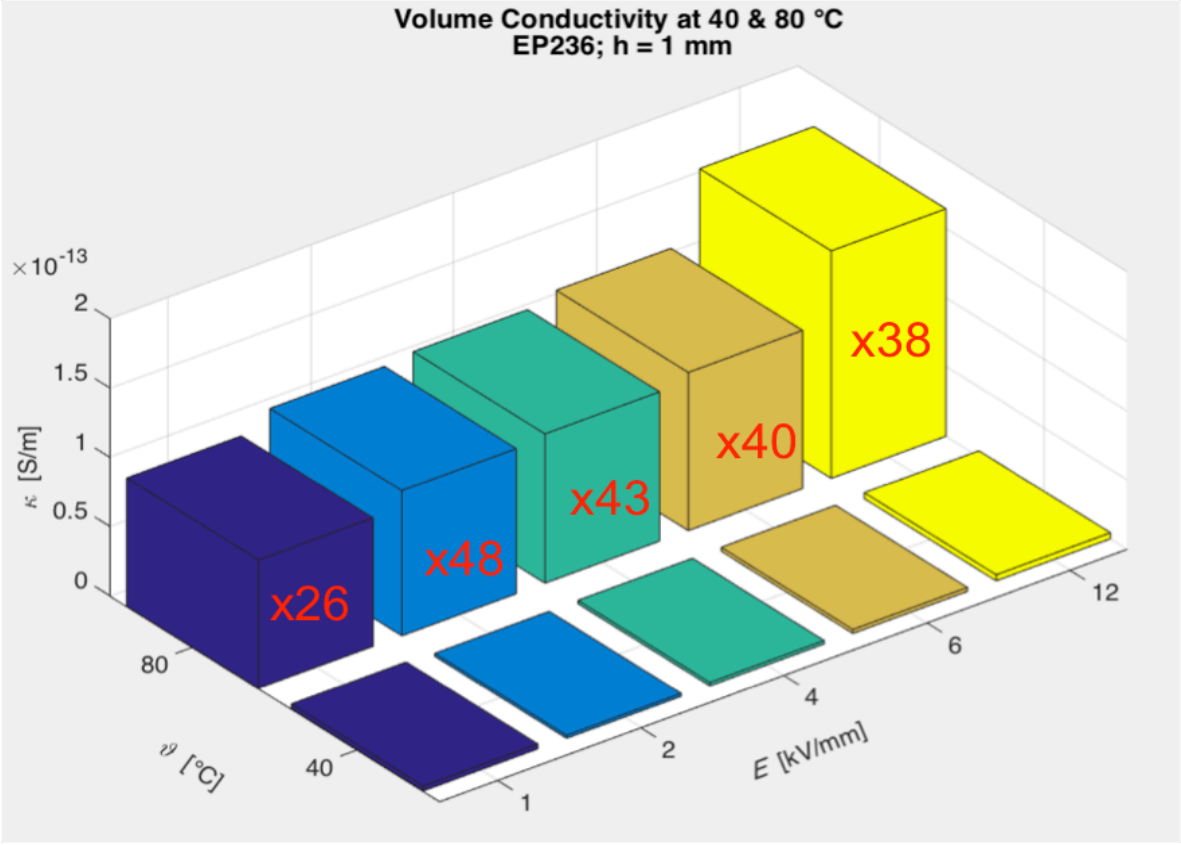

Fig. 5.5: Bar chart showing the difference in magnitude of the volume conductivity between 40 and 80 °C

The result was expected, as the volume conductivity of polymeric insulating materials is strongly dependent on the temperature and usually increases exponentially with it (Chapter 2). The strong temperature dependence of the volume conductivity of the material is also shown in [REM-12]. Going from 40 to 80 °C, at 1 kV/mm, the volume conductivity of the material is 26 times higher. Using the results of [REM-12], the volume conductivity at 1 kV/mm and temperatures from 40 to 100 °C has been plotted (Fig. 5.6 (a)) and then fitted with the Arrhenius equation (Fig. 5.6 (b)). It is to be noted that the volume conductivity of the material, at 1 kV/mm and within the range of 40 to 100 °C, fits well an Arrhenius-type relationship, giving an activation energy of 0.76 eV.

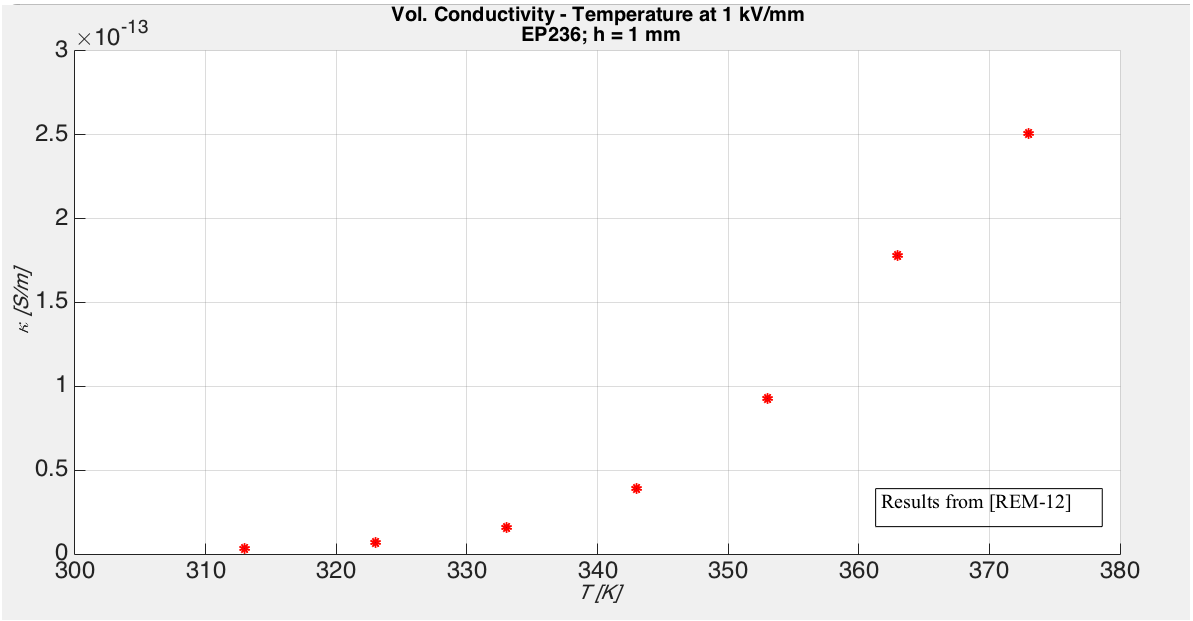

(a)

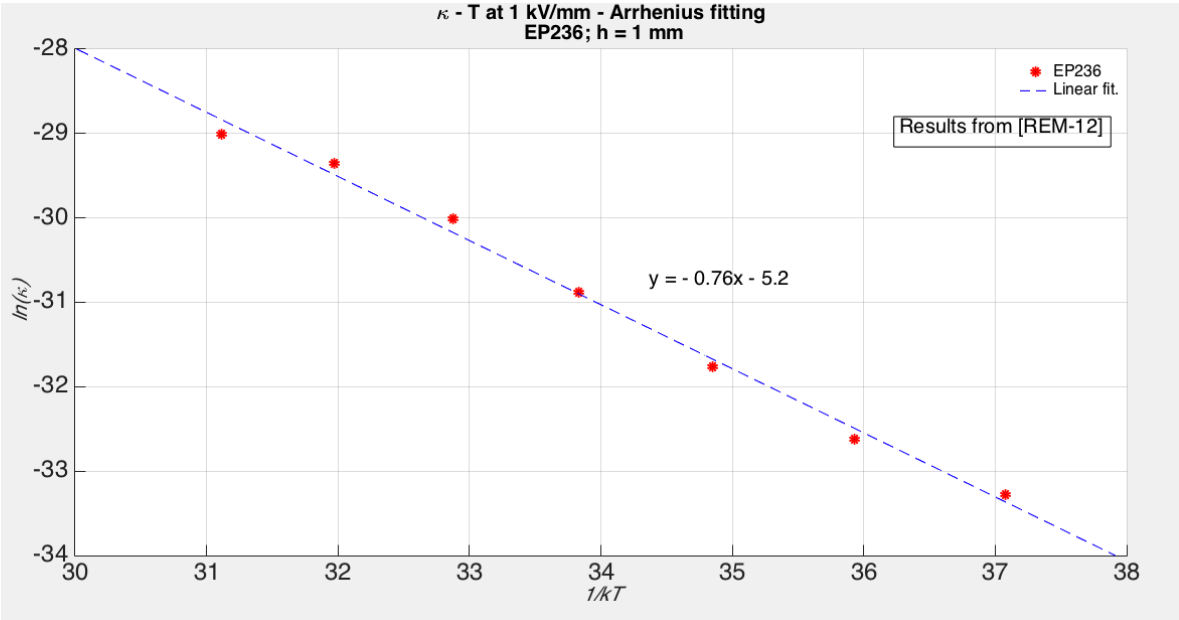

(b)

Fig. 5.6: (d) Volume conductivity with respect to temperature, at 1 kV/mm, from [REM-12]
(e) Arrhenius equation fitting at 1 kV/mm, using the results of [REM-12]

It should be noted that the activation energy is a parameter dependent on the electric field, meaning that it could be different at fields higher that 1 kV/mm. A good example is given in the study of [GAL-04] which investigates the current and space charge behavior in epoxy resin specimens under varying thermal and electric conditions, indicating an increase in activation energy as the field increases. In this case, the fitting of the Arrhenius equation proves the exponential dependence of the volume conductivity on temperature indicates the contribution of ions in the conduction, at least at low electric fields [JON-99].

5.3.2. Transient currents and dielectric response

In Fig. 5.7 below, a typical recording of the detected current is shown, with the steady-state current indicated. The specific measurement was performed at 2 kV/mm and 80 °C. The dielectric response of the material, as described in Chapter 2, is clear. The initial polarization current falls back to a steady-state current, after about 12 hours of polarization.

The time that the material needs to reach the steady-state condition decreases with temperature [PAT-08], as the polarization mechanisms are temperature dependent [KAO-04]. In our case, although the time that the material needed to reach the steady-state condition varied with temperature and field, no relation could result about the dependence of polarization time on those two parameters.

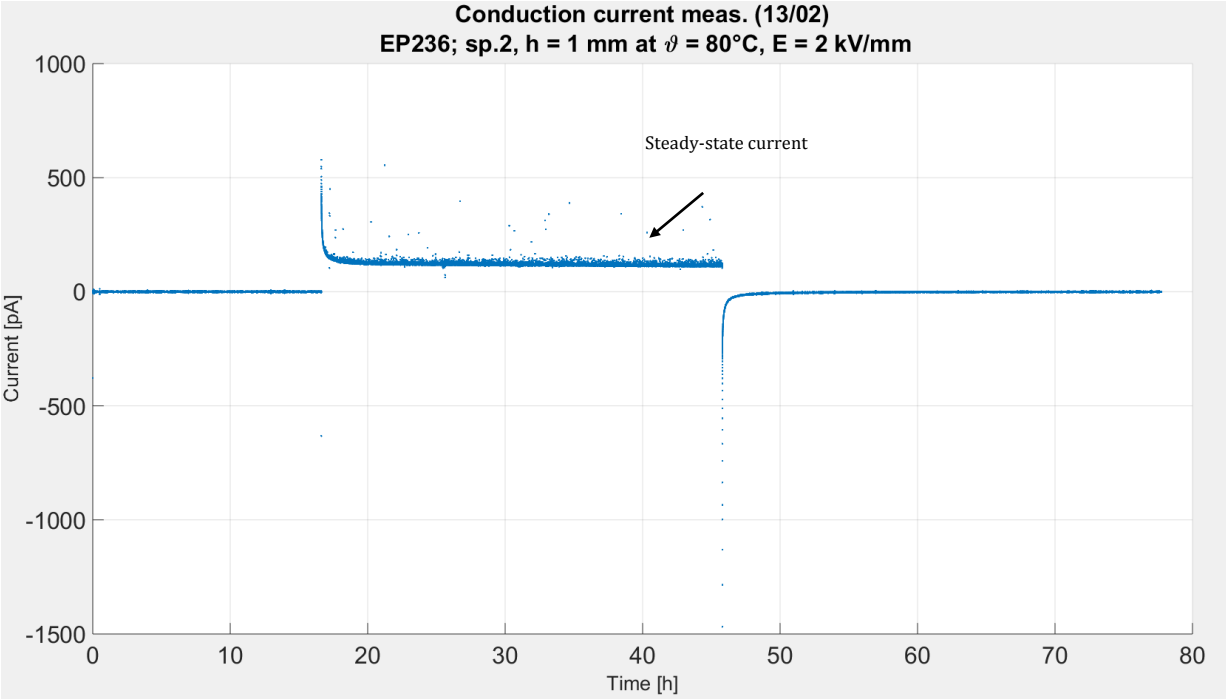

Fig. 5.7: Conduction current measurement result at 2 kV/mm and 80 °C

In Fig. 5.8 the time dependence of the charging currents at 40 and 80 °C for various fields is shown. The representation of the results is in log-log coordinates and only for the first 1000 minutes. A difference is indicated in the dielectric response of the material, depending on temperature and electric field.

At 40 °C and low fields (from 2 to 6 kV/mm) the current could be fitted with the Curie-von Schweidler law (Chapter 2). The equation used is from [LUT-11], taking into account the current one minute after polarization ($I_{1\mathrm{min}}$) and the final steady-state current (I_{ss}):

$$i_{40}(t) = (I_{1\mathrm{min}} - I_{\mathrm{ss}}) \cdot t^{-n} + I_{\mathrm{ss}} \qquad \text{Eq. 5.1}$$

The fitting of Eq. 5.2 to the results gave the following values of n:

$\vartheta = 40\ °C$			
E (kV/mm)			
	2	4	6
n	~ 0.6	~ 0.5	~ 0.4
Table 5.2			

At 12 kV/mm contrariwise, the response of the material is peculiar, indicating two different slopes, and reminding more of the General Response function (Chapter 2) with a slope of $n \sim 0.02$ for the first part, and a slope $m \sim 0.4$ for the second part.

At 80 °C on the other hand, the dielectric response of the material has the same shape for all applied fields, but indicating two different slopes, n and m, before it reaches the steady-state. The change in the slope of the graph happens at a time τ. Thus, the descending current can be described with the following equation:

$$i_{80}(t) = \begin{cases} \propto t^{-n}, & t < \tau \\ \propto t^{-m}, & t > \tau \end{cases} \qquad \text{Eq. 5.2}$$

The values of n and m for each field are shown in Table 5.3 below:

$\vartheta = 80\ °C$				
E (kV/mm)				
	2	4	6	12
n	~ 0.26	~ 0.26	~ 0.28	~ 0.29
m	~ 0.13	~ 0.11	~ 0.09	~ 0.06
Table 5.3				

It is important to note, that although the first part of the I-t response is called polarization current, at longer times, the current can still decrease for other reasons, such as [DAS-97]:

- Redistribution of space charge within the insulation bulk
- Electrode polarization
- Charge injection leading to trapped space charge effects
- Tunneling of charge from electrodes to empty charges
- Hopping of charge carriers from trap to trap from

This could also be the case here, as the investigated material is a filled polymer, where boundaries created from the host material and the fillers could lead to space charge trapping. Thus, different fields and temperatures could influence the above mentioned mechanisms and the descent of the current differently.

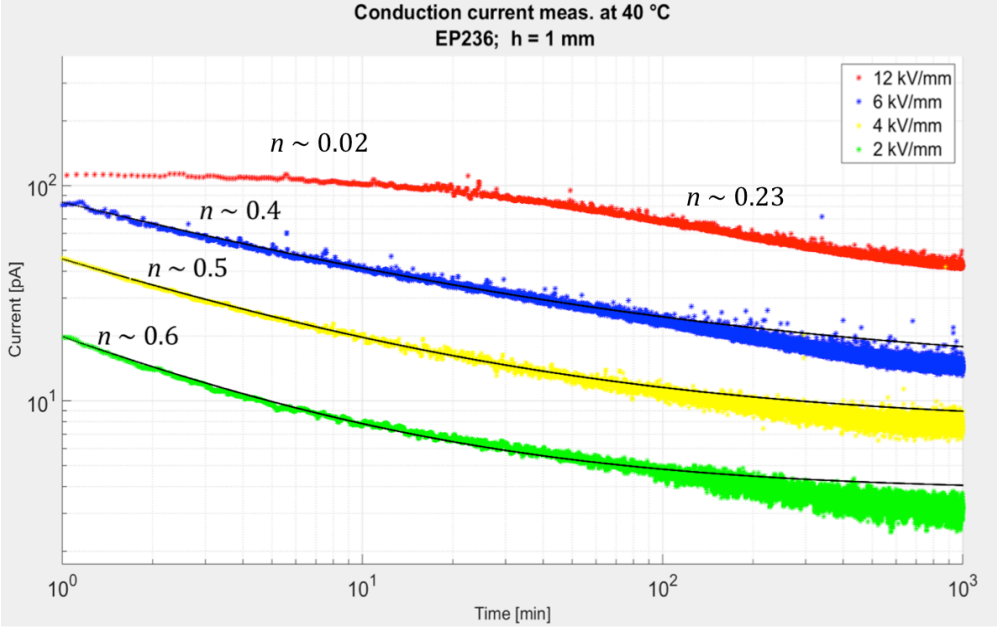

(a)

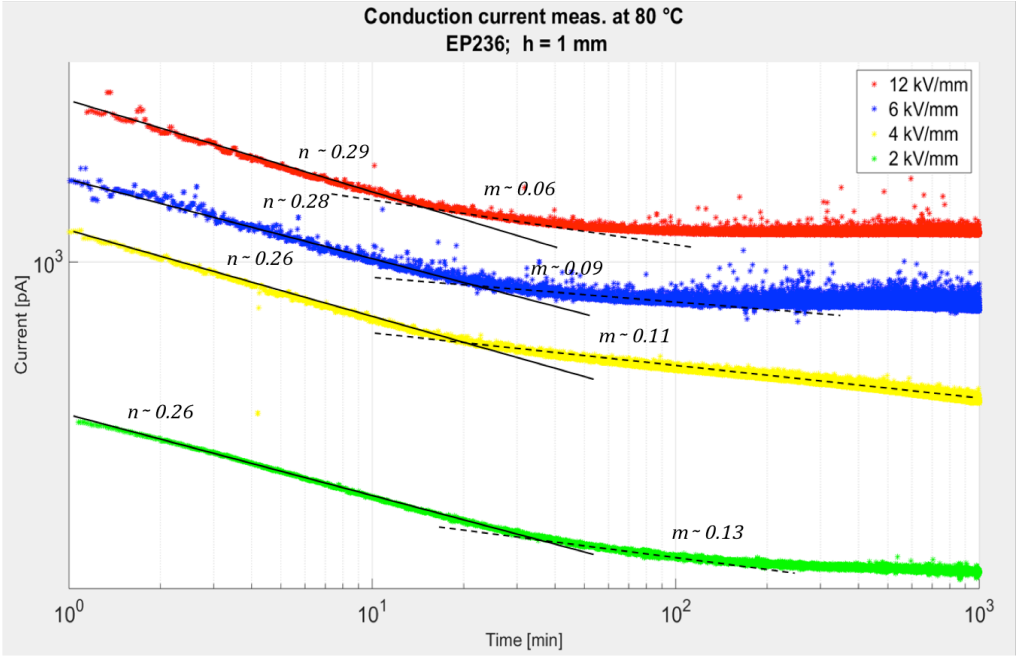

(b)

Fig. 5.8: *I-t* characteristics for the first 1000 minutes of polarization, in log-log scale:
(c) At 40 °C
(d) At 80 °C

Regarding the depolarization current, as explained in chapter 2, it normally flows in the opposite direction to the polarization current. However, under high electric fields the depolarization current can drop very rapidly and passes through the zero point. After that the current flows in the same direction as the polarization current and decays to zero gradually. The phenomenon has been experimentally observed by several researchers

[CHE-89], [MIZ-80], [PAT-90], [KIT-84]. So far no theory has been put forward except for an oversimplified model base on the bipolar charge injection [KIT-84].
The results on our material showed that the depolarization current flew always at the opposite direction of the polarization current.

5.3.3. Steady-state currents analysis

The steady-state current densities at 40 and 80 °C are plotted in log-log coordinates as a function of the applied electric field in Fig. 5.9. A good first step for the analysis of conduction currents consists of looking for a power law $I \sim E^a$ [GUI-06]. The curves in Fig. 5.9 point out a possible difference in the conduction mechanisms at low and high fields. At low fields (from 1 to 6 kV/mm), the linear interpolation of the results yields a slope of ~ 1.2 at 40 °C and of ~ 1.08 at 80 °C. At 12 kV/mm the current is higher than it would be, if the slope of the characteristic continued to be 1.2 and 1.08 at 40 and 80 °C respectively. In particular, it is 28.6 % higher at 40 °C and 33% higher at 80 °C (see Fig. 5.9). The change in the slope could indicate the inception of a high-field non-linear region (as discussed in chapter 4), with a threshold field between 6 and 12 kV/mm. Nevertheless, the difference between the expected and the real value is not big enough in order to interpret the results with certainty. Higher fields have to be investigated, and more measurements at each temperature-field combination have to be performed in order to eliminate the random measurement errors as much as possible. During this research, measurements at 16 kV/mm were tried, but failed due to the introduction of partial discharges. Furthermore, an impermanent damage of the measuring instrument as well as time limitations did not allow the performance of more measurements at each temperature-electric field combination.

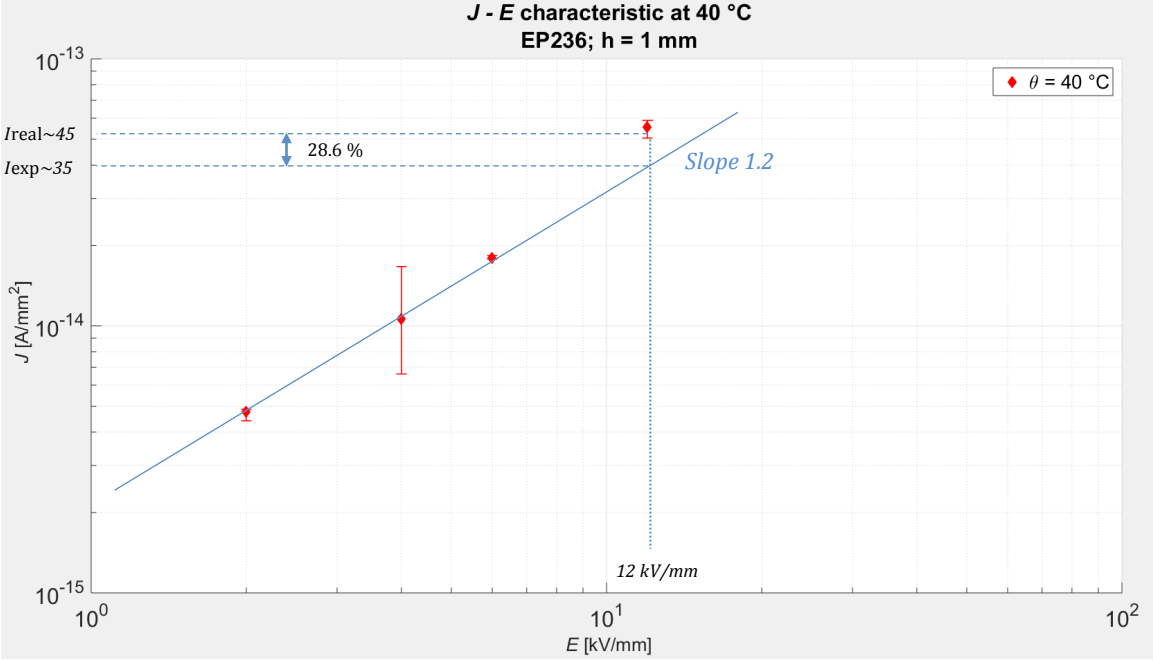

(a)

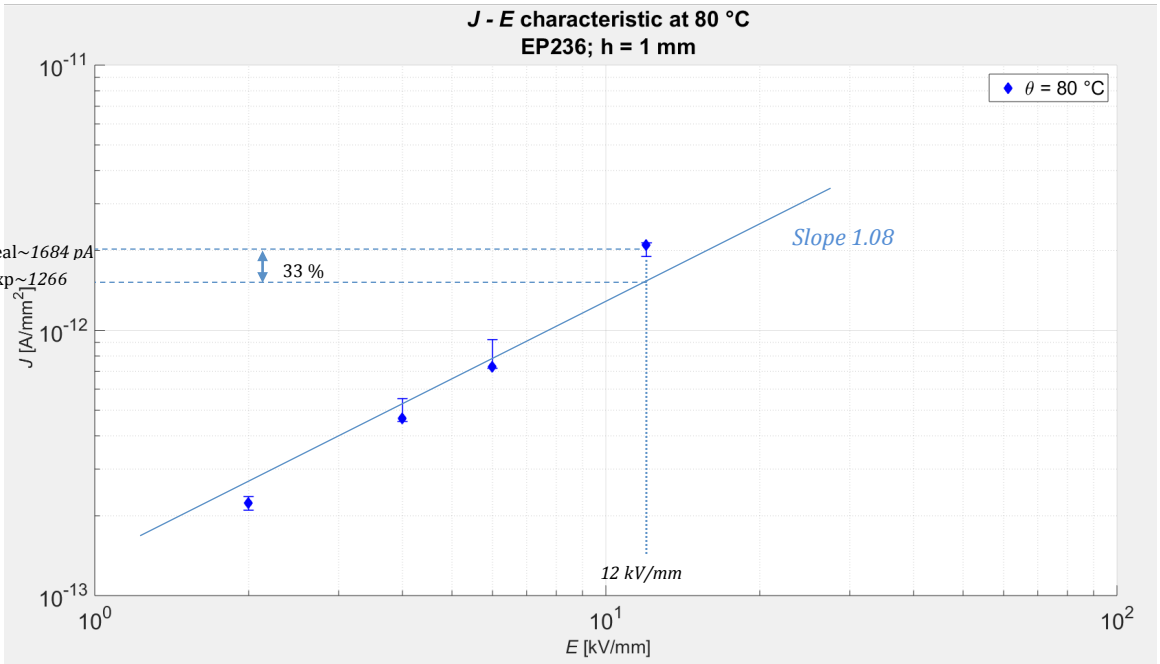

(b)

Fig. 5.9 | Current density with respect to electric field
(c) At 40 °C
(d) At 80°C

As explained in Chapter 4, the conduction currents can give us information about the conduction mechanisms occurring in the material. This is the goal here: using the results up to 12 kV/mm, the bulk and contact conduction phenomena will try to be fitted, as it was shown in Chapter 4. The slopes of 1.2 and 1.08 at 40 and 80 °C respectively refer to an almost Ohmic conduction, leaving however room for other mechanisms to occur. Bulk and contact phenomena discussed in Chapter 3, are examined here separately.

Bulk phenomena:

1. Space charge limited currents (SCLC)

The basic SCLC model at high electric fields is represented from the equation:

$$J = \frac{9}{8}\varepsilon_0\varepsilon_r\mu\frac{V^\alpha}{L^3} \qquad \text{Eq. 5.3}$$

where the current density is proportional to the square of the voltage. According to the SCLC theory, the case of $\alpha = 2$ corresponds to either a lack of traps or to a single trap distribution. The extension of the SCLC gives $\alpha > 2$, which corresponds to traps with multiple levels in the material. In order to examine the suitability of the SCLC model, the *J-E* characteristic must be plotted in log-log coordinates. If the slope of the characteristic is about 1 at low fields and 2 or greater at high fields, then the SCLC is a possible mechanism. That would indicate the accumulation of space charge in the bulk of the material, as the SCLC model bases the nonlinearity of the *J-E* characteristic at high fields on the intensive formation of space charge above a threshold field.

However, as seen in Fig. 5.9, the slope of the *J*-*E* characteristic in the field range between 2 and 6 kV/mm is 1.2 at 40 °C and 1.08 at 80 °C, indicating a low-field, almost Ohmic conduction region. At 12 kV/mm the resulting current is higher, indicating the inception of a high-field conduction region, but no slope can be found from the existing results.

The SCLC model is not suitable for the investigated field and temperature range, but has to be further investigated at higher fields, as the value of the current at 12 kV/mm indicates the inception of a high-field conduction region. The best way to validate the SCLC theory is of course the performance of both conduction current and space charge measurements as well as the comparison of the threshold field indicated from these two methods. In addition, as the SCLC theory is strongly dependent on the thickness specimen (see Eq. 5.3), the performance of conduction current measurements using specimens with different thicknesses could also show the presence and especially the intensity of the mechanism.

2. Poole-Frenkel Mechanism

In the Poole-Frenkel mechanism, barriers that are localizing carriers within the dielectric are lowered by the applied electric field (Chapter 3). The current density is given by:

$$J = \sigma_0 E \exp\left[-\frac{\beta_P E^{1/2}}{2kT}\right] \qquad \text{Eq. 5.4}$$

In order to examine if the Poole-Frenkel mechanism is present in the material for the investigated field and temperature values, the results have to be plotted in a $\ln(J/E) = \ln(\kappa)$ versus $E^{1/2}$ graph, and if the mechanism is present, it should give a straight line and sensible values for the unknown fitting parameters. At 1kV/mm, the results of [REM-12] are used. The fitting of the Poole-Frenkel mechanism is shown in Fig. 5.10 below and does not yield a straight line, suggesting that the model is not suitable in this case.

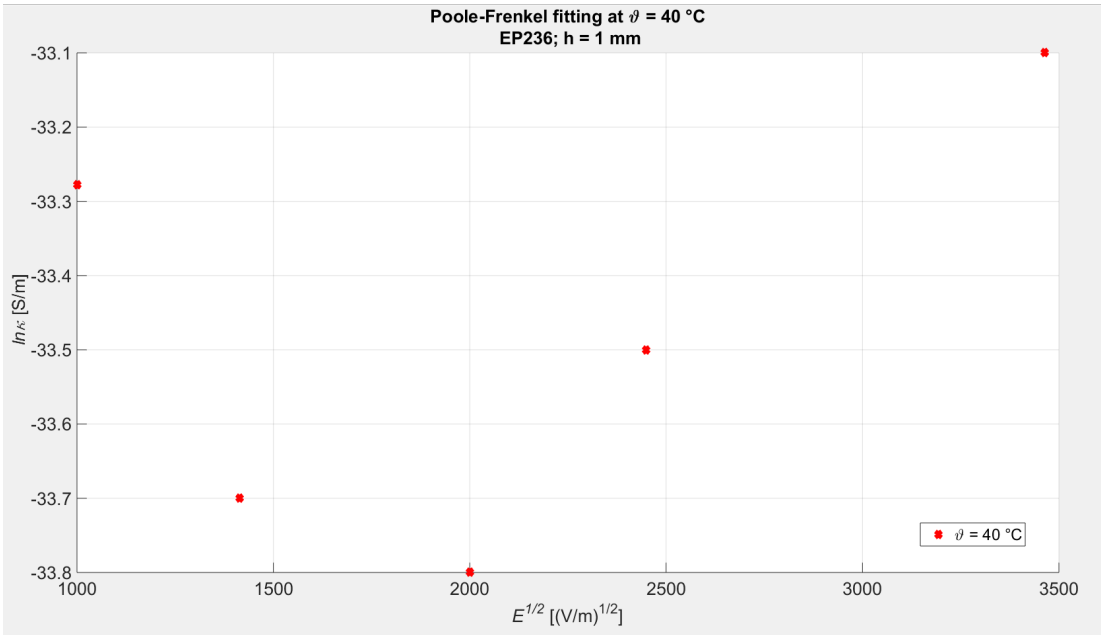

(a)

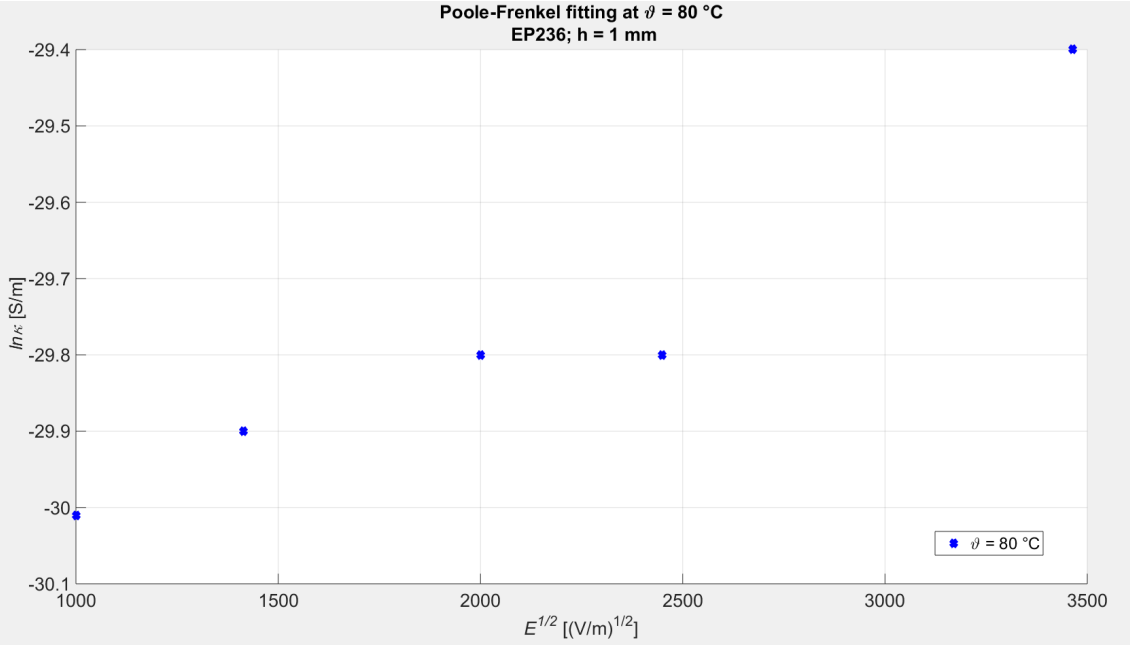

(b)

Fig. 5.10: For the investigation of the Poole-Frenkel mechanism, the ln(J/E) versus $E^{1/2}$ characteristic is plotted:
(c) At 40 °C
(d) At 80 °C

3. Bulk ionic conduction

In the Bulk ionic conduction model the current density is related to the field as follows:

$$J = J_0 \sinh\left(\frac{\lambda q_i E}{2kT}\right) \qquad \text{Eq. 5.5}$$

where E is the electric field, λ is an ionic jump distance, q_i is the ionic charge, and T is the absolute temperature. The applicability of this model has been investigated in several studies, giving the following values for λ:

Material		λ (nm)	Study
Epoxy resin	Unfilled	4	[GUI-06]
	Filled	5.6	
PVC		1.65-4.5	[KOS-71]
Epoxy resin unfilled		22.3	[CAO-88]
Polyether ether ketone		5	[DAS-87]
Epoxy resin unfilled		1.04	[GRI-00]
HDPE		0.9	[MIZ-79]
PET		6.9	[AMB-62]
Epoxy resin	Unfilled	9.8	[KRI-12]
	Filled	13.8-23	

Table 5.4

Summarizing, the value of the jump distance in epoxy samples is in the range of 1.04 to 23 nm. In order to find out if the specific mechanism takes place in the investigated material, the current density J has to be plotted with respect to sinh $(\lambda q_i E/2kT)$ for values of λ between 1.04 and 23 nm. However, in this case, the ionic charge is not known, as the exact composition of the material is not known. So, no conclusion can come out about the suitability of the Bulk ionic conduction model.

Contact phenomena

4. Schottky Injection

The Schottky injection model assumes field-assisted thermo-ionic injection of electrons from the electrodes into the conduction band of the material. The current density is described by:

$$J = A_s T^2 \exp\left\{-\frac{\left[\Phi_0 - \beta_s (E)^{\frac{1}{2}}\right]}{kT}\right\} \qquad \text{Eq. 5.6}$$

Φ_0 is the height of the potential barrier at the metal-dielectric interface without any applied field, or, more precisely, the barrier that the electronic carrier has to overcome, in order to leave the metal and enter the polymer.
The Schottky constant is given by:

$$\beta_s = \left[\frac{q^3}{4\pi\varepsilon_0\varepsilon_r}\right]^{\frac{1}{2}} \qquad \text{Eq. 5.7}$$

with $\varepsilon_r = 5$. In order to examine, if the Schottky effect is present in the material for the investigated field and temperature values, the results have to be plotted in a $logJ$ versus E graph, and if the mechanism is present, it should give a straight line and sensible values for the unknown fitting parameters. This is true, as seen in Fig. 5.11. The Eq. 5.6 takes the following form:

$$\boldsymbol{logJ} = \underbrace{\frac{\beta_s}{kT}}_{\boldsymbol{a_i}} \boldsymbol{E^{1/2}} + \underbrace{logA_s T^2 - \frac{\Phi_0}{kT}}_{\boldsymbol{b_i}} \qquad \text{Eq. 5.8}$$

and the coefficients a_i, b_i are found from the linear interpolation of the plotted results in Fig. 5.11.

The values of the parameters used are shown in Table 5.5:

$\boldsymbol{A_s}$	1.2×10^6	$A\, m^{-2} K^{-2}$
$\boldsymbol{T}$	313,353	K
$\boldsymbol{\beta_s}$	2.71×10^{-24}	$C\, V^{1/2} m^{1/2}$
$\boldsymbol{k}$	1.38×10^{-23}	$J\, K^{-1}$

Table 5.5

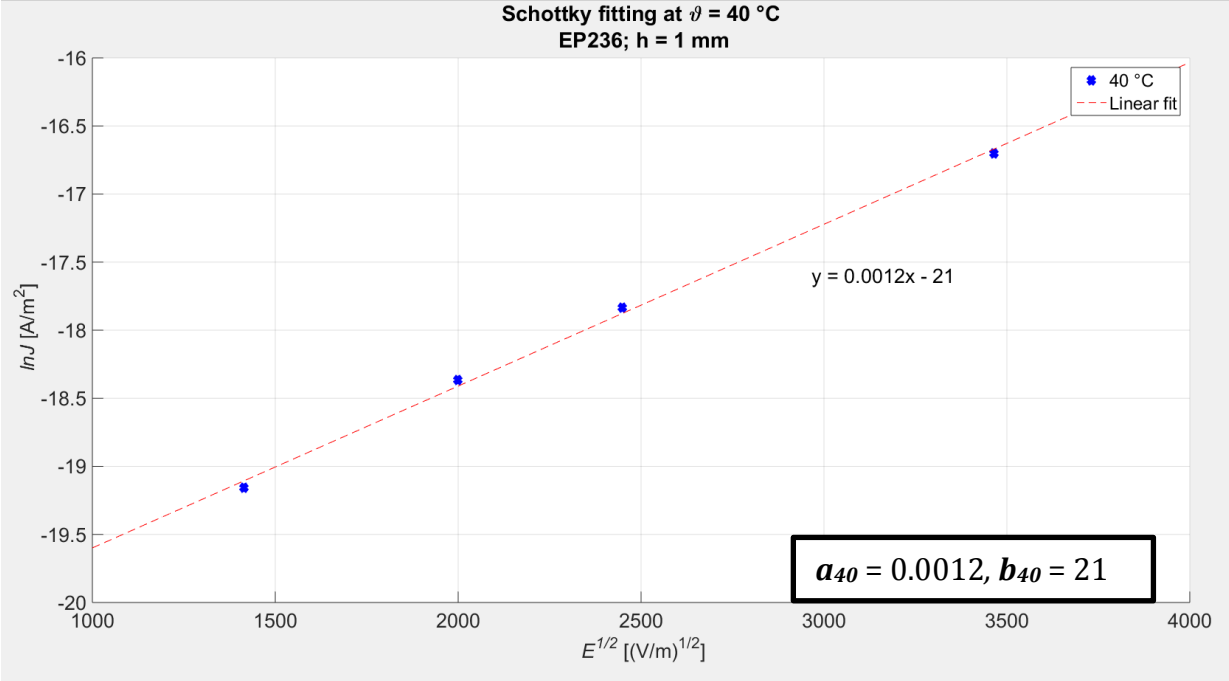

(a)

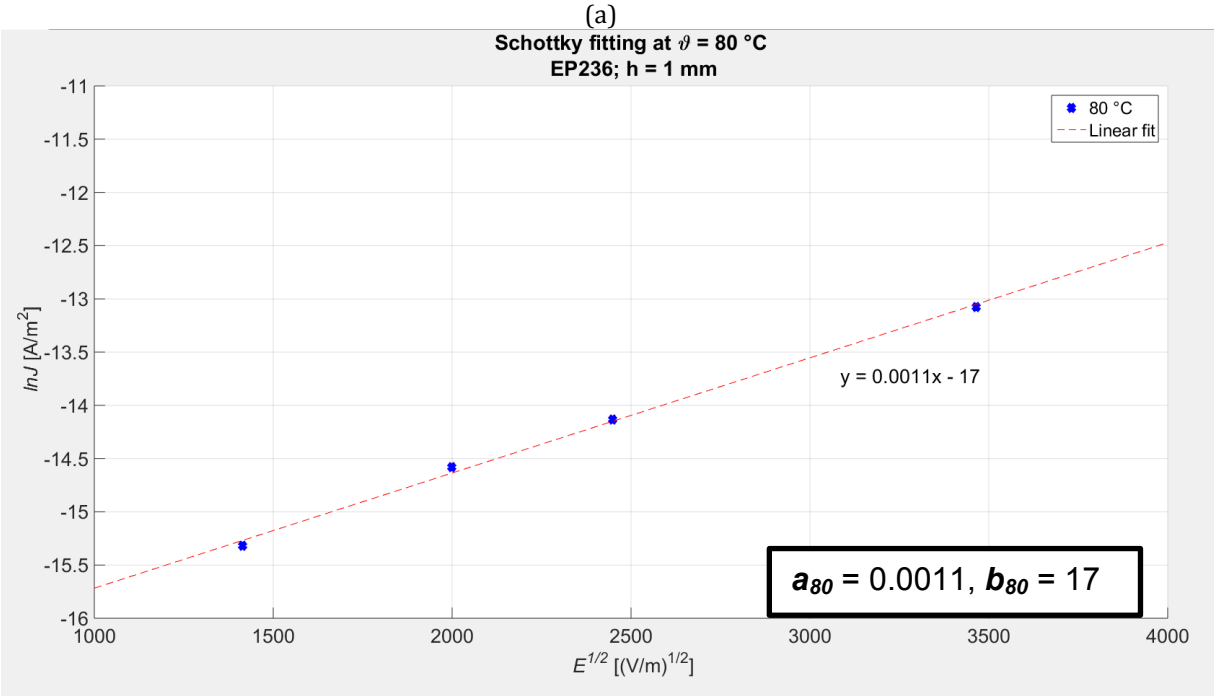

(b)

Fig. 5.11: For the investigation of the Schottky mechanism, the ln(J) versus $E^{1/2}$ characteristic is plotted:
(a) At 40 °C
(b) At 80 °C

The value of A_s is calculated using the electron mass and charge, which means that we are testing the case of electronic injection. Using Eq. 5.6 we calculate the unknown variables:

ϑ (°C)	Φ_0 (eV)	ε_r
40	1.25	1.36
80	1.29	1.56
Table 5.6		

The calculated values for Φ_0 are in a reasonable range, in agreement with previous measurements (e.g. [LEN-66], [KRI-12]). The value of ε_r on the other hand is much lower than the theoretical value, ε_r= 5. A possible explanation is that the field that we used in Eq. 5.6 (Schottky) is not the real field at the metal-dielectric interface, but the Laplace field. Assuming a Laplacian field at the interface could lead to wrong conclusions, as the accumulation of space charge at the interface can create a strong distribution of the field there. This is also shown in the study of [KRI-12], where both space charge and conduction current measurements are performed. The fitting of the latter leads to the presence of the Schottky emission, while the fist proves the presence of great space charge at the metal-dielectric interfaces at both the anode and the cathode. The effect of the field divergence at the electrode-dielectric interface can be taken into account by a multiplying factor γ, which expresses the difference of the field at the electrode over the charge-free value [LEN-66]:

$$E_c = \gamma \frac{V}{L} \qquad \text{Eq. 5.8}$$

Now, using the theoretical value of ε_r = 5, the γ parameter is calculated by:

$$\gamma = (slope\ kT)^2 4\pi\varepsilon_0\varepsilon_r/q^3 \qquad \text{Eq. 5.9}$$

The calculated values of γ are shown in Table 5.7 and are reasonable, compared to previous investigations like [KRI-12], in which it is indicated that the value of γ > 1 shows heterocharge at the positive electrode, which tends to decrease the energy barrier at the contact. However, only the performance of space charge measurements could validate the presence of Schottky emission and the suspicion for space charge accumulation near the electrodes.

ϑ (°C)	γ
40	3.65
80	3.22
Table 5.7	

5. Fowler-Nordheim Injection

The Fowler-Nordheim Injection assumes injection of electrons from the electrodes to the material through tunneling. The current density is described as:

$$J = BE^2 \exp\left[-\frac{C\varphi^{\frac{3}{2}}}{E}\right] \qquad \text{Eq. 5.10}$$

If the Fowler-Nordheim injection is present in the material, the log(J/E²) versus 1/E should give a straight line. This is not true, as seen in Fig. 5.12 below:

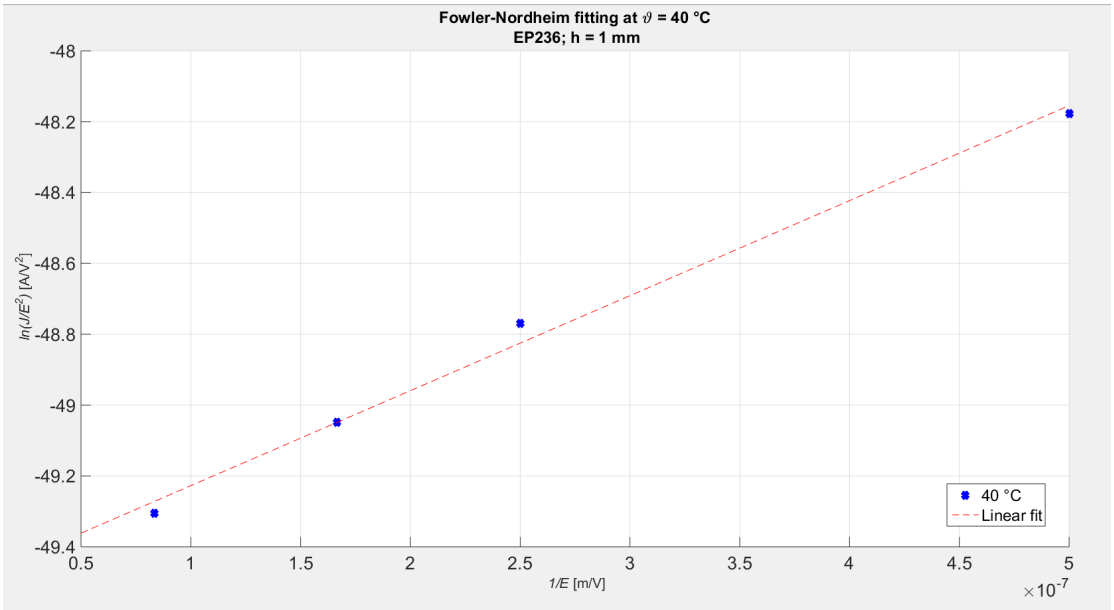

(a)

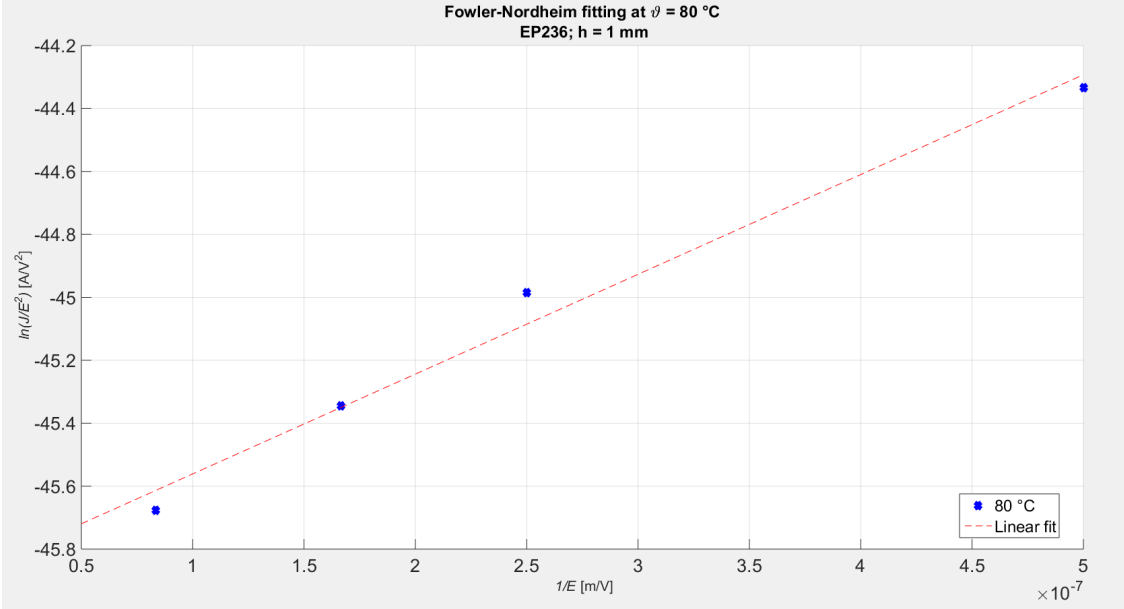

(b)

Fig. 5.12 | For the investigation of the Fowler-Nordheim mechanism, the ln(J/E²) versus E^{-1} characteristic is plotted:
(a) At 40 °C
(b) At 80 °C

As seen from graph 5.12, the Fowler.Nordheim mechanism does not fit as good as the Schottky emission, which was expected, as the specific mechanism requires fields of at least 100 kV/mm.

5.4. Conclusions and suggestions for further research

Conduction current measurements varying temperature and electric field provided useful information on the volume conductivity of the material and its dependence on the investigated parameters. Regarding the temperature dependence, the difference between the investigated temperatures was significant. At double temperature the resulting conductivity was 26 to 48 times higher. The fitting of the results of [REM-12] with an Arrhenius equation, at 1 kV/mm, leads to the conclusion of a dominating ionic conduction at low fields. Regarding the electric field, no obvious transition from low to high field mechanisms was revealed for the investigated fields. However, the fact that the slope of the J-E characteristic in a log-log scale was not exactly 1, gave room for the investigation of other mechanisms than the simple Ohmic conduction. These mechanisms can be either bulk or injection. Trying to fit the results with these mechanisms, only the Schottky effect fitted the results quite well, leading to possible electronic conduction due to charge injection at fields higher than 1 kV/mm. In addition, from the Schottky effect, a space charge accumulation is indicated that has to be investigated.

Although a lot of information is given from the results, the narrow range of the investigated fields does not allow us to be sure about the correct interpretation of them. Conduction current measurements at higher fields have to be performed, for the investigation of high field mechanisms taking place. In addition, with the performance of space charge measurements as well, a validation could come out for the suitability of Schottky effect and the creation of heterocharge. Space charge measurements could validate or deny the applicability of the SCLC theory at higher fields, as it is directly connected to the presence of space charge. Another experimental method that could give useful information regarding the trapping sites in the material is the method of Thermally Stimulated Depolarization Currents (TSDC). Three experiments using this method have also been tried in this thesis, in order to examine its potential for further research. These will be presented in the next chapter.

6. Thermally Stimulated Currents (TSC)

6.1. Theory of TSC spectroscopy

As explained in Chapter 3, polymers are materials with complicated physical structure, containing trapping sites in the forbidden gap (FG), between the valence band (VB) and the conduction band (CB). In addition, the concentration of traps is greater at the area near the electrodes, as the presence of surface roughness, imperfect contact etc. (discussed in paragraph 3.5) introduces traps as well, and these traps are numerous and deeper [VEL-95], [VELL-95].

The presence of these traps leads to the existence of trapped charges in the material. These charges, come either from injection at the contacts, or are introduced to the material from manufacturing (e.g. ions coming from making process). Either way, traps can help in the conduction process through these disordered materials when the carriers are thermally activated. In this case, the carriers are detrapped and contribute to the conduction current through hopping from trap to trap.

The Thermally Stimulated Current (TSC) spectroscopy is a method to characterize shallow and deep trapping levels in insulating and semiconducting materials [MAN-11]. Except for storage phenomena, TSC measurements have been used in the past in order to study decay phenomena, dipolar relaxation events, space charge redistribution and the migration of ionic charges.

The TSC spectroscopy is divided into two methods: the Thermally Stimulated Polarization Current method and the Thermally Stimulated Depolarization Current method (TSDC). Both consist of measuring, with a definite heating rate, the currents generated by the buildup (TSPC) and the release (TSDC) of a polarized state of a dielectric [VAN-82]. In this thesis, only the TSDC method is considered.

In order to perform TSDC, the same test arrangement as in Conduction current measurements can be used (see Fig. 6.1). The procedure for the performance of a TSDC consists of the following steps:

i. The sample is excited, either by photoexcitation or by strong field injection from the electrodes. In the framework of this thesis, only the latter will be used. So, as the first step: a polarization voltage (V_p) at a polarization temperature (T_p) for a polarization time (t_p) is applied.
ii. The sample is cooled to a deposit temperature (T_d), while the polarization voltage is still switched on, and stays at this temperature for some time (t_d), until homogenous temperature conditions are achieved.
iii. Finally, the polarization voltage is switched off, and the temperature is elevated gradually, usually with a constant heating rate, from T_d to a maximum temperature (T_{max}).

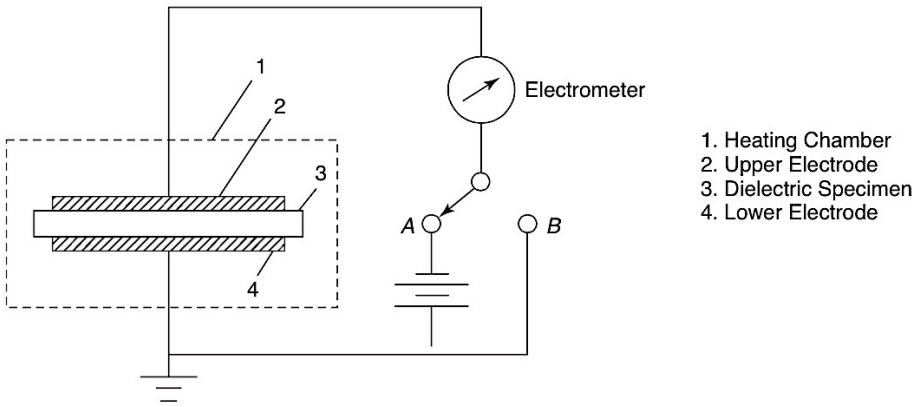

Fig. 6.1: Test arrangement for the performance of Thermally Stimulated Depolarization Currents (TSDC), from [KAO-05]

6.2. Experimental procedure

A quite different experimental procedure was followed here. The plaque EP236 specimen was heated at 80 degrees and then polarized at 12 kV/mm. A usual conduction current measurement was performed (as described in Chapter 2), and when the current had reached steady-state, the voltage source was switched off. The specimen was then depolarized for almost 2 days, at 80 °C. After this long depolarization period, the temperature was gradually increased from 80 to 150 °C, with steps of 10 °C. The climate chamber needed 10 minutes to increase the temperature by 10 °C, and then the temperature was kept constant for another 10 minutes before it was increased again (see Fig. 6.2 (a)). After the completion of this procedure, the specimen was cooled down to 80 °C and was kept at this temperature for 1 hour. Then, the temperature was increased again to 150 °C, two times, following the same heating rate.

The results of the measurements are shown in Fig. 6.2 below:

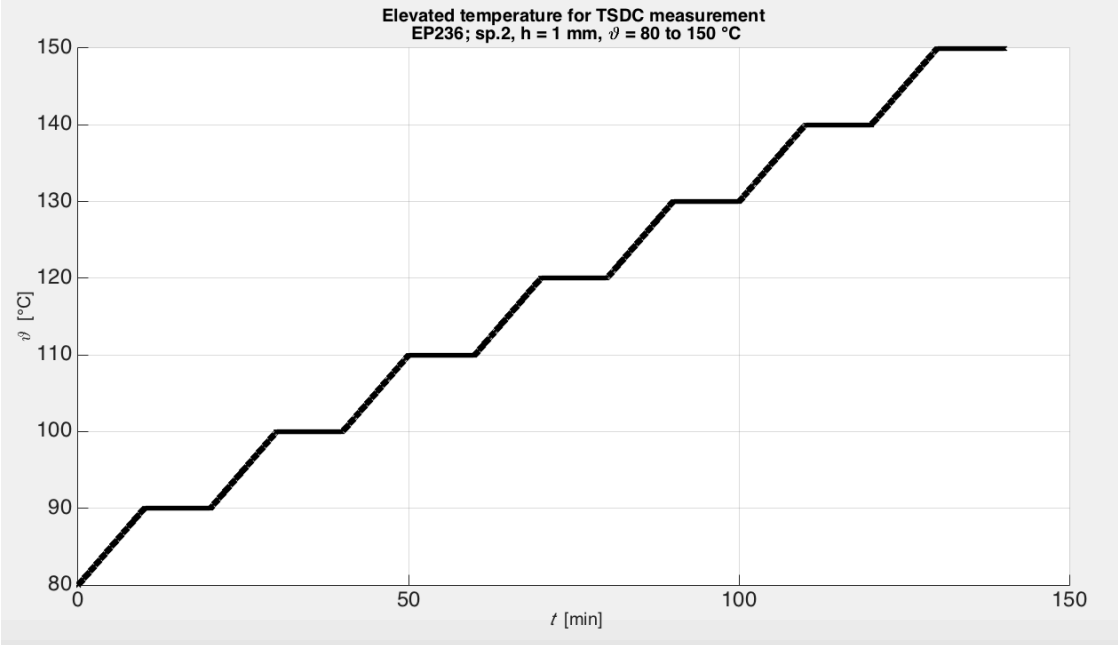

(a)

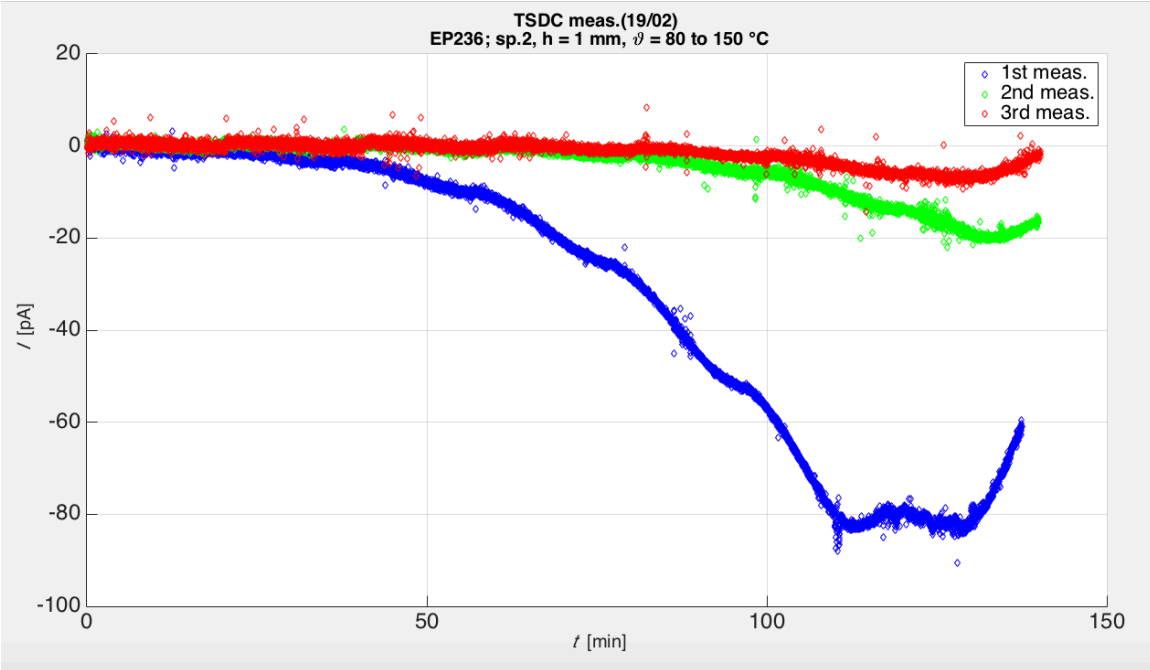

(b)

Fig. 6.1 Thermally Stimulated Depolarization Current measurement (TSDC) on EP236:
(a) Heating rate, from 80 to 150 °C
(b)Three subsequent depolarization current measurements with temperature elevated from 80 to 150 °C

6.3. Conclusions

From the TSDC measurements, we expect the thermal emission of trapped carriers through heating. When a trapped carrier acquires the required thermal energy, it leaves the trap and contributes to the conduction current. This detrapping is identified in the TSDC *I-t* characteristic with distinct peaks. The TSDC measurement on the investigated material revealed two peaks (at about 110 and 130 °C) the first time, and one peak (at about 140 °C) the second and third time. It can be, thus, said that there is charge trapped in the material, which is gradually detrapped due to thermal excitation of the carriers in the volume of the material. These peaks can be related to the activation energies of the associated traps. Equations have been developed in previous studies (e.g. [FAN-05], [LOO-83]) in order to calculate these activation energies. However, these equations are not further investigated here. It is also to be noted that the reason that such a long depolarization time was selected was to avoid the influence of depolarization mechanisms on the measured current. Especially because, as mentioned above, this method is also suitable for the investigation of relaxation times in solids.

The results deriving from the TSDC are very interesting and can provide useful information on the trapping sites of the material. Thus, further investigation is suggested. It is also proposed to use UV light illumination of the material prior TSDC performance (as in [MAN-11]), in order to fill the traps and enhance the detrapping phenomena observed later.

7. Appendix A

Technical specifications of the Conduction Current Measurement setup for plaques

- High resolution electrometer

Manufacturer	Keithley
Model	6517B
Measuring range	10aA – 21mA

Fig. A1: Keithley 6517B Electrometer

4. DC High Voltage Power Supply

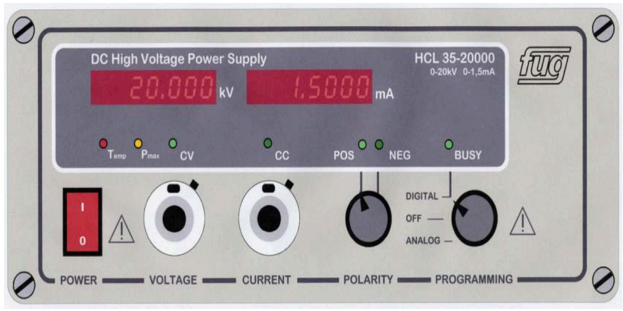

Manufacturer	FUG
Model	HCL 350-12500
Input	230 ± 10% V 47-63 Hz
Output	12.5 kV 25 mA

Fig. A2: FUG HCL 350-12500 DC High Voltage Power Supply

- Electrode arrangement

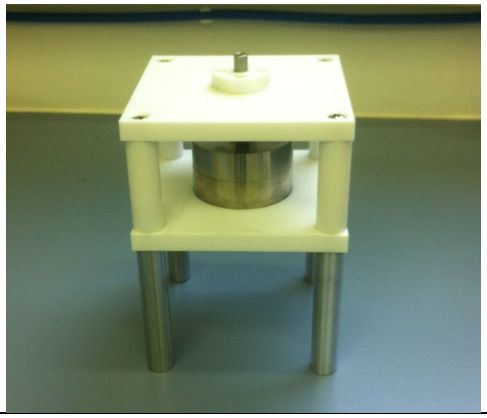

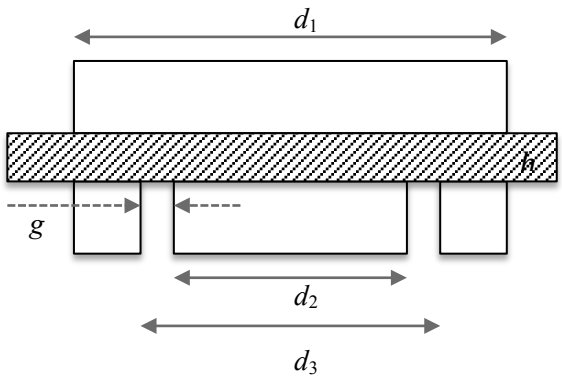

d_1 = *40 mm*, d_2 = *32 mm*, d_3 = 34 mm, g = 1 mm

Electrode material: Aluminum

Fig. A3: Electrode arrangement for plaque specimens

5. Climate chamber

Manufacturer	WEISS
Model	WK3 – 180/40
Input	230 ± 10% V 50 Hz
Temperature range	-42 to 180 °C

Fig. A4: WEISS WT3 Climate chamber

6. Computer with the suitable software (LabVIEW) for the data acquisition

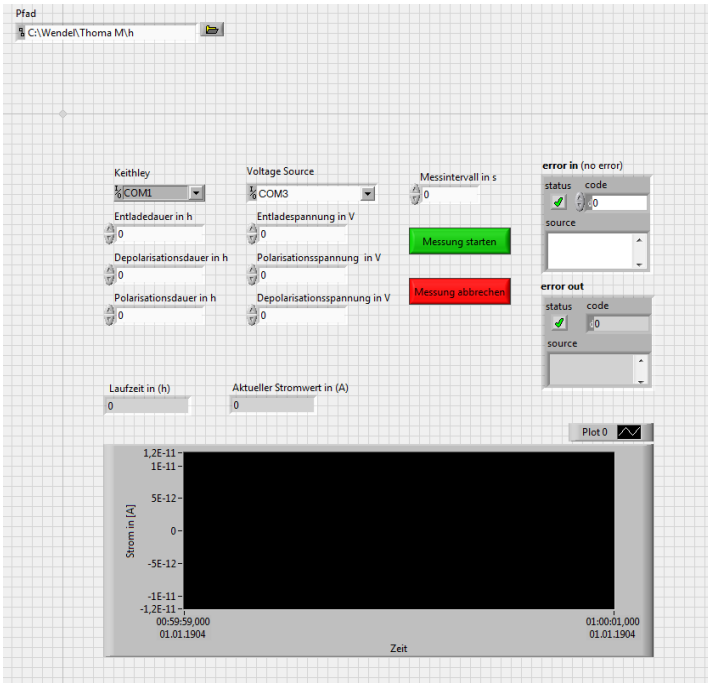

LabVIEW 2009
Values pm. : ~ 75

Fig. A5: LabVIEW file for the data acquisition and recording

- Keithley protection circuit

Adding a resistor and two diodes (1N3595) as shown in Fig. x.y below will provide considerable extra protection. The resistance must be large enough (x MOhms in our case) to limit the current through the diodes to 10 mA or less. It must also be large enough to withstand the supply voltage. The protection circuit should be enclosed in a light-tight conductive shield [Keithley-2].

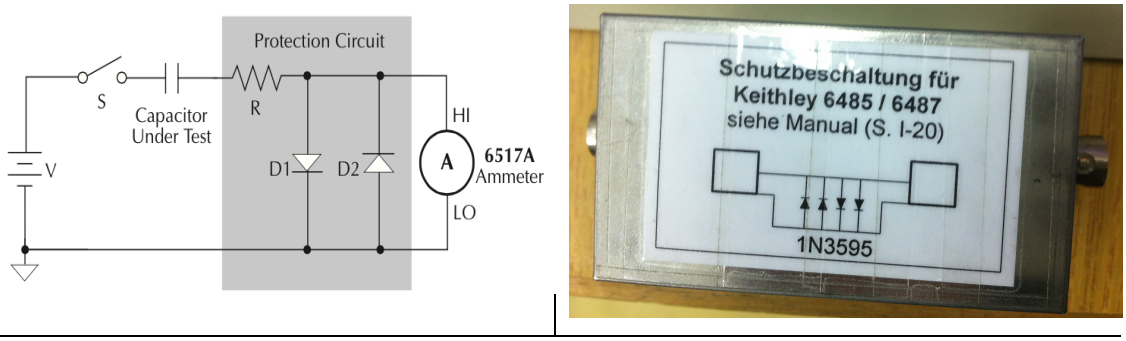

D1,D2: 1N3595 Diodes, R = 47 MOhms

Fig. A6: Keithley 6517B Diode protection circuit

- Humidity control

In order to control the humidity of the environment (climate chamber) and keep it at low levels (< 5%), silica gel bags are used. These silica gels are firstly put in the oven at 100 °C for at least 24 hours and then in the climate chamber.

Fig. A7: Silica gel bags for the control of humidity

8. Appendix B

Experimental results from the conduction current measurements on Al_2O_3 – filled epoxy specimens

E = 2 kV/mm

Steady-state current I_{ss} (pA)					
ϑ (° C)	**sp1**	**sp2**	**sp3**	**sp4**	**sp5**
40	3.5		3.84		3.92
80		113.13	189.86		168.70
Volume Conductivity κ (S/m)					
ϑ (° C)	**sp1**	**sp2**	**sp3**	**sp4**	**sp5**
40	2.06 E-15		2.24 E-15		2.29 E-15
80		6.61 E-14	1.11 E-13		9.86 E-14

E = 4 kV/mm

Steady-state current I_{ss} (pA)					
ϑ (° C)	**sp1**	**sp2**	**sp3**	**sp4**	**sp5**
40	5.33		13.46		8,49
80	364.50		444.74		373.46
Volume Conductivity κ (S/m)					
ϑ (° C)	**sp1**	**sp2**	**sp3**	**sp4**	**sp5**
40	1.55 E-15		3.58 E-15		2.09 E-15
80	1.07 E-13		1.30 E-13		1.09 E-13

E = 6 kV/mm

Steady-state current I_{ss} (pA)					
ϑ (° C)	**sp1**	**sp2**	**sp3**	**sp4**	**sp5**
40	14.75	14.45	14.19		
80	578.54		742.08		586.23
Volume Conductivity κ (S/m)					
ϑ (° C)	**sp1**	**sp2**	**sp3**	**sp4**	**sp5**
40	2.87 E-15	2.82 E-15	2.76 E-15		
80	1.13 E-13		1.45 E-13		1.14 E-13

E = 12 kV/mm

Steady-state current I_{ss} (pA)					
ϑ (° C)	**sp1**	**sp2**	**sp3**	**sp4**	**sp5**
40	44.72		47.74		40.63
80	1527.85		1718.66		1684.10
Volume Conductivity κ (S/m)					
ϑ (° C)	**sp1**	**sp2**	**sp3**	**sp4**	**sp5**
40	4.35 E-15		4.65 E-15		3.96 E-15
80	1.49 E-13		1.67 E-13		1.64 E-13

Note: For currents lower than 20 pA, the final depolarization current prior voltage application is added to the final steady-state conduction current I_{ss}.

9. Bibliography

[AMP-62] L. E. Amborski, "Structural dependence of the electrical conductivity of polyethylene terephthalate", Journal of polymer science, Vol. 62, 1962

[AND-10] Thomas Andriatsch, Roman Kochetov, Peter H. F. Morshuis and Johan J. Smit, "DC Conduction in epoxy based nano- and mesocomposites", Delft University of Technology, the Netherlands, 2010 annual report conference on electrical insulation and dielectric phenomena

[BAER-10] Ronald Bärsch, Andreas Küchler, "Beanspruchungen und elektrisches Verhalten von Isoliersystemen bei Gleich- und Mischfeldbeanspruchungen", 2010, Köln

[BLY-05] T. Blythe, D. Bloor, "Electrical properties of polymers", 2nd edition, Cambridge university press, 2005

[BOD-04] R. Bodega, G. C. Montanari, P. H. F. Morshuis, "Conduction current measurements on XLPE and EPR insulation", 2004 Annual Report Conference on Electrical Insulation and Dielectric Phenomena

[BOG-01] Steven Boggs, Fellow, IEEE, Dwight H. Damon, Jesper Hjerrild, Joachim T. Holboll, Senior Member, IEEE, and Mogens Henriksen, Senior Member, IEEE, "Effect of Insulation Properties on the Field Grading of Solid Dielectric DC Cable"

[BOG-93] S. A. Boggs, IEEE Trans. EI 28, 115 (1993)

[BOG-95] S. A. Boggs, IEEE Trans. DEI 2, 97 (1995)

[BÖT-85] H. Böttger and V. V. Bryskin, Hopping Conduction in solids, Akademie-Verlag, Berlin, 1985

[BRU-06] Jerilyn Brunson and J. R. Dennison, "E-field conditioning and charging memory in Low density polyethylene", American physical society four corner section meeting, Utah State University, Logan, UT, October 6-7-2006

[CAS-11] J. Castellon, H. N. Nguyen, S. Agnel, A. Toureille, M. Frechette, S. Savoie, A. Krivda, L. E. Schmidt, "Electrical properties analysis of micro and nano composite epoxy resin materials", IEEE Transactions on Dielectrics and Electrical Insulation, Vol. 18, No. 3; June 2011

[CHA-08] Ch. Chakradhar Reddy and T. S. Ramu, "on the DC conductivity of HVDC cable insulation, cautions in using the empirical models", Department of electrical engineering, Indian institute of science Bangalore, India, 2008

[CHE-09] G. Chen, "Anomalous phenomena in solid dielectrics under high electric fields", 9th international conference on properties and applications of dielectric materials, IEEE, 2009, Harbin, China

[CHE-89] G. Chen, H. M. Banford, R. a. Fouracre, D. J. Tedford, "Electrical conduction in low density polyethylene", 3rd international conference on electrical conduction and breakdown in solid dielectrics, pp. 277-281, 1989

[CHO-08] W. Choo, G. Chen, Electric field determination in DC polymeric cable in the

presence of space charge and temperature gradient under dc conditions, University of Southampton, School of electronics and computer science, United Kingdom, 2008

[CHO-10] W.Choo, G.Chen and S.G.Swingler, "Electric Field in Polymeric Cable due to Space Charge Accumulation under DC and Temperature Gradient", School of Electronics and Computer Science, University of Southampton, SO17 1BJ, United Kingdom

[CHR-10] Thomas Christen, Lise Donzel, and Felix Greuter, "Nonlineal Resistive Electric Field Grading Part 1: Theory and Simulation", ABB Switzerland, Corporate Research, Baden-Daettwill, Switzerland

[CHR-12] Thomas Christen, Nonstandard High-Voltage Electric Insulation Models, ABB Corporate Research, Theoretical physics

[CHR-98] Thomas Christen, "Charge injection instability in perfect insulators", ABB Corporate Research, Baden-Dättwil Switzerland, 1998

[CIGRE-01] CIGRE Working group 15.01.09, Dielectric response methods for diagnostics in power transformers, 2001

[COE-93] R. Coehlo and B. Aladenize, "Les Dielectriques", Hermes, Paris, 1993

[DAK-06] T. W. Dakin, Conduction and polarization mechanisms and trends in dielectrics, Formerly with Westinghouse Research labs, Pittsburgh, PA

[DAK-72] T. W. Dakin et al., CIGRE Rep. 15-04, 1972 Session

[DAK-74] T. W. Dakin, "Application of epoxy resins in electrical apparatus", IEEE Transactions on electrical insulation. Vol. EI-9, pp. 121-128, 1974

[DAS-12] Supriyo Das and Nandini Gupta, Department of Electrical Engineering, Indian institute of technology Kanpur, India, 2012 IEEE

[DAS-87] D. K. Das-Gupta, K. Doughty, "Dielectric and conduction processes in polytherether ketone (PEEK)", IEEE, 1987

[DAS-97] Dilip K. Das-Gupta, "Conduction mechanisms and high field effects in synthetic insulating polymers", IEEE Transactions on dielectrics and electrical insulation, School of electronic engineering and computer systems, Universioty of Wales, Bangor, UK, April 1997

[DIS-05] L. A. Dissado, C. Laurent, G. C. Montanari, P. H. F. Morshuis, "Demonstrating a threshold for trapped space charge accumulation in solid dielectrics under DC field", IEEE Trans. On DEI, vol. 12, no. 3, pp. 612-620, 2005

[DIS-92] L. A. Dissado and J. C. Fothergill, "Electrical degradation and breakdown in polymers", (Peter Peregrinus Ltd., London, 1992)

[DIS-97] L. A. Dissado, G. Mazzanti, G. C. Montanari, "The role of trapped space charges in the electrical ageing of insulating materials", IEEE Trans. Dielectr. Electr. Insul., Vol. 4, pp. 496-506, 1997

[DOM-12] Domininghaus, H.: Kunststoffe, Eigenschaften und Anwendungen, 8. Aufl., Springer-Verlag, 2012

[DWY-73] J. J. O'Dwyer, "The theory of electrical conduction and breakdown in solid dielectrics", (Clarendon Press, 1973)

[FAB-09] D. Fabiani, G. C. Montanari, L.A. Dissado, C. Laurent, G. Teyssedre, "Fast and slow packets in polymeric materials under DC stress", IEEE Transactions on Dielectrics and Electrical Insulation, Vol. 16, No 1; February 2009

[FAN-05] Z. Q. Fang, B. Claflin, D. C. Look, L. Polenta, W. C. Mitchel, "Thermally stimulated current spectroscopy of high-purity semi-insulating 4H-SiC substrates", Journal of electronic materials 34, pp. 336-340, 2005

[FAS-05] Fasching, G.: Werkstoffe für die Elektrotechnik, 4. Aufl., Wien: SpringerWienNewYork, 2005

[GAL-04] O. Gallot-Lavallée, G. Teyssedre, C. Laurent, S. Rowe, "Current and Space Charge Behaviour in an Epoxy Resin under Thermo-Electric", 5th Int. Conf. on Electric Charges in Non-Conductive Materials, Tunisia, 2004

[GIL-92] R. Gilbert, J. P. Crine, B. Noirhomme and S. Pelissou, "Measurement of organic and inorganic ions in cable insulation and shields". Proc. IEEE Conf. Electrical Insulation and Dielectric Phenomena, Leesburg, 18-20 Oct 1992, pp. 235-240

[GRE-14] R. Gremaud, F. Molitor, C. Doiron, T. Christen, U. Riechert, U. Straumann (ABB Switzerland Ltd. Switzerland)), R. Källstrand, K. Johansson, O. Hjortstam (ABB AB Sweden), Solid insulation in DC Gas-insulated Systems, CIGRE 2014, D1-103

[GRI-00] V. Griseri, K. Fukunaga, C. Laurent, D. Mary, L. A. Dissado, J. C. Fothergill, "Charge injecti, on, electroluminescence, and againg of an epoxy resin in high divergent fields", Dielectric materials, measurements and applications, No. 473, IEEE 2000

[GU-09] Jin GU, Xuguang LI, "Calculation of Electric Field and Temperature Field Distribution in MVDC Polymeric Cable", School of Electronic Information and Electrical Engineering, Shanghai Jiao Tong University, Shanghai, 200240, China

[GUI-06] Transient and steady-state currents in epoxy resin, Christophe Guillermin1,2, Pascal Rain2,3 and StephenW Rowe1, Published 20 January 2006, J. Phys. D: Appl. Phys. 39 (2006), pp. 515–524

[HIB-86] T. Hibma and H. R. Zeller, J. Appl. Phys. 59, 1614 (1986)

[HJE-01] Jesper Hjerrild, Steven Boggs, J. T. Holboll and M. Henrisken, "DC-field in solid dielectric cables under transient thermal conditions", 7th International Conference on Solid Dielectrics, June 25-29, 2001, Eindhoven, the Netherlands

[HO-01] Y. F. F. Ho, G. Chen, A. E. Davies, R. N. Hampton, S. G. Swingler and S. J. Sutton, "Do semicons affect space charge?" Prot. Int. Conf. Solid Dielectrics, Eindhoven, 25-29 June 2001, pp. 105-108

[HOF-91] R. Hoffmann, C. Janiak and C. Kollmar, "A chemical approach to the orbitals of organic polymers", Macromolecules, Vol. 24, pp. 3725-3746, 1991]

[IED-71] Masayuki Ieda, Goro Sawa, Sousuke Kato, “A consideration of the Poole-Frenkel effect on electric conduction in insulators”, Journal of applied physics, Vol. 42, No. 10, 1971

[IED-84] M. Ieda, “Electrical conduction and carrier traps in polymeric materials”, IEEE Transactions on electrical insulation Vol. EI-19, Department of electrical engineering, Nagoya University, Nagoya, Japan, June 1984

[JON-83] A. K. Jonscher, Dielectric relaxation in solids, Chelsey Dielectrics Press, 1983

[KAH-89] Manfred Kahle, “Elektrische Isoliertechnik”, Springer, 1989

[KAO-04] Kwan Chi Kao, “Dielectric phenomena in solids, with emphasis on physical concepts of electronic processes”, 2004

[KAS-01] Safa O. Kasap, “Principles of electronic materials and devices”, McGraw-Hill Science/Engineering/Math; 2 edition (July 18 2001)

[Keithley-01] Keithley Application note series, Volume and surface resistivity measurements of insulating materials using the model 6517A electrometer/high resistance meter, 2001

[KIT-84] I. Kitani, Y. Tsuji, A. Arii, “Analysis of anomalous discharge current in low density polyethylene”, Japan, Journal of applied physics, Vol. 23, pp. 855-860, 1984

[KNA-08] P. Knauth, Joop Schooman, “Nanocomposites: Ionic conducting materials and structural spectroscopies”, Springer, 2008

[KOS-71] Masamitsu Kosaki, Koichi Sugiyama, Masayuki Ieda, “Ionic jump distance and glas transition of polyvinyl chloride”, Journaal of applied physics, Vol. 24, No. 9, 1971

[KRE-95] F. H. Kreuger, Industrial high DC voltage. Delft University Press, 1995. F

[KRI-12] A. Krivda, T. Tanaka, M. Frechette, J. Castellon, D. Fabiani, G. C. Montanari, R. Gorur, P. Morshuis, S. Gubanski, J. Kindersberger, A, Vaughn, S. Pelissou, Y. Tanaka, L. E. Schmidt, G. Iyer, T. Adriatsch, J. Seiler, M. Anglhuber, “Characterization of epoxy microcomposite and nanocomposites materials for power engineering applications”, IEEE Electrical insulation magazine, 2012

[LAM-70] M. A. Lampert and P. Mark, “Current injection in Solids”, Academic Press, New York, 1970

[LAU-05] Lautenschläger, K-H, W. Schröter, A. Wanninger, “Taschenbuch der Chemie”, Frankfurt am main: Verlag Harri Deutsch, 2005

[LEN-66] G. Lengyel, “Schottky emission and conduction in some organic insulating materials”, Journal of applied physics, volume 37, number 2, February 1966

[LES-73] K. J. Less and E. G. Wilsor, “Intrinsic photoconduction and photoemission in polyethylene”, J. Phys. C: Solid state Phys., Vol. 6, pp. 3110-3120, 1973

[LOO-83] D. C. Look, "The electrical and photoelectronic properties of semi-insulating

GaAs", Semiconductors and semimetals, pp. 75-170, 1983

[LOV-74] R. Lovell, „Decaying and steady-state currents in an epoxy polymer at high electric fields“, J. Phys. D.: Appl. Phys., Vol. 7, 1974

[LUT-10] A. Lutz, J. Kindersberger, Lehrstuhl für Hochspannungs- und Anlagentechnik, Technische Universität München, Munich, Germany, 2010 International conference on solid dielectrics, IEEE, Potsdam, Germany], [STI-84, U. Stietzel, Untersuchungen zum Einfluss von von Feuchtigkeit auf die elektrischen Eigenschaften organisher Isolierstoffe für Freiluft-Hochspannungs-Anwendung, Dissertation, Technical University of Braunschweig, 1984

[LUT-11] B. Lutz, „ Einflussfaktoren auf die elektrische Feldverteilung in Isoliersystemen mit polymeren Isolierstoffen bei Gleichspannungsbelastung“, Doktor-Ingenieur Dissertation, Technische Universität München, Lehrstuhl für Hochspannungs- und Anlagentechnik, 2011

[MAC-00] J. W. Mackersie, M. J. Given and R. A. Fouracre, The electrical properties of filled and unfilled commercial epoxy resins, University of Strathelyde, United Kingdom, Dielectric Materials, measurements and applications conference Publication No. 473, IEEE 2000

[MAC-01] J. W. Mackersie, M. J. Given, S. J. MacGregor and R. A. Fouracre, The electrical properties of filled epoxy resin systems- A comparison, Centre for electrical power engineering, University of Strathclyde, Glasgow, United Kingdom, 2001 IEEE 7th international conference on solid dielectrics, Eiidhoven, the Netherlands

[MAC-97] Mackevich J., Shah M.,“Polymer Outdoor Insulating Materials Part I: Comparison of Porcelain and Polymer Electrical Insulation”, IEEE electrical insulation magazine, May/June 1997 -Vol. 13, No. 3

[MAE-98] Maekawa Y., Nizuno Y., Naito K., Koshino H., Shinokubo H., Ishiwari M., “Electrical insulating characteristics of polymeric materials under wetting and contaminated conditions, results of CIGRE round robin test”, Japan, Proceedings of 1998 International Symposium on Electrical Insulating Materials, in conjunction with 1998 Asian International Conference on Dielectrics and Electrical Insulation and the 30th Symposium on Electrical Insulating Materials, Toyohashi, Japan, Sept. 27-30, 1998, IEEE

[MAI-08] P. Maity, S. V. Subramanyam, V. Parameswaran, S. Basu and N. Gupta, “Improvement in surface Degradation Properties of polymer composites due to pre-processed nanometric alumina fillers”, IEEE, Trans. On Dielectr. And Electr. Insul., vol. 15, pp. 63-72, 2008], [PAT-08, R. R. Patel, Nandini Gupta, “Volume resistivity of epoxy containing nano-sized AL2O3 fillers”, 15th national power systems conference (NPSC), IIT Bombay, December 2008

[MAI-08] P. Maity, S. V. Subramanyam, V. Parameswaran, S. Basu, N. Gupta, “Improvement in surface degradation properties of polymer composites due to pre-processed nanometric alumina fillers”]

[MAN-11] K. C. Mandal, P. G. Muzykov, R. Krishna, T. Hayes, T. S. Sudarshan, “Thermally stimulated current and high temperature resistivity measurements of 4H semi-insulating silicon carbide”, Solid state communications, 2011

[MAR-62] P. Mark and W. Helfrich, “Space charge limited currents in organic crystals”, J. Appl. Phys., Vol. 33, pp. 205-215, 1962

[MAR-67] Peter Mark, Thomas E. Hartman, “On distinguishing between the Schottky and Poole-Frenkel effects in insulators”, 1967

[MAS-71] Masayuki Ieda, Goro Sawa, and Sousuke Kato, “A consideration of Poole-Frenkel effect on electric conduction in insulators”, Department of Electrical Engineering, Nagoya University, Nagoya, Japan, 1971

[MAZ-05] G. Mazzanti, G. C. Montanari, L. A. Dissado, “Electrical ageing and life models: the role of space charge “, IEEE Trans. Dielectr. Electr. Insul., Vol. 12, pp. 876-890, 2005

[MAZ-13] Giovanni Mazzanti, Massimo Marzinotto, Extruded cables for high voltage direct current transmission, Advances in research and development, IEEE Press, 2013

[MIK-01] Mikrajuddin, F. G. Shi, K. Okuyama, “Temperature dependent electrical conduction in porous silicon: Non-Arrhenius behavior”, Europhysics letters, pp. 234-240, 2001

[MIZ-79] T. Mizutani, M. Ieda, “Carrier transport in high-density polyethylene”, Journal of applied physics, Vol. 12, 1979

[MIZ-80] T. Mizutani, T. Tsukahara, M. Ieda, “The effects of oxidation on the electrical conduction of polyethylene”, Journal of applied physics, Vol. 13, pp. 1673-1679, 1980

[MON-00] G. C. Montanari, “The electrical degradation threshold of polyethylene investigated by space charge and conduction current measurements”, IEEE trans. Dielectr. Electr. Insul., Vol. 7, pp. 1255-1263, 2007

[MON-11] G. C. Montanari, “Bringing an insulation to failure: the role of space charge”, IEEE Trans. Dielectr. Electr. Insul., Vol. 18, No. 2, April 2011

[MOR-60] M. J. Morant, Equilibrium space charge at the contact of a metal and a pure highy insulating liquid and its influence on high-field conductivity, Journal of Electrochem. Soc. J. Electrochem. p. 671-677, 1960

[MOT-40] N. F. Mott, R. W. Gurney, “Electronic processes in ionic crystals, Oxford at the Clarendon press, 1940”

[NIN-13] Xin Ning, Zhen Xiang, Peng Liu, Hua Feng, Zongren Peng, “Space charge behavior of epoxy resin at high temperature”, State key laboratory of Electrical Insulation and power equipment, Xi’an Jiaotong University, 2013 IEEE, Annual report conference on electrical insulation and dielectric phenomena

[PAI-75] D. M. Pai and R. C. Enck, “Onsager mechanism of photogeneration in amorphous selenium”, Phys. Rev. B, Vol. 11, pp. 5163-5174, 1975

[PAT-08] R. R. Patel and Nandini Gupta, “Volume resistivity of epoxy containing nanosized Al_2O_3 fillers”

[PAT-90] R. Patsch, “Space charge phenomena in polyethylene at high electric fields”, Journal of applied physics, Vol. 23, pp. 1497-1505, 1990

[PHI-78] P. Phillips, “Morphology-Electical property relations in polymers”, IEEE Transactions on electrical insulation, Vol. 13, pp. 69, 1978

[QI-04] X. Qi, Z. Zheng, S. Boggs, “Engineering with nonlinear dielectrics”, November/December 2004, Vol. 20, No. 6

[RAJ-03] Gogur G. Raju, “Dielectrics in electric fields”, University of Windsor, Windsor, Ontario, Canada, 2003

[RED-08] C. C. Reddy and T. S. Ramu, “On the DC conductivity of HV DC cable insulation-cautions in using empirical models”, 2008 IEEE International Symposium on Electrical Insulation. 2008: 39-42

[ROS-55] A. Rose, “Space charge limited currents in solids”, Phys. Rev., Vol. 97, pp. 1538-1544, 1955

[SAR-07] R. Sarathi, R. K. Sahu, P. Rajeshkumar, “Understanding of the thermal, mechanical, and electrical properties of epoxy nanocomposites”, Materials science and engineering, Elsevier, 2007

[SEA-82] Seanor D. A., Electrical properties of polymers, Academic press, London New York, 1982

[SIE-12] Gas-insulated transmission lines (GIL), High-power transmission technology, Siemens Brochure, 2012

[TAK-99] T. Takeda, N. Hozumi, H. Suzuki and T. Okamoto, “Factors of hetero space charge generation in XLPE under DCD field of 20 kV/mm”, Elect. Eng. Jpn., Vol. 119, pp. 13-21, 1999

[TEY-01] G. Teyssedre, C. Laurent, G. C. Montanari, F. Palmieri, A. See, J. C. Fothergill and L. Dissado, “Charge Distribution and electroluminescence in XLPE under dc field”, J. Phys. D: Appl. Phys., Vol. 34, pp. 2830-2844, 2001

[VAN-82] J. Vanderschueren, M. Ladang, J. Niezette, “The effect of the temperature dependence of the dielectric constant on thermally stimulated currents in polymers”, IEEE, 1982

[VEL-95] N. Vella, A. Toureile, U. Nilsson, “Study of the origin of space charges created during preparation of PE plaques”, Jicable, Junie 1995

[VELL-95] N. Vella, “About traps origin in PE samples”, Jicable, June 1995

[WAG-24] Wagner. K. W., Theoretische Grundlagen, In “Die Isoliestoffe den Elektrotechnik” von H. Schering, Verlag von Julius Springer, Berlin, 1924

[WIN-13] A. Winter, J. Kindersberger, “Transient field distribution on epoxy resin insulators in air under DC voltages”, 18th International Symposium on High Voltage Engineering, 2013, Seoul, Korea

[WIN-14] A. Winter, J. Kindersberger, M. Tenzer, V. Hinrichsen, L. Zavattoni, O. Lesaint, M. Muhr, D. Imamovic, "Solid/Gaseous insulation systems for compact HVDC solutions", CIGRE 2014

[ZEL-84] H. R. Zeller and W. R. Schneider, J. Appl. Phys. 56, 455 (1984)

[ZEL-87] H. R. Zeller et al., "The physics of electrical breakdown and pre-breakdownin solid dielectrics", in Festkörperprobleme 27 (Vieweg1987) p.223

[ZHE-05] Z. Zheng, S. Boggs, "Defect tolerance of solid dielectric transmission class cable", IEEE Electr. Insul. Mag., Vol. 21, No. 1, pp. 35-41, 2005